HHS Public Access

Author manuscript

Brain Behav Immun. Author manuscript; available in PMC 2019 May 01.

Published in final edited form as:

Brain Behav Immun. 2018 May ; 70: 398–422. doi:10.1016/j.bbi.2018.03.031.

Lung-injury depresses glutamatergic synaptic transmission in the nucleus tractus solitarii via discrete age-dependent mechanisms in neonatal rats

David G Litvin[1,2,3], **Thomas E Dick**[2,4], **Corey B Smith**[1], and **Frank J Jacono**[2,3,*]

[1]Department of Physiology & Biophysics, Case Western Reserve University School of Medicine, Cleveland, OH 44106, United States

[2]Division of Pulmonary, Critical Care and Sleep Medicine, Department of Medicine, Case Western Reserve University School of Medicine, Cleveland, OH 44106, United States

[3]Division of Pulmonary, Critical Care and Sleep Medicine, Louis Stokes VA Medical Center, Cleveland, OH, 44106, United States

[4]Department of Neurosciences, Case Western Reserve University School of Medicine, Cleveland, OH, 44106, United States

Abstract

Transition periods (TPs) are brief stages in CNS development where neural circuits can exhibit heightened vulnerability to pathologic conditions such as injury or infection. This susceptibility is due in part to specialized mechanisms of synaptic plasticity, which may become activated by inflammatory mediators released under pathologic conditions. Thus, we hypothesized that the immune response to lung injury (LI) mediated synaptic changes through plasticity-like mechanisms that depended on whether LI occurred just before or after a TP. We studied the impact of LI on brainstem 2nd-order viscerosensory neurons located in the nucleus tractus solitarii (nTS) during a TP for respiratory control spanning (postnatal day (P) 11 – 15). We injured the lungs of Sprague-Dawley rats by intratracheal instillation of Bleomycin (or saline) just before (P9 – 11) or after (P17 – 19) the TP. A week later, we prepared horizontal slices of the medulla and recorded spontaneous and evoked excitatory postsynaptic currents (sEPSCs/eEPSCs) *in vitro* from neurons in the nTS that received monosynaptic glutamatergic input from the tractus solitarii (TS). In rats injured before the TP (pre-TP), neurons exhibited blunted sEPSCs and TS-eEPSCs compared to controls. The decreased TS-eEPSCs were mediated by differences in postsynaptic α-amino-3-hydroxy-5-methyl-4-isoxazolepropionic-acid receptors (AMPAR). Specifically, compared to

[*]**Corresponding Author**: Frank J. Jacono M.D., Division of Pulmonary, Critical Care & Sleep Medicine, Case Western Reserve School of Medicine, 11100 Euclid Ave, Wearn 622, Mailstop 5067, Cleveland, OH 44106, Phone: (216) 368-4625, Fax: (216) 844-2187, fjj@case.edu.

Competing interests: The authors declare no competing financial interests.

Author contributions: D.G.L.: conception; design; analysis of data; interpretation of data; drafting and revising content of manuscript; final approval. T.E.D.: drafting and revising content of manuscript; final approval. C.B.S.: design; revising content of manuscript; final approval. F.J.J.: conception; interpretation of data; revising content of manuscript; final approval.

controls, LI rats had more Ca^{2+}-impermeable AMPARs (CI-AMPARs) as indicated by: 1) the absence of current-rectification, 2) decreased sensitivity to polyamine, 1-Naphthyl-acetyl-spermine-trihydrochloride (NASPM) and 3) augmented immunoreactive staining for the CI-AMPAR GluA2. Thus, pre-TP-LI acts postsynaptically to blunt glutamatergic transmission. The neuroimmune response to pre-TP-LI included microglia *hyper*-ramification throughout the nTS. Daily intraperitoneal administration of minocycline, an inhibitor of microglial/macrophage function prevented *hyper*-ramification and abolished the pre-TP-LI evoked synaptic changes. In contrast, rat-pups injured after the TP (post-TP) exhibited microglia *hypo*-ramification in the nTS and had increased sEPSC amplitudes/frequencies, and decreased TS-eEPSC amplitudes compared to controls. These synaptic changes were not associated with changes in CI-AMPARs, and instead involved greater TS-evoked use-dependent depression (reduced paired pulse ratio), which is a hallmark of presynaptic plasticity. Thus we conclude that LI regulates the efficacy of TS➔nTS synapses through discrete plasticity-like mechanisms that are immune-mediated and depend on whether the injury occurs before or after the TP for respiratory control.

Keywords

Viscerosensory; Microglia; Neuroinflammation; Developmental Plasticity; Developmental Transition Period; Lung Injury; GluR2; Calcium Impermeable AMPA Receptor; Nucleus Tractus Solitarii; Bleomycin

1. Introduction

In many central nervous system (CNS) circuits, the mechanisms governing synaptic plasticity of glutamatergic synapses transition during development. Stimuli applied before versus after these transitions can alter synaptic efficacy through distinctly different mechanisms (Nosyreva and Huber, 2005; Bellone and Nicoll, 2007; Corlew et al., 2007; Ho et al., 2007). The timing of these transitions periods (TPs) often coincides with transient shifts in glutamate-receptor subunit stoichiometry and the closure of critical periods for CNS-circuit development (Crair and Malenka, 1995; Heynen et al., 2003; Bellone and Nicoll, 2007). The plasticity expressed before the transitions can confer heightened sensitivity to sensory-relevant stimuli, but may also render CNS-circuits more vulnerable to lasting maladaptive changes caused by pathologic stimuli such as hypoxia, injury and inflammation (Berardi et al., 2000; Hensch, 2005; Levelt and Hubener, 2012; Bavis and MacFarlane, 2017).

In the current study we investigate the immune response to a neonatal lung injury (LI) and its impact on brainstem (medulla oblongata) viscerosensory function to determine whether discrete synaptic plasticity mechanisms are recruited when the injury occurs before versus after a TP for the neural control of respiratory function (Bavis and MacFarlane, 2017). We examined the impact of LI on viscerosensory projections of the tractus solitarii (TS), which consist of vagal, glossopharyngeal and facial nerve pathways that synapse with 2^{nd}-order neurons in the nucleus tractus solitarii (TS➔nTS synapses). We elected to study these glutamatergic synapses because: I) they exhibit synaptic plasticity for a variety of pathologic respiratory stimuli, which raises the possibility of LI-evoked changes (Chen et al., 2003;

Kline et al., 2007; Sekizawa et al., 2008a; Zhang et al., 2008; Kline, 2009; Pozo and Goda, 2010); II) they are modulated by proinflammatory cytokines, which suggests the immune response to LI may regulate synaptic efficacy (Xu et al., 2006; Marty et al., 2008; Jacono et al., 2011; Rogers and Hermann, 2012; Razavi-Azarkhiavi et al., 2014; Skurikhin et al., 2015); III) They are developmentally regulated during the TP, in part through abrupt shifts in the stoichiometry of low conductance Ca^{2+}-impermeable (CI) $GluR_2$ containing AMPA receptor (GluA2s) (Liu and Wong-Riley, 2005; Balland et al., 2006). Based on work within other CNS sites, this suggests the timing of the TP may serve as a point of demarcation between immature and mature synaptic plasticity mechanisms in the nTS (Nosyreva and Huber, 2005; Ho et al., 2007; Henley and Wilkinson, 2016); and IV) The timing of the GluA2 shift also coincides with a window of heightened vulnerability to respiratory challenges (P11–15), which suggests the transition process may underlie the enhanced vulnerability (Bavis and MacFarlane, 2017). Taken together, this raises the possibility that if an LI is present during the TP, synaptic efficacy changes may occur through impairment of developmentally regulated processes such as postsynaptic GluA2 insertion/removal.

Our preliminarily evidence showed that LI evoked in rat-pups by intratracheal bleomycin (Bleo) just before the TP (P9–11, pre-TP) augmented GluA2s in the nTS 7d after injury (P16–18) (Litvin et al., 2016). Several recent studies have reported that GluA2-mediated synaptic plasticity in some CNS-circuits can be evoked by peripheral and/or central inflammation (Park et al., 2009; Zhang et al., 2014; Riazi et al., 2015; Sullivan et al., 2017). Because Bleo LI can potentiate proinflammatory cytokine production in the peripheral circulation or in the nTS, it raised the possibility that this immune response could evoke GluA2-mediated synaptic plasticity at TS➔nTS synapses (Xu et al., 2006; Jacono et al., 2011; Razavi-Azarkhiavi et al., 2014; Skurikhin et al., 2015). Thus, we hypothesized that the immune response to pre-TP-LI contributed to a GluA2-dependent synaptic plasticity mechanism that was not active in post-TP-LI rat-pups.

There is considerable evidence P11–15 represents a TP for breathing control in the rat-pup. Firstly, during this period excitatory and inhibitory transmission systems within several brainstem respiratory sites (including the nTS) undergo abrupt changes towards adult neuronal expression levels (Wong-Riley and Liu, 2008; Liu and Wong-Riley, 2010a, 2012a, 2013; Turner and Johnson, 2015; Bavis and MacFarlane, 2017), which are similar to TPs in other CNS sites (Kumar et al., 2002; Tyzio et al., 2007; Brill and Huguenard, 2008; Roberts et al., 2009; Isoo et al., 2016). Secondly, the ventilatory responses to acute hypoxia or hypercapnia become transiently blunted between P12 and P15 and exposure to chronic hypoxia during this period can prolong the hypoxic insensitivity; this suggests the TP may be an important step towards the development of some ventilatory functions (Liu et al., 2009; Teran et al., 2014; Bavis and MacFarlane, 2017). Finally, several forms of respiratory plasticity that are present in juvenile and adult rats become functional just after the end of this TP (Dutschmann et al., 2009, 2014; Fuller et al., 2009; Bavis and MacFarlane, 2017). We therefore induced LI in rat-pups at P9–11, which was just before the presumed onset of the TP (at P11), so that progressively worsening LI would develop during the TP (Kaminski et al., 2000; Borzone et al., 2001; Cutillo et al., 2002; Babin et al., 2011). We contrasted this with the impact of LI initiated after the TP by inducing injury at P17–19. In these more mature rat-pups, the LI progressively worsened during a time period when: I) several forms

of mature respiratory plasticity are present (Dutschmann et al., 2009, 2014; Fuller et al., 2009; Bavis and MacFarlane, 2017), II) neurotransmitter and receptor expression changes in brainstem respiratory sites become stabile (Liu and Wong-Riley, 2005, 2010a, 2010b, 2013; Wong-Riley and Liu, 2008; Dufour et al., 2010), and III) the vagally-mediated Hering Breuer inflation reflex and inspiratory off-switch are active, indicating increased maturation of respiratory control (Dutschmann et al., 2009, 2014).

We now report that LI weakens TS➔nTS synaptic transmission efficacy before and after the TP. However, distinctly different synaptic plasticity mechanisms are responsible for this loss of efficacy depending on the temporal relationship of the injury to the TP. In pre-TP-LI rat pups, the loss of efficacy occurs through a *post*-synaptic CI-AMPAR-dependent mechanism that is concurrent with microglia *hyper*-ramification in the nTS, all of which can be reversed by the microglia/macrophage inhibitor minocycline. Alternatively, rats injured after the TP (post-TP) exhibit microglia *hypo*-ramification and a loss of synaptic efficacy that is CI-AMPAR-independent and consistent with *pre*-synaptic plasticity (Kline, 2009). Together, these data indicate mechanisms governing LI-evoked synaptic plasticity of viscerosensory transmission undergo a developmental switch during the TP. This switch is analogous to that exhibited by some forms of long term synaptic plasticity mechanisms; whereby a stimulus (i.e. electrical, pharmacological or environmental) applied before versus after a TP can alter synaptic efficacy at different sites (pre- vs. post-synaptically) or through different mechanisms (LTD vs. LTP) depending on the temporal relationship of the stimulus to the TP (Nosyreva and Huber, 2005; Bellone and Nicoll, 2007; Corlew et al., 2007; Ho et al., 2007).

2. Materials & Methods

2.1. Animals

Sprague Dawley dams with litters containing 10 cross-fostered male pups were purchased from Envigo (Indianapolis, IN, USA), and delivered at least 24h prior to the induction of LI. Rats were delivered pathogen free, and housed under specific-pathogen free conditions with a 12h light/dark cycle. Even though rat-pups were cross-fostered, we controlled for litter effects by ensuring that experimental treatments were distributed across multiple litters. All procedures were conducted in accordance with the National Institute of Health guidelines for care and use of laboratory animals and were approved by the Institutional Animal Care and Use Committee at Case Western Reserve University.

2.2. Treatment Groups

Rat-pups referred to as pre-TP-LI received a single intratracheal (IT) instillation of Bleo or Saline on P9 or 10 or 11, and were euthanized for electrophysiological or immunohistochemical experiments 7d later on P16 or 17 or 18.

In a separate set of studies, a cohort of pre-TP-LI rat-pups also received once daily IP minocycline or saline treatment for 7d. Pre-TP-LI rats that received Bleo-IT and saline or minocycline IP were referred to as B+S or B+M respectively, and sham-injured rat-pups that received saline IT and saline or minocycline IP were referred to as S+S or S+M respectively.

In the final set of studies, rat-pups referred to as post-TP LI received a single IT instillation of Bleo or Saline on P17 or 18 or 19, and were euthanized for electrophysiological or immunohistochemical experiments 7d later on P24 or 25 or 26.

The sample number required for each study was selected based on a power analysis (http://www.stat.uiowa.edu/rlenth/Power) to achieve a desired power of 0.8 at an alpha value of 0.05, assuming an effect size of 30% and standard deviations that were 15-20% of the mean in a given treatment group (Lenth, 2001).

2.3. Bleomycin induced lung injury

Bleomycin sulfate (Bleo) is a chemotherapeutic routinely used in animal models of acute lung injury and pulmonary fibrosis (Borzone et al., 2001). The toxicity of Bleo is inversely proportional to the cellular expression of its deactivating enzyme Bleomycin hydrolase, which exhibits low expression in pulmonary alveolar cells (Schwartz et al., 1999). Following intratracheal instillation, Bleo induces inflammatory and histological hallmarks associated with LI that are detectable at 48h, and peak at 7d (Borzone et al., 2001).

The Bleo solution was freshly prepared ~30 min before instillation by dissolving 30 U (20 mg) of lyophilized Bleo powder (1.5 U/mg, BIOTANG Inc. Lexington, MA) in 0.5 ml sterile saline (0.9% NaCl). Rat pups were sedated with 3% isoflurane at a flow-rate of 2 liters/min (Vetflo™, Kent Scientific, Torrington, CT, USA). Once anesthetized, rat pups were placed on a surgical board, and anesthesia was maintained with 1.5 - 2 % isoflurane delivered through a nose cone. The surgical site was disinfected with betadine, and the ventral surface of the trachea was exposed via midline incision. In both pre-TP-LI and post-TP-LI rat-pups, we intratracheally instilled 0.06 U of Bleo solution per gram body mass (or equivalent volume of sterile saline in sham controls) using a 27G needle attached to a 1 ml syringe in a Stepper™ Repetitive Dispensing Pipette (Indicon Inc., Brookfield, CT). The incision site was sealed using (Vetbond™, St. Paul, MN, USA). Rats were observed during recovery and, returned to the animal facility, and monitored daily. Rat-pups were considered injured if they exhibited significant bilateral lesions on the lung surface associated with extravasated blood, which was visualized post-mortem in both age-groups (Hattori et al., 2000). Due to the secondary sequelae associated with LI (weight loss and tachypnea) electrophysiological and immunohistochemical experiments were not blinded (Savani et al., 2001; Jarman et al., 2013).

2.4. Brainstem slice preparation

A week after inducing LI, rats were anesthetized with isoflurane and decapitated. The brainstem was dissected in ice-cold artificial cerebrospinal fluid (aCSF); containing (in mM): 116 NaCl, 3 KCl, 2 CaCl2, 1.2 MgSO4, 1.5 NaHPO4, 25 NaHCO3, 11 D-glucose, 9-12 Mannitol, pH 7.4 (300 mOsm) gassed with carbogen (95 % O2, 5 % CO2, Airgas, Radnor, PA, USA). After removing the meninges, the ventral surface of the brainstem was attached to a mounting block with cyanoacrylate (Krazy Glue®, Elmer's Products Inc., High Point, NC, USA) and affixed in the vibratome. Horizontal brain slices (250 μM) containing the nTS and TS fibers were cut and placed in ice-cold carbogen infused aCSF (Doyle et al., 2004). Brainstem slices were transferred rapidly to a low profile (~2 mm height)

polycarbonate chamber (26GLP, Warner Instruments, Hamden, CT, USA) and held in place using a slice anchor (26GH/15 and 26H/15, Warner instruments, Hamden, CT, USA). The chamber was fitted to the fixed stage of an Olympus BW50WI microscope (Center Valley, PA, USA). The slice was visualized with a ×10 (NA = 0.3) dry and ×40 (NA = 0.8) water-dipping contrast-enhancing objectives and was continuously perfused with carbogen-gassed aCSF at 30-32°C at 3ml/min^{-1} (~0.5 ml bath volume). The slice equilibrated for approximately 30 min.

2.5. NTS electrophysiological recordings

Experimental protocols were based on studies of CI-AMPARs in other CNS sites (Liu and Cull-Candy, 2002; Bellone and Lüscher, 2006; Adesnik and Nicoll, 2007; Riazi et al., 2015), and were adapted to protocols examining glutamatergic transmission at TS➔nTS synapses (Balland et al., 2006, 2008; Khlaifia et al., 2013; Zhao et al., 2015). Blind (×20) and visual (×40) whole-cell voltage-clamp recordings were made in the commissural and medial subnuclei of the caudal nTS, which receive input from various viscerosensory projections. Patch pipettes had a ~1 μm tip diameter and 3 - 5 MΩ resistance. The intrapipette solution used throughout the entire study contained (in mM): 100 Cs-methanesulfonate, 10 CsCl, 5 NaCl, 1 $MgCl_2$, 5 Tetraethylammonium-Cl, 8 EGTA, 1 $CaCl_2$, 10 HEPES, 5 QX-314, 3 NaATP, 0.2 MgGTP, and spermine tetrahydrochloride (0.1 mM). The pH was adjusted to 7.3 with CsOH and osmolarity adjusted to 280 - 290 mOsmol with mannitol. All aCSF solutions used throughout the study contained Picrotoxin (100 μM, sc-202765A, Santa Cruz Biotechnology, Dallas, TX, USA), a selective $GABA_A$ receptor antagonist that also shows specificity for several chloride conducting inhibitory receptors (Pribilla et al., 1992; Das et al., 2003; Erkkila et al., 2004; Wang and Slaughter, 2005) that have been reported in the nTS (Smith and Uteshev, 2008; Liu and Wong-Riley, 2013). The micropipette was attached directly to a pre- amplifier (EPC9, HEKA Elektronik, Bellmore, NY, USA) and was maneuvered to the nTS location by micromanipulator (MP-285, Sutter Instruments, Novato, CA).

The TS was stimulated with concentric bipolar electrode (FHC, Bowdoin, ME, USA), delivering a square pulse from an isolation unit (PSIU6) attached to a stimulator (S48, Grass Technologies, Warwick, RI, USA). The tip of the bipolar electrode was positioned atop the TS fiber bundle approximately 1.5 mm from the recording site. The duration of the stimulus pulse was 0.1ms with an interval of 10s. The magnitude of the TS stimulus was determined for each recording; TS stimulus intensity was increased until an EPSC was evoked and further increased until a maximal EPSC was evoked (at ~50-250 μA) (Doyle and Andresen, 2001; Bailey et al., 2006; McDougall et al., 2009). TS-eEPSCs were considered maximal when further increases in stimulus intensity were unable to elicit further amplitude increases. There were no significant differences between maximally evoked TS-eEPSCs in any of the treatment groups. NTS neurons with TS-eEPSCs exhibiting short, fixed latencies (jitter<250 μs) that could follow pairs of closely timed shocks (10 pairs, 0.1s between shocks, 10s between pairs) were considered monosynaptically connected to TS afferent terminals (Doyle and Andresen, 2001). NTS neurons with jitter ≥ 250 μs were excluded.

All experiments were completed in the whole-cell voltage clamp configuration. TS➔nTS synaptic recordings were accepted for analysis if access resistance was < 30 mΩ. Recordings were filtered at 10 kHz, amplified using an EPC-9 amplifier with “Pulse” (version 8.8 software; HEKA Electronik, Bellmore, NY, USA), digitized and recorded at 20 kHz with PowerLab data acquisition system (PowerLab hardware and LabChart version 8 software, AD Instruments, Colorado Springs, CO, USA).

We measured the AMPA to NMDA ratio (AMPA/NMDA) to determine the relative contribution of AMPA and NMDA receptors to TS-eEPSCs; this also serves as a reliable index for detecting changes in glutamatergic receptors (Bellone and Lüscher, 2006; Hall et al., 2007; Brill and Huguenard, 2008; Roberts et al., 2009; Riazi et al., 2015). All EPSCs were evoked by maximal TS-stimulation (0.1ms duration, used in all studies). Following successful break-in, ~10 min stabilization, and determination that putative 2^{nd}-order neurons were monosynaptic, we measured the NMDAR-component of TS-eEPSCs. To do this we increased the membrane potential (+10 mV step size, 5s between steps) from baseline (−60mV) to +40mV, where the cationic driving force produces outward currents. For each cell, we measured the average TS-evoked outward current at 50 ms after the stimulus artifact to determine the NMDAR component (Forsythe and Westbrook, 1988; Zhao et al., 2015); the average was comprised of 10 TS-eEPSCs stimulated at 0.1 Hz. The membrane potential was than returned to −60mV using −10mV steps (5s between steps) and the NMDAR blocker *DL*-2-amino-5-phosphonopentanoic acid (*DL*-AP5, 50μM; #14539, Cayman Chemical, Ann Arbor, MI, USA) was delivered into the perfusate. 5 min following *DL*-AP5 wash-on, we checked that input resistance changes greater than 20% were absent, and began measuring the AMPAR component of TS-eEPSCs; this consisted of 10 TS-eEPSCs (0.1 Hz) that were averaged. The average AMPAR and NMDAR components for each cell were divided to determine their ratio.

To assess current rectification, maximally evoked TS-eEPSCs were recorded using the same cesium based intrapipette solution as before, and with bath applied *DL*-AP5 and Picrotoxin. Following stabilization, confirmation of monosynaptic status and measurement of input resistance, the cell holding potential was decreased from −60 mV to −80 mV using 10 mV hyperpolarizing steps (5 s between steps). The membrane potential was held for 20 s before beginning TS-stimulation (10 TS-eEPSCs, 0.1 Hz). After TS-stimulation the holding potential was increased using 10 mV depolarizing steps, and TS-eEPSCs were measured at 20 mV intervals between −80 mV and +60 mV. At positive holding potentials intracellular spermine blocks the conductance pore of Ca^{2+}-permeable AMPARs (CP-AMPARs), and diminishes the magnitude of outward currents (Isaac et al., 2007). This spermine-dependent reduction in outward conduction is referred to as inward-current rectification, and can be quantified by making a ratio of the average TS-eEPSC amplitude evoked at +40 mV and −60 mV (Isaac et al., 2007). This is referred to as the rectification index (RI), where the magnitude of inward-current rectification is inversely proportional to the RI. The RI can detect changes in the contribution of CI- or CP-AMPARs to excitatory glutamatergic synaptic currents (Isaac et al., 2007). We additionally, assessed current-rectification by plotting the current-voltage (I–V) relationship, which normalizes all TS-eEPSCs measured at varying holding potentials to value of TS-eEPSCs at −80 mV. Changes in rectification can be visualized as shifts from a curvilinear I–V relationship to a more linear I–V relationship

or vice-versa. This normalization provides a way to assess current rectification when electrical normalization to a fixed eEPSC amplitude (using graded synaptic currents) cannot be used (Doyle and Andresen, 2001; Bailey et al., 2006; McDougall et al., 2009).

To further investigate changes in the contribution of CI- or CP-AMPARs, we washed on NASPM an antagonist of CP-AMPARs that is more sensitive to changes in AMPAR stoichiometry than inward-current rectification (Isaac et al., 2007). Changes in NASPM-dependent current depression reflect changes in CP- and CI-AMPARs; where CI-AMPAR expression is inversely proportional to the magnitude of NASPM-dependent depression (Isaac et al., 2007). NASPM-dependent depression of TS-eEPSCs was measured at −60 mV using the same cesium based intrapipette solution as before, and with bath applied *DL*-AP5 and Picrotoxin. The TS was stimulated every 30 s and the magnitude by which NASPM depressed the amplitude of TS-eEPSCs from baseline (3 min average) to 13 min after wash-on was measured. The access and input resistance were measured before and 13 min after NASPM wash-on.

In post-TP-LI studies, 10Hz stimulation of the TS was used to measure use-dependent depression and the paired-pulse ratio (PPR, eEPSC2/eEPSC1) (Kline et al., 2007; Almado et al., 2012a). TS-eEPSCs were evoked at −60 mV in the presence of bath applied Picrotoxin. The TS was stimulated (0.1 ms pulse duration) using a 500 ms train duration, 0.05 Hz train frequency and 2 min protocol duration.

2.6. Minocycline treatment

Following intratracheal Bleo or saline instillation, P9–11 rats were randomly assigned to groups that received IP minocycline hydrochloride (25 mg/kg, M9511, Sigma-Aldrich Co., St. Louis, MO, USA) or saline. Minocycline is highly acidic when reconstituted in water or saline, which contributes to a painful response that may stimulate immune pathways in the CNS (Ren and Dubner, 2010). The pH of our minocycline solution was adjusted with 10N NaOH (to pH 7.4) to minimize pain from the IP injection. All rat-pups were closely monitored and none exhibited any obvious signs of pain or discomfort. Rats received their first IP minocycline or saline injection ~24h following instillation of Bleo or saline, and continued to receive injections once daily until euthanized on day 7.

2.7. Immunohistochemistry (IHC), imaging and quantification

Rats were anesthetized deeply with isoflurane and euthanized by exsanguination and transcardial perfusion of ice-cold phosphate buffered saline (PBS, 0.9% saline + 0.1M phosphate buffer, pH 7.4) followed by ice-cold 4% paraformaldehyde (RT15714, Electron Microscopy Sciences, Hatfield, PA, USA). For histologic processing we: 1) removed the brainstems, 2) post-fixed the tissue for 2h in ice-cold 4% PFA, 3) cryoprotected it in 30% sucrose overnight, 4) trimmed the brainstem to reduce tissue size, 5) froze the tissue with dry ice, 6) embedded in Tissue-Tek® OCT compound (Sakura Finetek, Torrance, CA, USA), and then stored at −80 °C. Serial 20 μm coronal sections (Leica CM1850 cryostat. Leica Biosystems Inc., Buffalo Grove, IL, USA) were mounted on gelatin-coated slides and stored at −20 °C.

The slides containing sections were thawed, and rehydrated with PBS washes. Sodium citrate buffer (10mM tri-sodium citrate, 0.05 % tween-20, pH 6, heated to 75 °C) was used for antigen retrieval. The sections were permeabilized with PBS containing 0.1 % Triton X-100 (PBST), and incubated for 1h in blocking buffer (PBST, 5% bovine serum albumin (# 9048-46-8, Millipore Sigma, Temecula, CA, USA), and 5% normal donkey serum and then incubated overnight at room temperature with primary antibody diluted in blocking buffer. Dilutions and sources for the primary antibodies were as follows: rabbit anti-Iba-1 (1:500, #019-19741, Wako Pure Chemical Industries, Osaka, Japan), mouse anti-GluR2 (1:100, MAB397, Millipore Sigma), rabbit ant-GluR1 (1:1000, ABN241, Millipore Sigma), rabbit anti-GluR4 (1:1000, AB1508, Millipore Sigma) and rabbit anti IL-1β, which detects both the mature and pro-peptide versions of IL-1β (1:500, AB9722, Abcam). Following primary antibody incubation, the slides were washed in PBST (5 × 5 min) and incubated in blocking buffer containing donkey anti-rabbit Alexa 488 (1:500, # 111-545-144, Jackson Immunoresearch Laboratories, West Grove, PA, USA) or donkey anti-mouse Alexa 488 (1:500, # 715-545-150, Jackson Immunoresearch Laboratories) secondary antibodies. Following secondary antibody incubation, the slides were washed in PBST followed by PBS, and cover-slipped with Prolong Gold™ anti-fading medium (P36930, ThermoFisher Scientific, Waltham, MA). Slides were sealed with CoverGrip™ coverslip sealant (# 23005, Biotium, Fremont, CA, USA) and stored in the dark at 4 °C until the time of imaging. All brainstem sections from a particular study (e.g. pre-TP Bleo vs. saline) were immunostained in parallel for a particular antibody. In particular, sections from comparable groups were simultaneously incubated in the same: i) antigen retrieval solution, ii) blocking buffer, iii) primary antibody, and iv) secondary antibody. This insured that IHC protocol variability did not contribute to potential differences in immunostaining between Bleo- and saline-treated rats.

For reasons unrelated to our experiment, we used two different inverted microscopes (TCS SP8, Leica Biosystems Inc., Buffalo Grove, IL, USA for figures 3, 4, & 6; and a Leica TCS SP2 for figures 8 and 10). For both confocal microscopes, brainstem sections were imaged at ×40 (APO, 1.3 NA, oil objective) using Argon (SP2) or “White Light” (SP8) lasers tuned for Alexa 488. Brainstem sections imaged with the SP8 were never compared to brainstem images acquired by SP2. Images used for quantification were acquired within the same imaging session as 512 × 512 three-dimensional “z-stacks” with 8-bit resolution. Identical confocal conditions were used to image brainstem sections within datasets (i.e. IL-1β IHC). This included the same settings for: i) photomultiplier gain ii) pinhole (airy), iii) frame average and accumulation, iv) optical section thickness (z-axis step-size), and v) z-stack thickness. Three sections per rat were imaged bilaterally for all quantifications. Representative images were displayed as 8-bit maximum projections at a pixel resolution of 1024 × 1024.

Quantification was done using the open-source image analysis software FIJI (Schindelin et al., 2012). For densitometric analysis, we used a thresholded binary image from each optical slice within a z-stack and calculated the immunoreactive area within a region of interest using the “measure” function in ImageJ software (Schindelin et al., 2012). Cell number and area per cell were measured on maximum projected, segmented binary images using the “analyze particle” function. Iba-1+ branch endpoints/cell, and total branch length/cell were

quantified in a given region of interest using maximum projected binary masks that were "skeletonized" and measured using the "analyze skeleton" function without "pruning" (Arganda-Carreras et al., 2010; Morrison and Filosa, 2013).

2.8. Bronchial alveolar lavage fluid (BALF) acquisition and analysis

Rats-pups were euthanized with isoflurane and placed on a surgical board. The chest cavity and trachea were surgically exposed and visualized. A 25 or 27 gauge needle was inserted in the trachea and was sutured in place. A 1ml tuberculin syringe was used to inject and withdraw (lavage) PBS (500 μl). Three aliquots from successive PBS flushes were pooled to collect ~1.3 ml total volume of BALF per rat. The BALF was then centrifuged (1500 rpm, 10 min), and the pellet was re-suspended in PBS and stained with trypan blue to exclude dead cells. Nucleated cells were counted using a hemocytometer. The supernatant was stored at −80 °C protein analysis, for which 100 μl of BALF supernatant was incubated with 5 ml of diluted modified Bradford Protein Assay (Bio-Rad Laboratories, Hercules, CA, USA) for 10 min and analyzed spectrophotometrically (595 nm). Protein concentration was determined by comparing the BALF samples to standards. The results were expressed as micrograms of protein per microliter of BALF. BALF was collected from a set of S+S, S+M, B+S, and B+M rat-pups to quantitatively determine whether minocycline altered pulmonary inflammation in conjunction with its systemic and/or central actions (Yrjänheikki et al., 1999; Riazi et al., 2008, 2015). These rat-pups were not utilized in electrophysiological or immunohistochemical studies because the process of BALF collection interfered with these experimental procedures. As minocycline was not administered to post-TP-LI rat-pups, BALF was not examined in the older age group.

2.9. Measurement of breathing patterns

We recorded respiratory waveforms in awake, freely moving rat-pups within a temperature equilibrated whole-body plethysmographic (pleth) chamber (BUXCO Research Systems, Wilmington, NC, USA) (Jacono et al., 2006, 2011). Pressure changes detected within the chamber were transmitted through a pre-amplifier (Max II, BUXCO Research Systems, Wilmington, NC, USA) and recorded at 200 Hz by PowerLab data acquisition system (PowerLab hardware and LabChart version 8 software, AD Instruments, Colorado Springs, CO, USA).

Rat-pups were allowed to acclimate to the pleth chamber for at least 45 min before recording commenced. Baseline breathing was measured for 30 min before testing ventilatory responses to hypoxic-hypercapnia (H/H). To induce H/H exposure, inflow to the pleth chamber was switched to the test gas (10% O_2, 5% CO_2) for 5 min followed by a 10 min return to normoxia and an additional 5 min H/H exposure. The respiratory rate (breaths per minute, bpm) during the 1^{st} min of the H/H exposure was normalized to the baseline respiratory rate to assess ventilatory responses and averaged between exposure episodes. Apneas were defined as respiratory cycles with duration >2.5× baseline, and were quantified manually in LabChart using the "Cyclic Measurements" function by plotting the instantaneous period of respiratory cycles over time.

2.10. Data analysis

All statistical analysis was performed using GraphPad Prism 7. Data are presented here mean ± SEM. The probability for statistical significance was set at $P < 0.05$. A D'Agostino-Pearson omnibus normality test was performed on each data set to determine whether they conformed to a Gaussian distribution. Parametric statistics were used for data sets conforming to a Gaussian distribution. These statistics included an unpaired two-tail t-test, a two-way ANOVA with Bonferroni's repeated measure test, and a one-way ANOVA with Tukey multiple comparisons test. When non-Gaussian distribution was present, the Kruskal-Wallis test, a one-way ANOVA on ranks, was used with Dunn's multiple comparison's test.

In the patch-clamp studies, we initially pooled and plotted spontaneous EPSC (sEPSC, 60 s recording) events from each cell in a given treatment group by cumulative probability graph. Statistical differences were not tested for these graphs. For quantifying statistical differences between treatment groups, the amplitude or frequency of sEPSC events were averaged from a 60 s recording for a given cell and the difference in the distribution of these values between treatment groups was tested for significance using two-tail t-tests. In presenting the origin of the data, we show values for the number of neurons, followed by the number of slices from a particular rat followed by the number of rats per group.

For immunohistochemical experiments, measurements from 3 - 4 brainstem sections per rat were averaged and compared between groups.

3. Results

3.1. Bleomycin (Bleo) lung injury (LI) induced prior to the transition period (TP) reduces the efficacy of glutamatergic transmission to 2nd-order neurons in the nTS

We recorded TS-evoked (TS-e) excitatory postsynaptic currents (TS-eEPSCs) and measured the AMPAR (−60 mV, inward) and NMDAR (+40 mV, outward) components of maximally evoked currents using distal stimulation of the TS (Figure 1A). Figure 1B shows representative raw traces of inward and outward currents recorded from the same 2nd-order nTS neuron of a Bleo (magenta) and saline (black) treated rat-pup. The sign (−/+) associated with the amplitude of the TS-evoked current indicates direction rather than magnitude; at more depolarized holding potentials the direction of cationic current flow is outward (positive current), and at hyperpolarized holding potentials current flow is inward (negative current).

We observed significantly smaller AMPAR-mediated TS-eEPSC amplitudes in the Bleo- compared to the saline treated group ((Figure 1B, 1C) Bleo: 264.8 ± 12.4 pA, n = 8 (1 neuron was recorded from 8 different slices from 8 different rats); saline: 534.8 ± 60.3 pA, n = 8 cells/slices/rats, $t_{14} = 4.3$, $P = 0.0006$, Two-tail t-Test). Also, we observed significantly larger NMDAR mediated TS-eEPSC amplitudes recorded from Bleo- compared to saline-treated rats (Figure 1C) Bleo: 104.3 ± 15.6 pA vs. saline: 68.7 ± 5.6 pA, $t_{14} = 2.2$, $P = 0.049$, Two-tail t-Test). The AMPAR to NMDAR ratio serves as a reliable index for detecting alterations in glutamatergic transmission mediated through receptor composition changes (Bellone and Lüscher, 2006). The AMPAR/NMDAR ratio of TS-eEPSCs was significantly

lower in Bleo- compared to saline- treated rats ((Figure 1C) Bleo: 3.2 ± 0.9; saline: 8.3 ± 0.9, $t_{11} = 3.97$, $P = 0.002$, Two-tail t-Test).

Unlike TS-eEPSCs, the synaptic source of sEPSCs is comprised of TS and non-TS related inputs, which allows sampling of a larger population of glutamatergic transmission to 2nd-order neurons. We observed significantly smaller sEPSC amplitudes in Bleo versus saline treated rats, which was reflected in a leftward shift of the cumulative probability plot ((Figure 1D, 1E) Bleo: 31.7 ± 1.7 pA, n = 12 cells, 11 slices, 11 rats vs. saline: 39.6 ± 2.0 pA, $t_{20} = 3.04$, $P = 0.006$, n = 10 cells/slices/rats, Two-tail t-Test). This decrease in sEPSC amplitude occurred without significant changes in the sEPSC frequency ((Figure 1F, inset) Bleo: 13.8 ± 2.0 Hz; saline: 16.1 ± 3.4 Hz, $t_{20} = 0.59$, $P = 0.56$, Two-tail t-Test). Also, the rise and decay times were not significantly different between measured groups (rise time: Bleo: 3.7 ± 0.3 ms vs. saline: 3.3 ± 0.2 ms, $t_{20} = 0.97$, $P = 0.345$, Two-tail t-Test) (decay time: Bleo: 3.9 ± 0.3 ms vs. saline: 3.7 ± 0.3 ms, $t_{20} = 0.53$, $P = 0.600$, Two-tail t-Test). These findings indicate that sEPSC transmission efficacy is depressed following LI, and suggests that LI affects TS and non-TS associated synaptic sites on the 2nd-order neuron (Fortin and Champagnat, 1993).

3.2. Lung injury prior to the transition period enhances the contribution of Ca^{2+}-impermeable AMPA receptors to TS-evoked synaptic currents

We examined whether changes in GluA2s or $GluR_2$-lacking AMPARs (non-GluA2s) were concurrent with altered efficacy; this was because pre-TP-LI evoked decreases in EPSC amplitude were likely AMPAR dependent (Doyle and Andresen, 2001; Bailey et al., 2006). To do this we took advantage of the sensitivity of non-GluA2s to intracellular polyamines such as spermine (Isaac et al., 2007). In the presence of intrapipette spermine, blockade of non-GluA2's channel-pore occurs at positive holding potentials, which reduces outward cationic current conduction (relative to inward conduction) (Bowie and Mayer, 1995; Isaac et al., 2007). This is referred to as inward-current rectification and can be visualized as a curvilinear plateau in a current-voltage (I–V) plot. Contrastingly, GluA2s, which are resistant to intracellular polyamine block, and conduct cations with similar efficacy at positive and negative membrane potentials, are said to lack inward-current rectification. The amino acid substitution that confers resistance to polyamine block in GluA2s precludes Ca^{2+}-conduction; GluA2s are therefore also referred to as CI-AMPARs, and exhibit a linear I–V relationship.

TS-eEPSCs of Bleo treated rats exhibited a linear I–V relationship and had a significantly larger rectification index (RI, mean TS-eEPSCs at +40 mV/mean TS-eEPSCs at −60 mV, where RI is inversely proportional to inward current rectification) compared to saline treated rats ((Figure 2A, 2B) Bleo: 0.7 ± 0.2, n = 10 cells/slices/rats; saline 0.21 ± 0.02, n = 9 cells/slices rats, $t_{17} = 2.9$, $P = 0.008$, Two-tail t-Test). This indicates pre-TP-LI promotes a loss of inward-current rectification, and suggests changes in the stoichiometry of GluA2s (increase) or non-GluA2s (decrease) may be responsible (Liu and Cull-Candy, 2000; Mameli et al., 2007).

We measured the effect of NASPM, an inhibitor of non-GluA2s, to assess whether changes in AMPAR subunits were related to the reduced TS-evoked currents (protocol in methods).

Wash-on of NASPM (50 μM) caused a decrease in the amplitude of TS-eEPSCs in saline treated animals (n = 6 cells/slices/rats), suggesting that non-GluA2s comprise a significant amount of the AMPA-mediated current (Figure 2C, 2D). We observed that Bleo treated rats (n=6 cells/slices/rats) were significantly less sensitive to NASPM, consistent with a decrease in TS-eEPSC amplitude due to a difference in AMPAR subunit composition in the Bleo- versus saline-treated rats ((Figure 2C, 2D) Bleo: 82.6 ± 5.0 % of baseline; saline: 47.7 ± 6.5 %, Two-way ANOVA with Bonferroni correction: treatment effect $F_{1,10} = 23.5$, NASPM effect F16,160 = 19.68, treatment*NASPM interaction F16,160 = 4.92, $P < 0.0001$). The blunted NASPM sensitivity and smaller current-rectification likely reflect altered postsynaptic AMPAR function because AMPARs in the nTS are exclusively expressed postsynaptically (Kessler and Baude, 1999; Aicher et al., 2003; Lachamp et al., 2003; Balland et al., 2006).

We next determined whether changes in current rectification and NASPM sensitivity were related to alterations in specific AMPAR subunits by immunohistochemically labeling AMPARs containing GluR1, 2 or 4 subunits in coronal brainstem sections (Figure 3). The density of GluA2 positive (GluA2+) immunostaining in the nTS was greater in Bleo- than in saline- treated rats ((Figure 3C) Bleo: 0.19 ± 0.01 AUs, n = 4; saline treated 0.10 ± 0.02 AUs n = 4, $t_6 = 3.3$, $P = 0.02$, Two-tail t-Test), but the densities of GluA1+ and GluA4+ immunostaining in the nTS were not significantly different between groups (GluA1+ (Figure 3B) Bleo: 0.052 ± 0.01 AUs, n = 5; saline: 0.042 ± 0.004 AUs n = 5, $t_8 = 0.89$, $P = 0.4$, Two-tail t-Test; and GluA4+ (Figure 3D) Bleo: 0.22 ± 0.01 AUs, n = 5; saline: 0.20 ± 0.03 AUs, n = 5, $t_8 = 0.62$, $P = 0.55$, Two-tail t-Test). Together these results are consistent with a current-rectification and NASPM-sensitivity decrease that is mediated through augmented postsynaptic GluA2 expression rather than reduced non-GluA2 expression.

3.3. Lung injury prior to the transition period promotes microglia hyper-ramification in the nTS

Microglia can mediate synaptic plasticity under pathophysiological conditions by altering postsynaptic GluA2s (Zhang et al., 2014; Riazi et al., 2015). Therefore, we examined whether microglia morphologic changes in the nTS were concurrent with the GluA2 dependent synaptic depression. First we assessed whether pre-TP-LI altered microglia number and morphology in the nTS, because changes in these variables can correlate with changes to microglial synaptic engagement (Miyamoto et al., 2016; Sipe et al., 2016). Coronal nTS-containing sections from Bleo and saline treated rats did not exhibit significant differences in the average number of Iba-1 positive (Iba-1+) cells within a set region of the nTS (186.2×10^4 μm^2) (Bleo: 162 ± 5 cells, n = 5; saline: 150 ± 12 cells, n = 5, $t_8 = 0.88$, $P = 0.4$, Two-tail t-Test) (Figure 4A, 4B). However, the average area per Iba1+ cell did increase significantly in the nTS from Bleo- compared to saline-treated rats (Bleo: 9.0 ± 0.4 × 10^2 μm^2, n = 5: saline: 6.9 ± 0.6 × 10^2 μm^2, n = 5, $t_8 = 2.97$, $P = 0.018$, Two-tail t-Test) (Figure 4C). This was associated with significant increases in the number of branch endpoints (BEP) (Bleo: 11.2 ± 1.4 BEP, n = 5; saline: 7.4 ± 0.6 BEP, n = 5, $t_8 = 2.49$, $P = 0.04$, Two-tail t-Test) (Figure 4D), and in the average total branch length in Bleo versus saline treated rats (Bleo: 120.2 ± 18.2 μm, n = 5 rats; saline: 67.5 ± 7.9 μm, n = 5, $t_8 = 2.65$, $P = 0.03$, Two-tail t-Test) (Figure 4E). Thus, in pre-TP-LI, microglia appear to express

hyper-ramification in their appendages, which raises the possibility that microglia may contribute to altered TS➔nTS synaptic efficacy.

Changes in microglia morphology are also associated with the production and release of neuroinflammatory factors (Riazi et al., 2008, 2015; Roumier et al., 2008; Lewitus et al., 2016). Therefore, we determined whether microglia *hyper*-ramification was associated with changes in the levels of the inflammatory cytokine Interleukin 1 beta (IL-1β), which has been shown to depress TS-eEPSC amplitude *in vitro* (Marty et al., 2008). Immunohistochemical staining using an antibody that detected IL-1β and its inactive precursor pro-IL-1β indicated that pre-TP-LI augmented IL-1β/pro-IL-1β immunoreactivity throughout the nTS in Bleo- versus saline- treated rats ((Figure 5A, 5B) Bleo: 47.0 ± 8.3 AUs, n = 7; saline: 16.4 ± 2.1 AUs, n = 8, t_{13} = 3.8, P = 0.0022, Two-tail t-Test). The apparent widespread increase in IL-1β/pro-IL-1β immunoreactivity in the nTS suggested that the neuroimmune response to pre-TP-LI extended beyond respiratory viscerosensory pathways in the nTS. We measured IL-1β/pro-IL-1β immunoreactivity on the same coronal brainstem sections in the: I) area postrema (AP, Figure 5C), a circumventricular organ that senses circulating immune factors and projects to the nTS, II) gracile nucleus (Gr, Figure 5D), a non-respiratory medullary site with 2nd-order neurons receiving input from spinal projections that are posterior to T6, and III) dorsal motor nucleus of the vagus (DMNX, Figure 5E), which receives input from the nTS and has a visceromotor efferent component of the vagus nerve. These three sites had significant increases in IL-1β/pro-IL-1β immunoreactivity in Bleo-compared to saline treated rats (Bleo AP: 12.6 ± 2.5 AUs vs. saline AP: 3.3 ± 1.0 AUs, t_{13} = 3.6 P = 0.0032, Two tail t-Test; Bleo Gr: 10.9 ± 2.9 AUs vs. saline Gr: 2.04 ± 0.70 AUs, t_{13} = 3.2, P = 0.0071; Bleo DMNX: 9.1 ± 2.5 AUs vs. saline DMNX: 2.1 ± 0.8 AUs, t_{13} = 2.8, P = 0.02). We conclude that LI evokes IL-1β/pro-IL-1β production throughout the dorsal brainstem, which suggests that LI may impact CNS function beyond respiratory or viscerosensory control. Furthermore, the augmented IL-1β/pro-IL-1β immunoreactivity observed in the AP raises the possibility that systemically released cytokines may be mediating CNS production of IL-1β in response to LI (Vitkovic et al., 2000; Goehler et al., 2006).

3.4. Daily minocycline treatment during the course of pre-TP-LI prevents loss of synaptic efficacy and microglia hyper-ramification

We next tested whether the systemic and/or central immune response to pre-TP-LI contributed to synaptic changes in the nTS. A day after inducing pre-TP-LI we injected minocycline (IP once daily for 7d), which is permeable to the blood brain barrier and inhibits microglia/macrophages (Figure 6A) (Yrjänheikki et al., 1999; Colovic and Caccia, 2003; Buller et al., 2009). We had the following four groups of rats: 1) Bleo, IT and minocycline IP, (B+M treated); 2) Bleo, IT and saline IP, (B+S treated); 3) Saline, IT and minocycline IP, (S+M treated); and 4) Saline, IT and saline IP, (S+S treated). B+M treated rats exhibited significantly larger TS-eEPSC amplitudes when compared to B+S treated rats ((Figure 6B, 6C) B+M: 382.6 ± 53.3 pA, n = 7 cells/slices/rats vs. B+S: 171.6 ± 17.4 pA, n = 8 cells/slices/rats, P = 0.0082, One-way ANOVA with Tukey test, treatment effect $F_{3,24}$ = 9.75, P = 0.0002). Further, TS-eEPSC amplitudes were not significantly different among B+M−, S+S−, and S+M− treated rats ((Figure 6C) B+M vs. S+S: 41.7 ± 2.6 pA, n = 12 cells,

9 slices, 9 rats, $P = 0.999$; B+M vs. S+M: 40.2 ± 2.3 pA, n = 9 cells, 7 slices, 7 rats, $P = 0.373$, One-way ANOVA with Tukey test). Consistent with our first experiments, TS-eEPSC amplitudes from B+S treated rats were significantly less than those of S+S− and S+M− treated rats.

Similarly, the amplitude of sEPSCs recorded from B+M treated rats was significantly greater than B+S treated rats, and was not significantly different from S+S− or S+M− treated rats ((6D, 6E) B+M: 41.4 ± 2.2 pA, n = 11 cells, 7 slices, 7 rats; vs. B+S: 31.4 pA± 1.4, n = 12 cells, 7 slices, 7 rats, $P = 0.01$, One-way ANOVA with Tukey test). Further, B+M treated rats were not significantly different from S+S− (S+S: 41.7 pA± 2.6, n = 12 cells, 9 slices, 9 rats, $P = 0.999$) and S+M− (S+M: 40.2 pA± 2.3, n = 9 cells, 7 slices, 7 rats, $P = 0.983$) treated rats. Finally, the amplitudes of sEPSCs recorded from B+S-treated rats were significantly smaller than those recorded from S+S− and S+M− treated rats ((Figure 6D, 6E) B+S versus S+S: $P = 0.006$; B+S versus S+M: $P = 0.041$, One-way ANOVA with Tukey test: treatment effect $F_{3,40} = 5.42$, $P = 0.0032$). As we expected, the frequencies of sEPSCs were not significantly different among the groups ((Figure 6D, 6F) B+M: 9.8 ± 2.3 Hz vs. B+S: 11.4 ± 3.6 Hz, $P > 0.999$, Kruskal-Wallis with Dunn's test). There were also no significant differences in the frequency of sEPSCs measured between B+M- and S+S− or S+M− treated groups ((Figure 6D, 6F) B+M vs. S+S: 15.5 ± 2.7 Hz, $P = 0.6$; B+M vs. S+M: 13.5 ± 3.0 Hz $P > 0.999$, Kruskal-Wallis with Dunn's test, $H = 4.4$, $P = 0.2$).

We quantified the number and morphology of Iba-1+ cells in the nTS (Figure 7A–D) to assess whether microglia *hyper*-ramification was altered by minocycline. Consistent with our initial finding, the number of Iba-1+ cells did not significantly differ between groups ((Figure 7B) B+M: 114 ± 20 cells, n = 7, vs. B+S: 162 ± 17 cells, n = 7, $P = 0.4$; B+M vs. S+S: 117 ± 16 cells, n = 5, $P > 0.999$; B+M vs. S+M 119 ± 11 cells, n = 5, $P > 0.999$, Kruskal-Wallis with Dunn's test, $H = 5.1$, $P = 0.17$). Thus, minocycline treatment did not impact the number of Iba1+ cells in the nTS.

In contrast, daily minocycline treatment significantly reduced the number of branch endpoints per iba-1+ cell in B+M- compared to B+S treated rats, which were not significantly different from S+S treated or S+M treated rats ((Figure 7C) B+M: 8.4 ± 0.8 BEP vs. B+S: 12 ± 1.1 BEP, $P = 0.048$; B+M vs. S+S: 8.4 ± 0.9 BEP, $P > 0.999$; B+M vs. S+M: 7.8 ± 0.9, $P < 0.97$, One-way ANOVA with Tukey test, $F_{3,20} = 4.2$, treatment effect $P = 0.02$). As before, the number of branch endpoints in B+S-treated rats were significantly greater than those in S+M-treated rats, but did not attain significance when compared to S+S treated rats ((Figure 7C) B+S vs. S+M: $P = 0.03$; B+S vs. S+S: $P = 0.08$, One-way ANOVA with Tukey test).

We also measured the average total branch length for Iba-1+ cells and observed a significant reduction in the average total branch length measured in B+M− compared to B+S treated rats. This was not significantly different when compared to S+S or S+M treated rats ((Figure 7D) B+M: 68.1 ± 9.2 μm vs. B+S: 108.8 ± 10.4 μm, $P = 0.02$; B+M vs. S+S: 70.9 ± 8.9 μm, $P = 0.996$; B+M vs. S+M: 61.8 ± 8.3 μm, $P = 0.97$, One-way ANOVA with Tukey test, $F_{3,20} = 5.34$, treatment effect $P = 0.007$). The average total branch length per Iba-1 cell was significantly greater in B+S treated rats compared to S+M treated rats but was not

significantly different compared to S+S treated rats ((Figure 7D) B+S vs. S+M: $P = 0.014$; B +S vs. S+S: $P = 0.055$, One-way ANOVA with Tukey test). Together this demonstrates that minocycline treatment during the course of LI can attenuate the pre-TP-LI dependent *hyper*-ramification of microglia in the nTS. In summary, our electrophysiological and microglial morphologic data indicate that minocycline treatment administered after inducing pre-TP-LI can attenuate the LI-dependent depression to TS-eEPSCs and *hyper*-ramification of microglia in the nTS. Thus, brainstem inflammation is associated with depressed synaptic efficacy at the synapse that integrates viscerosensory information from the periphery.

We also assessed the possibility that minocycline treatment may have preserved synaptic efficacy and attenuated microglia/macrophage morphologic changes in the nTS by mitigating LI rather than by acting centrally. Therefore, to quantify the severity of LI, we sampled airway epithelial lining fluid by bronchial alveolar lavage and measured two hallmarks of LI, protein leak into the lung (Figure 7E) and the number of nucleated immune cells (Figure 7F) in the BALF (Jacono et al., 2006). Minocycline treatment did not significantly affect protein concentration in BALF measured from B+M− compared to B+S− treated rats ((Figure 7E) B+M: 0.51 ± 0.11 μg/μl, n = 6; vs. B+S: 0.26 ± 0.02 μg/μl, n = 7, $P > 0.999$, Kruskal-Wallis with Dunn's test, H = 17.8, $P = 0.0005$). Both LI groups had higher BALF protein concentrations compared to their respective control groups ((Figure 7E) B+M vs. S+M: 0.05 ± 0.01 μg/μl n = 5, $P = 0.002$; B+S vs. S+S: 0.03 ± 0.01 μg/μl, n = 5, $P = 0.04$, Kruskal-Wallis with Dunn's test). Similarly, nucleated cell counts from the same BALF indicated that B+M and B+S treated rats were not significantly different ((Figure 7F) B+M: 117.3 ± 15.3 $\times 10^4$ cells vs. B+S: 94.9 ± 6 $\times 10^4$ cells, $P = 0.3$, One-way ANOVA with Tukey test). Both LI groups showed greater cell counts when compared to their corresponding control groups ((Figure 7F): B+M vs. S+M: 4.2 ± 2.8 $\times 10^4$ cells, P < 0.0001; B+S vs. S+S: 58.4 ± 5 $\times 10^4$ cells, $P = 0.048$, One-way ANOVA with Tukey test, $F_{3,19} = 13.5$, treatment effect P < 0.0001). Thus, minocycline treatment did not reduce vascular leak or immune cell infiltration 7d following intratracheal instillation of Bleo. Our results indicate a magnitude of similar LI in the untreated and minocycline treated groups.

3.5. Minocycline treatment prevents the enhanced contribution of Ca^{2+}-impermeable AMPARs evoked by pre-TP-LI

Microglia/macrophages can mediate synaptic depression or potentiation by reducing postsynaptic GluA2 expression (Zhang et al., 2014; Riazi et al., 2015). Therefore, we assessed whether microglia/macrophages contributed to the reduced current-rectification and NASPM sensitivity observed following pre-TP-LI. First we tested the impact of daily minocycline treatment on current rectification (Figure 8A, 8B). The rectification index was smaller in B+M− compared to B+S− treated rats B+M ((Figure 8A) B+M: 0.35 ± 0.04, n = 6 cells, 5 slices, 5 rats; B+M vs. B+S: 0.75 ± 0.04, n = 8 cells/slices/rats, $P < 0.0001$, One way ANOVA with Tukey test: $F_{3,25} = 39.6$, treatment effect $P < 0.0001$). The rectification index did not differ between B+M−, S+S−, and S+M− treated groups ((Figure 8A, 8B) B+M vs. S +S: 0.23 ± 0.03, $P = 0.19$; B+M vs. S+M: 0.33 ± 0.04, $P = 0.99$). Consistent with our previous results, the rectification index was greater in B+S− than in S+S− or S+M− treated rats ((Figure 8A, 8B) B+S vs. S+S: P < 0.0001; B+S vs. S+M: P < 0.0001). The S+S− and S +M treated rats did not have different rectification indices ((Figure 8A, 8B) S+S vs. S+M: *P*

= 0.26, One way ANOVA with Tukey test). These data indicate that microglia/macrophages contribute to the loss of rectification evoked by pre-TP-LI.

Second, we tested whether minocycline affected the loss of NASPM-sensitivity in TS-eEPSCs that occurred after pre-TP-LI (Figure 8C, 8D). Treatment with minocycline prevented the loss of the NASPM-dependent depression of TS-eEPSCs as evident by comparing TS-eEPSCs of B+M− to: 1) those of B+S− treated rats, and 2) those of S+M− and S+S− treated rats. TS-eEPSCs of B+M− were more depressed compared to those of B +S− treated rats ((Figure 8C, 8D) B+M: 40.3 ± 6.9%, (n = 7 cells/slices/rats) vs. B+S: 82.1 ± 6.1% (n = 8 cells/slices/rats), P < 0.0001); whereas TS-eEPSCs of B+M− were similar to those from S+M− and S+S− treated rats (B+M vs. S+S: 41.9 ± 3.6%, n = 5 cells/slices/rats, $P = 0.998$; B+M vs. S+M: 32.1 ± 7.0%, n = 6 cells/slices/rats $P = 0.71$, Two-way ANOVA with Tukey test: treatment effect $F_{3,21} = 16.6$, NASPM effect $F_{16,336} = 65.4$, treatment*NASPM interaction $F_{48,336} = 3.97$, $P < 0.0001$). Also consistent with our earlier findings, the normalized TS-eEPSC amplitudes were greater in B+S− than those in S+S− and S+M− treated groups ((Figure 8C, 8D) B+S vs. S+S: $P < 0.0001$; B+S vs. S+M: P < 0.0001, Two-way ANOVA with Tukey test). These data indicate that microglia/macrophages contribute to the loss of NASPM sensitivity evoked by pre-TP-LI.

Finally, we measured the density of GluA2+ immunostaining in the nTS to determine if rescuing inward current rectification and NASPM-sensitivity was correlated with GluA2 expression (Figure 9A, 9B). GluA2+ immunostaining in the nTS was lower in B+M− than in B+S−, greater than that in S+S−, and did not differ from that in S+M− treated rats ((Figure 9A, 9B) B+M: 1.2 ± 0.2 AUs, n = 7 vs. B+S: 1.9 ± 0.2 AUs, n = 7, $P = 0.008$; B+M vs. S+S: 0.4 ± 0.1 AUs, n = 5, $P = 0.0079$; B+M vs. S+M: 0.75 ± 0.13 AUs, n = 5, $P = 0.234$, One-way ANOVA with Tukey test, $F_{3,20} = 18.6$, treatment effect $P < 0.0001$). Similar to our results from pre-TP-LI rats without treatment, GluA2+ immunostaining in the nTS increased after LI (B+S treatment) compared to controls ((Figure 9A, 9B) B+S vs. S+S: P < 0.0001; B +S vs. S+M: $P = 0.0002$). Finally, S+S− and S+M− treated groups did not differ ((Figure 9A, 9B) S+S vs. S+M: $P = 0.419$, One-way ANOVA with Tukey test). These results indicate that the minocycline dependent rescue of current rectification and NASPM sensitivity following pre-TP-LI is concurrent with reduced GluA2 expression in the nTS.

In summary, the rectification index and NASPM sensitivity data demonstrate that daily minocycline treatment prevents the enhanced contribution of CI-AMPARs, which occurs at TS➔nTS synapses following pre-TP-LI. The immunohistochemistry data suggest: I) microglia/macrophages enhance the contribution of CI-AMPARs to TS➔nTS synapses following pre-TP-LI by augmenting postsynaptic GluA2 expression, II) microglia/ macrophages reduce synaptic efficacy following pre-TP-LI, and III) microglia/macrophages do not developmentally regulate postsynaptic GluA2 insertion/removal during the TP.

3.6. Lung injury in pre-TP-LI rats promotes apnea and loss of ventilatory sensitivity to acute Hypercapnic-Hypoxia, which is ameliorated by minocycline treatment

The induction of LI during a window of vulnerability to respiratory challenges raised the possibility that pre-TP-LI promoted changes in neurally controlled respiratory functions (Feldman et al., 2003; Ramirez et al., 2013; Li et al., 2016). Moreover, changes in TS➔nTS

synaptic efficacy have been attributed to altered cardiorespiratory control (Kline, 2008). We first recorded respiratory patterns in awake, freely moving pre-TP-LI rat-pups using whole-body plethysmography (pleth). Representative pleth traces from pre-TP-LI rat-pups showed B+S treatment augmented the number of apneas (defined as breaths >2.5× longer than baseline cycle duration) when compared to saline-treated controls, which was prevented by minocycline treatment ((Figure 10A, 10C): B+S: 17 ± 3, n = 9 vs. S+S: 6 ± 1, n = 5, P = 0.041; B+S vs. S+M: 6 ± 1, n = 5, P = 0.041; B+S vs. B+M: 7 ± 2, n = 9, P = 0.027, One way ANOVA with Tukey test, $F_{3, 24}$ = 4.48, treatment effect P = 0.012). There were no significant differences in apnea number between the B+M treated group and saline-treated controls (B+M vs. S+S: P = 0.998; B+M vs. S+M: P = 0.998). We next examined the breathing rate of pre-TP-LI rats in normoxia and during an acute (5 min) hypercapnic-hypoxic (H/H) (10% O_2 with 5% CO_2) episode, which is commonly present during LI (Carlo, 2007; Ragaller and Richter, 2010; Vadász and Sznajder, 2017), and has been used to examine the neural control of breathing (Dergacheva et al., 2014; Dyavanapalli et al., 2014) (Figure 10A, 10B, 10D, and 10E). LI promoted significant breathing frequency increases (breaths per minute, bpm) in Bleo-treated rats compared to saline-treated controls, which were irrespective of minocycline treatment (B+S: 235.5 ± 10.5 bpm vs. S+S: 136.4 ± 6.5 bpm, P <0.0001; B+S vs. S+M: 145.3 ± 4.9 bpm, P = 0.0002; B+M: 213.2 ± 18.1 bpm vs. S +S: P = 0.002; B+M vs. S+M: P = 0.0078; One way ANOVA with Tukey test, $F_{3, 24}$ = 9.3, treatment effect P = 0.0003). Minocycline treatment did not significantly alter the breathing frequency in Bleo-treated rats (B+S vs. B+M: P = 0.718, One way ANOVA with Tukey test). In all treatment groups, H/H exposure significantly increased (relative to baseline (BL)) the respiratory rate during the 1st min (1m) of exposure ((Figure 10B, 10D) S+S BL vs. 1m: P < 0.0001; S+M BL vs. 1m: P < 0.0001; B+S BL vs. 1m: P < 0.0001; B+M BL vs. 1m: P < 0.0001, Two-way ANOVA with Sidak's test). However, Bleo-treated rats responded with a significantly smaller rate increase compared to rat-pups from saline-treated control groups; this effect was prevented by minocycline treatment ((Figure 10B, and 10E) B+S: 21.0 ± 2.7 % vs. S+S: 72.5 ± 5.8 %, P = 0.0008; B+S vs. S+M: 74.7 ± 6.1 %, P = 0.0005; B+S vs. B+M: 48.7 ± 10.5 %, P = 0.04; One way ANOVA with Tukey test, $F_{3, 24}$ = 10.41, treatment effect P = 0.0001). There were no significant differences in the ventilatory response to H/H in B+M measured rat-pups compared to the saline treated control groups (B +M vs. S+S: P = 0.187; B+M vs. S+M: P = 0.131). Together these data indicate LI increases the propensity for respiratory pausing while decreasing the ventilatory response to acute H/H exposure in pre-TP rat-pups. These effects are prevented by minocycline treatment, which suggests the neuroimmune response to pre-TP-LI alters central control of respiration.

3.7. Lung injury induced in rats after the transition period exerts a dual modulatory role on synaptic efficacy that is mechanistically distinct

So far, we have focused on the mechanisms by which LI evokes synaptic depression before a TP for respiratory control. Comparing these mechanisms of pre-TP-LI to those stimulated by post-TP-LI revealed that discrete synaptic plasticity-like changes were active in each of these age groups. In post-TP-LI studies Bleo or saline was IT instilled in rats aged P17–19 and euthanized 7d later (P24–26) (Figure 11A). The amplitudes of TS-eEPSCs (at −60 mV) were smaller in 2nd-order neurons from Bleo- than from saline- treated rats ((Figure 11B, 11C) Bleo: 263.7 ± 29.5 pA n = 10 cells, 8 slices, 8 rats vs. saline: 455.9 ± 57.6 pA, n = 10

cells, 8 slices, 8 rats, $t_{19} = 2.96$, $P = 0.007$, Two-tail t-Test). However, the amplitudes of sEPSCs were greater in Bleo- than those form saline- treated rats ((Figure 11D, 11E) Bleo 59.0 ± 4.4 pA, n = 16 cells, 13 slices, 13 rats vs. saline: 42.4 ± 3.6 pA, n = 16, 13 slices, 13 rats, $t_{31} = 2.94$, $P = 0.006$, Two-tail t-Test). Further, the frequencies of sEPSCs were greater in Bleo- than saline-treated rats ((Figure 11D, 11F) Bleo: 29.6 ± 3.5 Hz vs. saline: 19.9 ± 2.4, $t_{30} = 2.25$, $P = 0.03$, Two-tail t-Test). Thus, contrary to the depression in sEPSC amplitudes demonstrated in pre-TP-LI, these findings showed that post-TP-LI potentiated the amplitude and frequency of sEPSCs.

We measured the rectification index and GluA2+ immunostaining in the nTS to assess whether CI-AMPARs contributed to the decrease in synaptic efficacy in post-TP-LI rats. Unlike pre-TP-LI, the TS-eEPSC rectification index did not differ between LI and control rats ((Figure 12A, 12B) Bleo: 0.25 ± 0.02, n = 7 cells, 6 slices, 6 rats, vs. saline: 0.3 ± 0.02, n = 9 cells, 6 slices, 6 rats, $t_{15} = 1.62$, $P = 0.13$, Two-tail t-Test). Further, GluA2+ immunostaining in the nTS did not differ between Bleo- and saline- treated rats ((Figure 12C, 12D) Bleo: 6.2 ± 1.3 $\times 10^2$ AUs, n = 5 rats, vs. saline: 4.8 ± 0.9 $\times 10^2$ AUs, n = 7 rats, $t_{10} = 0.80$, $P = 0.44$, Two-tail t-Test). Together these results indicate that GluA2 are unlikely to be the source of the TS-eEPSC depression or the sEPSC amplitude potentiation following post-TP-LI.

In post-TP rats, short-term, use-dependent depression at TS➔nTS synapses was mediated presynaptically when a train of stimuli exceeded 3 Hz (Zhao et al., 2015). This depression can be altered by pathologic conditions that impact presynaptic efficacy in the nTS (Kline, 2009). Therefore, we determined whether post-TP-LI altered the ability to evoke short-term depression of TS➔nTS synapses. At 10 Hz TS-stimulation (full protocol in methods), we evoked use-dependent depression of the amplitude of TS-eEPSC in both injured and sham rats ((Figure 13A, 13B) Bleo: comparing stimulus 1 to responses to stimuli 2, 3, 4, & 5 were depressed, n = 6 cells, 5 slices, 5 rats, $P < 0.0001$; saline: stimulus 1 vs. 2, 3, 4 & 5, n = 7 cells, 6 slices, 6 rats, $P < 0.0001$, Two-way ANOVA with Tukey test). However, the TS-eEPSCs were depressed more after the 2nd, 3rd, and 5th stimuli in Bleo- than saline- treated rats ((Figure 13A, 13B) Bleo: stimulus 2: 31.5 ± 2.7 %, stimulus 3: 27.3 ± 2.9 %, stimulus 5: 28.7 ± 3.7 %; vs. Saline: stimulus 2: 46.0 ± 2.3 %, stimulus 3: 39.0 ± 2.3 %, stimulus 5: 38.8 ± 3.2 %, $P = 0.0008$, $P = 0.009$ and $P = 0.032$ respectively, Two-way ANOVA with Tukey test, treatment effect $F_{1,11} = 11.34$, $P = 0.006$; stimulus effect $F_{4,4} = 456.4$, $P < 0.0001$; treatment*stimulus interaction $F_{4,44} = 4.02$, $P = 0.0072$). The paired-pulse ratio (EPSC 2/EPSC 1) was reduced in Bleo- compared to saline- treated rats ((Figure 13C) Bleo: 0.31 ± 0.03, n = 6 vs. saline: 0.47 ± 0.02, n = 7, $t_{11} = 4.48$, $P = 0.0009$, Two-tail t-Test).

We measured the inverse coefficient of variation squared ($1/CV^2$) for stimulus-evoked EPSCs at 10 Hz. This analysis detects changes in synaptic efficacy due to alterations in the release probability (p) and the number of release sites (n), where the quantal content ($n \bullet p$) is directly proportional to the $1/CV^2$ (Malinow and Tsien, 1990; Kerchner and Nicoll, 2008; Almado et al., 2012b). This analysis has been applied in studies examining pathologically evoked synaptic efficacy changes at TS➔nTS synapses (Kline et al., 2007; Almado et al., 2012b; Accorsi-Mendonca et al., 2015). The $1/CV^2$ of EPSCs evoked by 10Hz TS-stimulation was less in Bleo- compared to saline-treated rats ((Figure 13D) Bleo: 1.95

± 0.32, n = 6 vs. saline: 3.85 ± 0.53, n = 7, t_{11} = 1.69, P = 0.013, Two-tail t-Test). These findings indicate that post-TP-LI depresses TS-evoked synaptic transmission in a GluA2-independent manner, which increases use-dependent depression, while reducing the PPR and $1/CV^2$. These data suggest diminished quantal content causes synaptic depression following post-TP-LI. Thus, unlike pre-TP-LI, post-TP-LI synaptic depression has a presynaptic mechanism.

Finally, we wanted to test whether post-TP-LI altered the morphology and number of microglia in the nTS (Figure 14). The number of Iba-1+ cells did not differ between Bleo- and saline- treated rats (Bleo: 145.9 ± 18.3, n = 7, vs. saline: 163.0 ± 7.2, t_{11} = 0.82, n = 6, P = 0.431, Two-tail t-Test) (Figure 14B). Further, in distinct contrast to pre-TP-LI the number of branch endpoints/Iba-1+ cells decreased in Bleo- compared to saline- treated rats (Bleo: 6.9 ± 0.7 BEP vs. saline: 9.6 ± 0.4 BEP, t_{11} = 3.23, P = 0.008, Two-tail t-Test) (Figure 14C). There was also a significant decrease in the average total branch length/Iba-1+ cell in Bleo treated rats compared to saline treated rats ((Figure 14D) Bleo: 53.8 ± 7.7 μm vs. saline: 75.4 ± 3.4 μm, t_{11} = 2.41, P = 0.035, Two-tail t-Test). Thus LI after the TP causes microglia *hypo*-ramification rather than *hyper*-ramification evoked by pre-TP-LI.

4. Discussion

4.1. Summary of our findings

We used a well-established model of bleomycin-based murine lung injury (Matute-Bello et al., 2008; Physiol et al., 2013) to examine its impact on 2nd-order viscerosensory integration within the dorsal medulla oblongata. We determined pre-TP-LI reduced the efficacy of AMPAR-mediated TS➔nTS transmission. This loss of synaptic efficacy occurred through an enhanced contribution of CI-AMPARs with increases in GluA2, a CI-AMPAR, in the nTS. Treatment with minocycline, an inhibitor of microglia/macrophages, reduced the increase in GluA2 expression and CI-AMPAR contribution and prevented the loss of synaptic efficacy, suggesting that these changes are mediated by the immune response to LI. In contrast, post-TP-LI augmented spontaneous transmission and blunted evoked synaptic transmission to 2nd-order neurons in the nTS. This post-TP-LI effect occurred in a CI-AMPAR-independent manner. Interestingly, the observed alterations in post-TP-LI synaptic function shared similarities with functional changes at TS➔nTS synapses evoked by other pathologic stimuli in adult rats (Kline, 2009). Taken together, these findings suggest that LI is a potent pathological stimulus that down-regulates fast glutamatergic signaling to 2nd order neurons in the nTS. Furthermore, the timing of the LI stimulus is important, as distinct synaptic mechanisms function just before and after the P11–15 TP.

4.2. Loss of synaptic efficacy following pre-TP-LI

Our findings demonstrate that synaptic sites associated with TS-evoked and spontaneous excitatory glutamatergic transmission become blunted by LI when the injury coincides with a TP for respiratory control and a window of heightened vulnerability to respiratory challenges (Bavis and MacFarlane, 2017). These findings are the first to demonstrate that LI can impact CNS function, broadly affecting a brainstem site where pulmonary afferents terminate (Berger and Dick, 1987). Previous work has shown that TS-evoked action

potential generation becomes blunted following ozone exposure in the neonatal rhesus macaque (Chen et al., 2003). Because ozone exposure at comparable doses has been shown to produce lung injury, it suggests our findings may be related (Connor et al., 2012).

There are indications that early-life respiratory challenges can impair viscerosensory integration in the nTS when they occur during a period of neurodevelopmental transition in the rat (P11–15) (Bavis and MacFarlane, 2017). Consequently, the timing of this developmental epoch has also been referred to as a period of respiratory vulnerability; that is, rodents faced with respiratory challenges are unable to produce a physiologically appropriate ventilatory response (Bavis and MacFarlane, 2017). Clinical studies also suggest respiratory insults in pre-term or full-term infants may cause deficits related to impaired brainstem viscerosensory integration; this includes apneas (Martin et al., 1986; Warren et al., 2010) reduced ventilatory drive (Reuter, 2014), blunted oral-motor reflexes (Stumm, 2008), and diminished parasympathetic tone (Smith et al., 2005). Our findings demonstrating that LI promotes reduced ventilatory sensitivity to acute H/H exposure and an increase in the number of apnea, mirror the observations of several of these studies. This raises the possibility that loss of TS➔nTS synaptic efficacy may contribute to impairments in ventilatory function during ear-life LI.

4.3. Reduced contribution of CI-AMPARs following pre-TP-LI

We found smaller current rectifications and a reduced sensitivity to the non-GluA2 antagonist NASPM, suggesting that pre-TP-LI enhances the contribution of CI-AMPARs upon TS-evoked transmission. These CI-AMPAR related changes were concurrent with augmented staining throughout the nTS for the low conductance CI-AMPAR subunit GluR2. Notably, changes to GluR1 or GluR4 were not observed. Taken together, these electrophysiological and immunohistochemical data suggest that the loss of synaptic efficacy is directly related to the enhanced contribution of CI-AMPARs. However, a contribution from non-stoichiometric changes in AMPAR-subunit function cannot be entirely excluded, as changes in transmembrane AMPAR regulatory proteins (TARPs) can modulate rectification and polyamine sensitivity (Soto et al., 2007, 2009).

At TS➔nTS synapses, efficacy changes evoked under pathological or environmental conditions have commonly been attributed to mechanisms of prolonged neurophysiological adaptation known as long-term (LT) synaptic plasticity. These mechanisms can occur in the range of hours to days, and can depress (LTD) or potentiate (LTP) synaptic transmission efficacy (Kline et al 2008). Our finding of a reduction in AMPAR-dependent currents following pre-TP-LI suggests that LI evokes a form of postsynaptic LTD, by lowering the sensitivity of 2nd-order neurons to presynaptically released glutamate. Several groups have reported GluA2-mediated LTD in other CNS sites, which raises the possibility that it may also be occurring in the nTS following pre-TP-LI (Liu and Cull-Candy, 2000; Ho et al., 2007; Mameli et al., 2007; Liu et al., 2010). This form of postsynaptic LTD can be evoked *in vitro* through NMDAR or mGluR activation. Because postsynaptic mGluR-LTD is not inducible at TS➔nTS synapses, it suggests our findings, if attributable to LTD, likely occur through an NMDAR-dependent mechanism (Chen et al., 2002; Jin et al., 2004). This is supported in part by *in-vitro* studies showing that low frequency TS-stimulation in P3–21

aged rats or P0 mice can evoke an NMDAR-dependent LTD, which reduces postsynaptic AMPAR currents (Zhou et al., 1997; Poon et al., 2000). We observed a rise in NMDAR-dependent currents following pre-TP-LI, which is also consistent with this form of LTD (Yashiro and Philpot, 2008).

4.4. Evidence for a neuroimmune response to pre-TP-LI

Previous studies labeling specific viscerosensory pathways identified that pathophysiologically evoked changes occurred at labeled and unlabeled synapses (de Paula et al., 2007; Accorsi-Mendonça et al., 2015). This is consistent with our finding that pre-TP-LI reduced synaptic efficacy in neurons that likely received input from a diverse range of afferent pathways. This apparent lack of specificity could be explained in part by the incomplete blood brain barrier (fenestrated capillaries) found within the caudomedial nTS, which allows central access to circulating factors (Gross et al., 1990). Thus, it is possible that the peripheral immune response to LI could promote widespread synaptic changes within and beyond the nTS (Lin et al., 1999; Sekizawa et al., 2008b; Park et al., 2009; Thibault et al., 2014; Riazi et al., 2015). Consistent with this, pre-TP-LI evoked changes in microglia within the nTS. Although there was no change in the number of microglia in the nTS, we did observe an increase in the average area per microglia. This increase in area was concurrent with an increase in branch endpoint number and total branch length. These changes indicate microglia *hyper*-ramification, which is consistent with the presence of hypertrophied processes that occurs in response to some noxious conditions (Streit et al., 1999; Hinwood et al., 2013; Karperien et al., 2013; Hellwig et al., 2016). Although microglia *hyper*-ramification is not well understood, several studies have suggested that it is not associated with a pro-inflammatory role for microglia (Hinwood et al., 2013; Hellwig et al., 2016). However, we observed augmented immunoreactivity for IL-1β/pro-IL-1β within the nTS and more generally throughout the dorsal brainstem in respiratory (DMNX) and non-respiratory (Gr, and AP) related nuclei. Because the antibody used to detect IL-1β exhibits specificity for both the inactive precursor and active mature version of the cytokine, it is unclear whether LI causes IL-1β release or simply provides greater substrate availability for the NLRP3 inflammasome (He et al., 2016; Kiernan et al., 2016). It remains an open question whether the described neuroimmune-related changes represent a pathophysiological event or a physiological adaptation to LI.

4.5. Preventing synaptic efficacy changes with minocycline

To further assess the role of microglia/macrophages and the neuroimmune response following pre-TP-LI, we examined the effect of minocycline treatment on the observed depression of glutamatergic transmission to 2nd-order nTS neurons. Daily IP minocycline treatment during the course of LI prevented TS-eEPSC and sEPSC amplitude reductions. Moreover, minocycline prevented augmented GluA2 expression in the nTS, and the loss of TS-eEPSC rectification and NASPM-depression. Together this argues for an immune mediated mechanism governing synaptic depression in pre-TP-LI, which acts by enhancing the postsynaptic contribution of CI-AMPARs at TS➔nTS synapses. Because we observed that minocycline treatment concurrently prevented microglia *hyper*-ramification, this provides an indirect link between microglia activation by LI and CI-AMPAR-dependent changes to glutamatergic transmission. Importantly, minocycline did not significantly alter

the augmented protein concentrations and cell counts measured in BALF from injured rat-pups, indicating comparable injury severity. The similar magnitude of LI suggests minocycline prevented synaptic efficacy changes through immune mechanisms beyond the lung, acting instead to inhibit the peripheral (Xu et al., 2006; Razavi-Azarkhiavi et al., 2014; Skurikhin et al., 2015) and/or central (Jacono et al., 2011) immune responses to intratracheal Bleo treatment. Together these findings are novel because they are the first to demonstrate that the immune response to a neonatal LI participates in synaptic plasticity of viscerosensory circuit function in the nTS. Furthermore, our data suggest that microglia/macrophages are critical to the described GluA2-dependent LTD-like mechanism following pre-TP-LI.

Some caution is required in attributing the proposed GluA2-dependent efficacy loss specifically to microglia/macrophages, given that minocycline may have more than one mechanism of action. On the one hand, there are indications that minocycline (at varying doses) can recapitulate many of the immune effects associated with microglia/macrophage specific perturbations such as: I) genetic deletion of complement receptor C3R (Schafer et al., 2012), II) antagonism of the fractalkine receptor (Clark et al., 2015), or III) microglia depletion (Miyamoto et al., 2016; Szalay et al., 2016). Moreover, microglia specific complement receptors or fractalkine receptors have been shown to mediate synaptic plasticity of glutamatergic synapses (Riazi et al., 2015; Lewitus et al., 2016); this includes a C3R-mediated form of LTD that contrastingly involves GluA2 internalization (Zhang et al., 2014). On the other hand, there are indications that minocycline also acts to inhibit protein kinase C (PKC) and mitogen-activated protein kinase (MAPK) signaling pathways primarily in microglia/macrophages (Nikodemova et al., 2006, 2007), but potentially also in neurons (Cho et al., 2012). This raises the possibility that minocycline prevented LI-dependent synaptic efficacy changes through direct inhibition of these pathways in neurons, which could regulate the AMPAR trafficking used in some forms of synaptic plasticity (Lüscher and Malenka, 2012; Chater and Goda, 2014). However, neuronal PKC or MAPK inhibition is less likely given that minocycline treated control rat-pups (S+M) did not exhibit signs of altered synaptic physiology relative to saline treated control rat-pups (S+S) (Gottschalk et al., 1999; Lanuza et al., 2002; Newbern et al., 2011; Sen et al., 2016; Sugawara et al., 2017) Nonetheless, we cannot fully exclude the involvement of minocycline-dependent PKC or MAPK inhibition in our study.

4.6. The Impact of post-TP-LI on TS➔nTS synapses

Our study also examined viscerosensory function when the LI was induced after the TP to determine whether distinct synaptic mechanisms were involved. Our findings show that post-TP-LI promotes a reduction in the amplitude of TS-eEPSCs. This indicates that glutamatergic transmission efficacy through the TS is also reduced in more mature post-TP-LI rats. However, contrary to pre-TP-LI rat-pups, we observed augmented sEPSC amplitude and frequency in rats injured after the TP. This suggests LI discretely affects synaptic sites receiving spontaneous vs. evoked glutamatergic transmission in post-TP rats (Sara et al., 2011; Lalanne et al., 2016). In further contrast, there were no differences in TS-eEPSC inward rectification or GluR2 immunoreactivity measured between Bleo- and saline treated post-TP-LI rat-pups. This indicates that TS-eEPSC amplitude reductions in post-TP-LI rats

are not mediated through changes in AMPAR stoichiometry. Taken together, these data suggest that discrete synaptic mechanism underlying the loss of efficacy occur depending on the temporal relationship of the LI to the TP. Tellingly, post-TP Bleo treated rat-pups exhibited greater TS-evoked short-term use-dependent depression compared to saline treated rat-pups. This was associated with a reduced PPR and $1/CV^2$, which are common hallmarks of presynaptic changes at TS➔nTS synapses (Kline et al., 2007; Zhang et al., 2009a; Li et al., 2015). For example in adult rats, exposure to chronic intermittent hypoxia (CIH) elicits adaptive depression of TS➔nTS synapses, reducing the amplitude and $1/CV^2$ of TS-eEPSCs, while increasing the frequency of sEPSCs (Kline et al., 2007). This plasticity is mediated presynaptically by calcium-calmodulin kinase II (CaMKII) a molecular switch involved in use-dependent LTD and could also be involved in mediating synaptic changes in post-TP-LI rat-pups (Ninan and Arancio, 2004; Lu and Hawkins, 2006).

Somewhat unexpectedly, microglia in the nTS from post-TP-LI rats had morphologic changes that were consistent with *hypo*-ramification, rather than the *hyper*-ramification observed following pre-TP-LI. This morphological response is consistent with the appendage retraction often attributed to phagocytic microglia during systemic or CNS inflammation (Yrjänheikki et al., 1999; Riazi et al., 2008; Karperien et al., 2013; Chen et al., 2014; Stokes et al., 2017). This suggests that the developmental status of nTS microglia could dictate their response to pathologic challenges. Related findings have been reported for microglia morphologic changes in the nTS of P10 vs. P25 rat-pups with chorda tympani transection, and could explain in part why P10 rat-pups are unable to regain sensory function (Sollars, 2005; Riquier and Sollars, 2017). It is tempting to attribute the divergent microglia morphologic changes following pre-TP- vs. post-TP-LI to the shift in synaptic plasticity-like changes we observed in these age groups. However, it is unclear whether mechanisms of synaptic plasticity that are evoked by microglia also undergo developmental regulation. This will be a focus of future investigation.

4.7. Technical caveats

In the nTS, AMPARs are exclusively postsynaptic (Kessler and Baude, 1999; Aicher et al., 2003; Lachamp et al., 2003; Balland et al., 2006). Thus, the observed changes to AMPAR-mediated TS-eEPSCs and sEPSCs, which were concurrent with changes to the polyamine sensitivity of AMPAR-currents strongly suggests a postsynaptic site of action. This does not exclude the possibility that presynaptic mechanisms may also be active during pre-TP-LI. For example, we reported that the amplitude of NMDAR-mediated TS-eEPSCs was augmented in Bleo treated rats, which could be mediated through changes in presynaptic NMDARs (Chen et al., 1999). However, because AMPAR TS-eEPSCs were recorded under low frequency stimulation (0.1Hz) with AP5 and Mg^{2+} in the perfusate, it is unlikely that changes to presynaptic NMDARs were misattributed to AMPARs (Zhao et al., 2015).

We stimulated the TS with a current injection intensity required to maximally evoke EPSCs from 2^{nd}-order neurons, as has been done in previous studies of these synapses (Kline et al., 2007; McDougall et al., 2009; Zhang et al., 2009b; Clark et al., 2011; Almado et al., 2012a; Li et al., 2015). This approach was used in lieu of a standardized eEPSC threshold as there is well-established evidence demonstrating 2^{nd}-order neurons in the nTS rely primarily on

single, and sometimes double or triple converging inputs from the TS, which evoke unitary (non-graded) EPSCs (Doyle and Andresen, 2001; Bailey et al., 2006; McDougall et al., 2009). This is in contrast to other CNS sites tasked with higher-order sensory integration (i.e. cortex), which rely upon the recruitment of many convergent inputs to produce graded eEPSCs (Allen and Stevens, 1994) that can be standardized to stimulus intensity (Kumar et al., 2002).

Evoked currents in nTS neurons have been shown to exhibit minimal inward-rectification and NASPM-depression (Balland et al., 2006; Li et al., 2015). However, in our study, we observed that TS-eEPSCs exhibited pronounced inward rectification and NASPM-dependent depression. These differences may be attributable to the differing internal/external polyamine sensitivities that can occur in distinct pathways sharing common neuronal targets (Sara et al., 2011; Lalanne et al., 2016). For example, in coronal-brainstem slices, stimulation may have recruited glutamatergic release from monosynaptic inputs of interneurons and collaterals in addition to TS-projections (Mifflin and Felder, 1988; Davis et al., 2004; Doyle et al., 2004; Fernandes et al., 2011). Thus, differences in experimental protocol may underlie the differing current-profiles observed between studies.

We recorded AMPAergic transmission in the presence of the NMDAR inhibitor *DL*-APV and $GABA_AR$ inhibitor Picrotoxin, which was based on previous studies in the nTS and other CNS sites (Liu and Cull-Candy, 2002; Balland et al., 2006; Bellone and Lüscher, 2006; Adesnik and Nicoll, 2007; Brill and Huguenard, 2008; Zhang et al., 2009b; Riazi et al., 2015; Zhao et al., 2015). Picrotoxin is also an antagonist of some but not all chloride conducting ionotropic ligand-gated receptors (Pribilla et al., 1992; Das et al., 2003; Erkkila et al., 2004; Wang and Slaughter, 2005) that have been reported in the nTS (Smith and Uteshev, 2008; Liu and Wong-Riley, 2013). This raises the possibility that some Glycinergic, Cholinergic and/or Serotonergic inhibition remained in our recordings of EPSCs. Based on a calculated chloride reversal potential (E_{Rev}) of −40 mV we would have expected chloride-related inward currents at holding potentials below E_{Rev} and outward currents at holding potentials above E_{Rev}; either could mask detection of glutamatergic EPSCs. However, assessment of TS-eEPSCs at E_{Rev} (from rectification studies), where chloride-related currents would expectedly be minimized (data not shown), yielded similarly significant effects to those measured at −60 mV. Thus it is unlikely that chloride-related currents are a significant source for the LI-induced TS-eEPSC changes reported in our study.

TS transmission is almost exclusively glutamate dependent, but is modulated by a variety of inhibitory transmitters (Kline, 2008). These inhibitory inputs may converge with TS-afferents onto 2^{nd}-order neurons, and likely constitute targets for synaptic efficacy changes (Tsukamoto and Sved, 1993; Kline, 2008). Investigating changes in GABA or Glycine-dependent transmission was beyond the scope of the present work. Although it is unlikely that inhibitory inputs contributed to the observed differences in glutamatergic transmission efficacy, we cannot completely exclude the possibility that LI also impacts inhibitory pathways. Future studies can address these possibilities.

Our findings (within both age-groups) represent a form of pathologically evoked viscerosensory synaptic depression. It is possible that this synaptic plasticity underlies

respiratory system plasticity occurring as a result of LI; increased apnea frequency and H/H ventilatory desensitization have been attributed to changes in brainstem respiratory control (Huang et al., 2005; Kamendi et al., 2009; Herlenius, 2011; Johnson et al., 2017). However, this remains an open question as we did not assess whether the 2nd-order neurons in our study project downstream to respiratory or non-respiratory circuits (Kubin, 2006; King et al., 2012; Dutschmann et al., 2014; McDougall et al., 2017). Further, the presence LTD-like changes is consistent with a Hebbian rather than homeostatic synaptic plasticity mechanism (Pozo and Goda, 2010). However, the apparent lack of specificity for LI-dependent viscerosensory pathway depression suggests a non-Hebbian mechanism (Naka et al., 2013; Clark et al., 2015). This form of plasticity has been reported in spinal nociceptive pathways that exhibit primary hyperalgesia following injury, which can spread to nearby non-stimulated pathways and promote secondary hyperalgesia (Sandkuhler, 2009; Naka et al., 2013; Kronschlager et al., 2016). The mechanism governing this form of non-Hebbian plasticity involves IL-1β release by microglia (Clark et al., 2015). In the nTS, exogenous IL-1β application *in vitro* depresses the amplitude of TS-evoked transmission to 2nd-order neurons without apparent specificity for viscerosensory pathways (Marty et al., 2008). Thus, it is possible that IL-1β upregulation following LI may promote a form of non-Hebbian plasticity in the nTS.

The primary aim of the current study was to investigate LI-evoked synaptic efficacy changes within a window of respiratory vulnerability. Post-TP-LI results were included simply as evidence for a switch in synaptic plasticity mechanisms during the TP. Thus, experiments involving minocycline treatment in post-TP-LI rat-pups were not undertaken. Developmental regulation of microglia/macrophage-mediated synaptic mechanisms is an important but separate question. Future studies will examine microglial-dependent mechanisms throughout development.

4.8. Conclusions

We identified that the timing of LI relative to a TP for the neural control of respiratory function results in a switch in the mechanisms governing the plasticity of TS➔nTS synapses. This conclusion is supported by a shift from post- to pre-synaptic mechanisms underlying the loss of synaptic efficacy when LI is induced before versus after the TP. These findings suggest P11–15 is a TP for TS➔nTS plasticity as well. Further, our data support a novel role for microglia/macrophages in mediating a synaptic LTD-like mechanism that augments the contribution of CI-AMPARs to early life respiratory insults. Future studies will address whether these LI-induced neuroimmune-related changes in synaptic plasticity represent a pathophysiological event or a physiological adaptation.

Acknowledgments

The authors thank the School of Medicine Light Microscopy Imaging Core at Case Western Reserve University for their technical support. The authors also thank Didi Mamaligas, Christopher Ford and Shyue-An Chan for support with experimental design, data analysis and manuscript editing.

Funding: This work was supported by grants from the National Institutes of Health T32 HL007913 (D.G.L.) and by Award Number IO1BX000873 from the Biomedical Laboratory Research & Development Service of the VA Office of Research and Development (F.J.J.).

Abbreviations

nTS	nucleus tractus solitarii
TS	tractus solitarii
EPSC	excitatory post synaptic current
TS-eEPSC	TS-evoked EPSC
GluA2	$GluR_2$-containing AMPA receptors
AMPAR	α-amino-3-hydroxy-5-methyl-4-isoxazolepropionic acid receptor
CI-AMPARs	Ca^{2+}-impermeable AMPA receptors
CP-AMPARs	Ca^{2+}-permeable AMPARs
Bleo	Bleomycin
LI	lung injury
pre-TP LI	lung injury induced before transition period
post-TP LI	lung injury induced after transition period
IT	intratracheal
IP	intraperitoneal
S+S	Saline IT + saline IP
S+M	saline IT+ minocycline IP
B+S	Bleomycin IT + saline IP
B+M	Bleomycin IT + minocycline IP
NASPM	1-Naphthyl-acetyl-spermine-trihydrochloride
NMDAR	N-Methyl-D-Aspartate Receptors
IL-1β	Interleukin 1 beta
BEP	branch end points
aCSF	artificial cerebrospinal fluid
TP	transition period
BALF	bronchial alveolar lavage fluid
PBST	phosphate buffered saline + triton-x
CNS	central nervous system

BEP	branch endpoints
RI	rectification index
AP	area postrema
DMNX	dorsal motor nucleus of the vagus
Gr	gracile nucleus
LTD	long term depression
LTP	long term potentiation
PPR	paired-pulse ratio

References

Accorsi-Mendonca D, Almado CEL, Bonagamba LGH, Castania JA, Moraes DJA, Machado BH. Enhanced Firing in NTS Induced by Short-Term Sustained Hypoxia Is Modulated by Glia-Neuron Interaction. J Neurosci. 2015; 35:6903–6917. [PubMed: 25926465]

Adesnik H, Nicoll RA. Conservation of Glutamate Receptor 2-Containing AMPA Receptors during Long-Term Potentiation. J Neurosci. 2007; 27:4598–4602. [PubMed: 17460072]

Aicher SA, Sharma S, Mitchell JL. Structural changes in AMPA-receptive neurons in the nucleus of the solitary tract of spontaneously hypertensive rats. Hypertension. 2003; 41:1246–1252. [PubMed: 12695422]

Allen C, Stevens CF. An evaluation of causes for unreliability of synaptic transmission. Proc Natl Acad Sci U S A. 1994; 91:10380–10383. [PubMed: 7937958]

Almado CEL, Machado BH, Leão RM. Chronic intermittent hypoxia depresses afferent neurotransmission in NTS neurons by a reduction in the number of active synapses. J Neurosci. 2012a; 32:16736–16746. [PubMed: 23175827]

Almado CEL, Machado BH, Leão RM. Chronic intermittent hypoxia depresses afferent neurotransmission in NTS neurons by a reduction in the number of active synapses. J Neurosci. 2012b; 32:16736–16746. [PubMed: 23175827]

Arganda-Carreras I, Fernández-González R, Muñoz-Barrutia A, Ortiz-De-Solorzano C. 3D reconstruction of histological sections: Application to mammary gland tissue. Microsc Res Tech. 2010; 73:1019–1029. [PubMed: 20232465]

Babin AL, Cannet C, Gérard C, Wyss D, Page CP, Beckmann N. Noninvasive assessment of bleomycin-induced lung injury and the effects of short-term glucocorticosteroid treatment in rats using MRI. J Magn Reson Imaging. 2011; 33:603–614. [PubMed: 21563244]

Bailey TW, Hermes SM, Andresen MC, Aicher SA. Cranial visceral afferent pathways through the nucleus of the solitary tract to caudal ventrolateral medulla or paraventricular hypothalamus: target-specific synaptic reliability and convergence patterns. J Neurosci. 2006; 26:11893–11902. [PubMed: 17108163]

Balland B, Lachamp P, Kessler J-P, Tell F. Silent synapses in developing rat nucleus tractus solitarii have AMPA receptors. J Neurosci. 2008; 28:4624–4634. [PubMed: 18448639]

Balland B, Lachamp P, Strube C, Kessler J-P, Tell F. Glutamatergic synapses in the rat nucleus tractus solitarii develop by direct insertion of calcium-impermeable AMPA receptors and without activation of NMDA receptors. J Physiol. 2006; 574:245–261. [PubMed: 16690712]

Bavis RW, MacFarlane PM. Developmental plasticity in the neural control of breathing. Exp Neurol. 2017; 287:176–191. [PubMed: 27246998]

Bellone C, Lüscher C. Cocaine triggered AMPA receptor redistribution is reversed in vivo by mGluR-dependent long-term depression. Nat Neurosci. 2006; 9:636–641. [PubMed: 16582902]

Bellone C, Nicoll RA. Rapid Bidirectional Switching of Synaptic NMDA Receptors. 2007:779–785.

Berardi N, Pizzorusso T, Maffei L. Critical periods during sensory development. Curr Opin Neurobiol. 2000; 10:138–145. [PubMed: 10679428]

Berger AJ, Dick TE. Connectivity of slowly adapting pulmonary stretch receptors with dorsal medullary respiratory neurons. J Neurophysiol. 1987; 58:1259–1274. [PubMed: 3437333]

Borzone G, Moreno R, Urrea R, Meneses M, Oyarzún M, Lisboa C. Bleomycin-induced chronic lung damage does not resemble human idiopathic pulmonary fibrosis. Am J Respir Crit Care Med. 2001; 163:1648–1653. [PubMed: 11401889]

Bowie D, Mayer ML. Inward rectification of both AMPA and kainate subtype glutamate receptors generated by polyamine-mediated ion channel block. Neuron. 1995; 15:453–462. [PubMed: 7646897]

Brill J, Huguenard JR. Sequential Changes in AMPA Receptor Targeting in the Developing Neocortical Excitatory Circuit. J Neurosci. 2008; 28:13918–13928. [PubMed: 19091980]

Buller KM, Carty ML, Reinebrant HE, Wixey JA. Minocycline: A neuroprotective agent for hypoxic-ischemic brain injury in the neonate? J Neurosci Res. 2009; 87:599–608. [PubMed: 18831005]

Carlo WA. Permissive hypercapnia and permissive hypoxemia in neonates. J Perinatol. 2007; 27:S64–S70.

Chater TE, Goda Y. The role of AMPA receptors in postsynaptic mechanisms of synaptic plasticity. Front Cell Neurosci. 2014; 8

Chen C-Y, Bonham AC, Plopper CG, Joad JP. Neuroplasticity in nucleus tractus solitarius neurons after episodic ozone exposure in infant primates. J Appl Physiol. 2003; 94:819–827. [PubMed: 12433861]

Chen C-Y, Horowitz JM, Bonham AC. A presynaptic mechanism contributes to depression of autonomic signal transmission in NTS. Am J Physiol - Hear Circ Physiol. 1999; 277:H1350–H1360.

Chen C-Y, Ling Eh E, Horowitz JM, Bonham AC. Synaptic transmission in nucleus tractus solitarius is depressed by Group II and III but not Group I presynaptic metabotropic glutamate receptors in rats. J Physiol. 2002; 538:773–786. [PubMed: 11826164]

Chen Z, Jalabi W, Hu W, Park H-J, Gale JT, Kidd GJ, Bernatowicz R, Gossman ZC, Chen JT, Dutta R, Trapp BD. Microglial displacement of inhibitory synapses provides neuroprotection in the adult brain. Nat Commun. 2014; 5:4486. [PubMed: 25047355]

Cho IH, Lee MJ, Jang M, Gwak NG, Lee KY, Jung HS. Minocycline markedly reduces acute visceral nociception via inhibiting neuronal ERK phosphorylation. Mol Pain. 2012; 8

Clark AK, Gruber-Schoffnegger D, Drdla-Schutting R, Gerhold KJ, Malcangio M, Sandkühler J. Selective activation of microglia facilitates synaptic strength. J Neurosci. 2015; 35:4552–4570. [PubMed: 25788673]

Clark CG, Hasser EM, Kunze DL, Katz DM, Kline DD. Endogenous brain-derived neurotrophic factor in the nucleus tractus solitarius tonically regulates synaptic and autonomic function. J Neurosci. 2011; 31:12318–12329. [PubMed: 21865474]

Colovic M, Caccia S. Liquid chromatographic determination of minocycline in brain-to-plasma distribution studies in the rat. J Chromatogr A. 2003; 791:337–343.

Connor AJ, Laskin JD, Laskin DL. Ozone-induced lung injury and sterile inflammation. Role of toll-like receptor 4. Exp Mol Pathol. 2012; 92:229–235. [PubMed: 22300504]

Corlew R, Wang Y, Ghermazien H, Erisir A, Philpot BD. Developmental switch in the contribution of presynaptic and postsynaptic NMDA receptors to long-term depression. J Neurosci. 2007; 27:9835–9845. [PubMed: 17855598]

Crair MC, Malenka RC. A critical period for long-term potentiation at thalamocortical synapses. Nature. 1995; 375:325–328. [PubMed: 7753197]

Cutillo AG, Chan PH, Ailion DC, Watanabe S, Rao NV, Hansen CB, Albertine KH, Laicher G, Durney CH. Characterization of bleomycin lung injury by nuclear magnetic resonance: Correlation between NMR relaxation times and lung water and collagen content. Magn Reson Med. 2002; 47:246–256. [PubMed: 11810667]

Das P, Bell-Horner CL, Machu TK, Dillon GH. The GABAAreceptor antagonist picrotoxin inhibits 5-hydroxytryptamine type 3A receptors. Neuropharmacology. 2003; 44:431–438. [PubMed: 12646280]

Davis SF, Derbenev AV, Williams KW, Glatzer NR, Smith BN. Excitatory and inhibitory local circuit input to the rat dorsal motor nucleus of the vagus originating from the nucleus tractus solitarius. Brain Res. 2004; 1017:208–217. [PubMed: 15261116]

Dean JB, Putnam RW. The caudal solitary complex is a site of central CO2 chemoreception and integration of multiple systems that regulate expired CO2. Respir Physiol Neurobiol. 2010; 173:274–287. [PubMed: 20670695]

Dergacheva O, Dyavanapalli J, Piñol RA, Mendelowitz D. Chronic intermittent hypoxia and hypercapnia inhibit the hypothalamic paraventricular nucleus neurotransmission to parasympathetic cardiac neurons in the brain stem. Hypertension. 2014; 64:597–603. [PubMed: 24958501]

Doyle MW, Andresen MC. Reliability of monosynaptic sensory transmission in brain stem neurons in vitro. J Neurophysiol. 2001; 85:2213–2223. [PubMed: 11353036]

Doyle MW, Bailey TW, Jin YH, Appleyard SM, Low MJ, Andresen MC. Strategies for cellular identification in nucleus tractus solitarius slices. J Neurosci Methods. 2004; 137:37–48. [PubMed: 15196825]

Dufour A, Tell F, Baude A. Perinatal development of inhibitory synapses in the nucleus tractus solitarii of the rat. Eur J Neurosci. 2010; 32:538–549. [PubMed: 20718854]

Dutschmann M, Bautista TG, Mörschel M, Dick TE. Learning to breathe: Habituation of Hering-Breuer inflation reflex emerges with postnatal brainstem maturation. Respir Physiol Neurobiol. 2014; 195:44–49. [PubMed: 24566392]

Dutschmann M, Mörschel M, Rybak IA, Dick TE. Learning to breathe: control of the inspiratory-expiratory phase transition shifts from sensory- to central-dominated during postnatal development in rats. J Physiol. 2009; 587:4931–4948. [PubMed: 19703965]

Dyavanapalli J, Jameson H, Dergacheva O, Jain V, Alhusayyen M, Mendelowitz D. Chronic intermittent hypoxia-hypercapnia blunts heart rate responses and alters neurotransmission to cardiac vagal neurons. J Physiol. 2014; 592:2799–2811. [PubMed: 24835174]

Erkkila BE, Weiss DS, Wotring VE. Picrotoxin-mediated antagonism of alpha3beta4 and alpha7 acetylcholine receptors. Neuroreport. 2004; 15:1969–1973. [PubMed: 15305147]

Feldman JL, Mitchell GS, Nattie EE. Breathing: rhythmicity, plasticity, chemosensitivity. Annu Rev Neurosci. 2003; 26:239–266. [PubMed: 12598679]

Fernandes LG, Jin YH, Andresen MC. Heterosynaptic crosstalk: GABA-glutamate metabotropic receptors interactively control glutamate release in solitary tract nucleus. Neuroscience. 2011; 174:1–9. [PubMed: 21129447]

Forsythe I, Westbrook GL. Slow Excitatory Postsynaptic Currents Mediated By N-Methyl-D-Aspartate Receptors On Cultured Mouse Central Neurones. J Physiol. 1988:515–533.

Fortin G, Champagnat J. Spontaneous synaptic activities in rat nucleus tractus solitarius neurons in vitro: evidence for re-excitatory processing. Brain Res. 1993; 630:125–135. [PubMed: 7906996]

Fu C, Xue J, Wang R, Chen J, Ma L, Liu Y, Wang X, Guo F, Zhang Y, Zhang X, Wang S. Chemosensitive Phox2b-expressing neurons are crucial for hypercapnic ventilatory response in the nucleus tractus solitarius. J Physiol. 2017:1–36.

Fuller DD, Dougherty BJ, Sandhu MS, Doperalski NJ, Reynolds CR, Hayward LF. Prenatal nicotine exposure alters respiratory long-term facilitation in neonatal rats. Respir Physiol Neurobiol. 2009; 169:333–337. [PubMed: 19818419]

Goehler LE, Erisir A, Gaykema RPA. Neural-immune interface in the rat area postrema. Neuroscience. 2006; 140:1415–1434. [PubMed: 16650942]

Gottschalk WA, Jiang H, Tartaglia N, Feng L, Figurov A, Lu B. Signaling mechanisms mediating BDNF modulation of synaptic plasticity in the hippocampus. Learn Mem. 1999; 6:243–256. [PubMed: 10492006]

Gross PM, Wall KM, Pang JJ, Shaver SW, Wainman DS. Microvascular specializations promoting rapid interstitial solute dispersion in nucleus tractus solitarius. Am J Physiol. 1990; 259:R1131–R1138. [PubMed: 2260724]

Hall BJ, Ripley B, Ghosh A. NR2B Signaling Regulates the Development of Synaptic AMPA Receptor Current. J Neurosci. 2007; 27:13446–13456. [PubMed: 18057203]

Hattori N, Degen JL, Sisson TH, Liu H, Moore BB, Pandrangi RG, Simon RH, Drew AF. Bleomycin-induced pulmonary fibrosis in fibrinogen-null mice. J Clin Invest. 2000; 106:1341–1350. [PubMed: 11104787]

He Y, Hara H, Núñez G. Mechanism and Regulation of NLRP3 Inflammasome Activation. Trends Biochem Sci. 2016; 41:1012–1021. [PubMed: 27669650]

Hellwig S, Brioschi S, Dieni S, Frings L, Masuch A, Blank T, Biber K. Altered microglia morphology and higher resilience to stress-induced depression-like behavior in CX3CR1-deficient mice. Brain Behav Immun. 2016; 55:126–137. [PubMed: 26576722]

Henley JM, Wilkinson KA. Synaptic AMPA receptor composition in development, plasticity and disease. Nat Rev Neurosci advance on. 2016:337–350.

Hensch TK. Critical period plasticity in local cortical circuits. Nat Rev Neurosci. 2005; 6:877–888. [PubMed: 16261181]

Herlenius E. An inflammatory pathway to apnea and autonomic dysregulation. Respir Physiol Neurobiol. 2011; 178:449–457. [PubMed: 21762793]

Heynen AJ, Yoon B-J, Liu C-H, Chung HJ, Huganir RL, Bear MF. Molecular mechanism for loss of visual cortical responsiveness following brief monocular deprivation. Nat Neurosci. 2003; 6:854–862. [PubMed: 12886226]

Hinwood M, Tynan RJ, Charnley JL, Beynon SB, Day TA, Walker FR. Chronic stress induced remodeling of the prefrontal cortex: Structural re-organization of microglia and the inhibitory effect of minocycline. Cereb Cortex. 2013; 23:1784–1797. [PubMed: 22710611]

Ho MT, Pelkey KA, Topolnik L, Petralia RS, Takamiya K, Xia J, Huganir RL, Lacaille J, Mcbain CJ. Developmental Expression of Calcium-Permeable AMPA Receptors Underlies Depolarization-Induced Long-Term Depression at Mossy Fiber – CA3 Pyramid Synapses indicate that the transient participation of CP-AMPARs at young MF – PYR synapses dictates the develop. 2007; 27:11651–11662.

Huang ZG, Wang X, Dergacheva O, Mendelowitz D. Prenatal nicotine exposure recruits an excitatory pathway to brainstem parasympathetic cardioinhibitory neurons during hypoxia/hypercapnia in the rat: Implications for sudden infant death syndrome. Pediatr Res. 2005; 58:562–567. [PubMed: 16148074]

Isaac JTR, Ashby M, McBain CJ. The Role of the GluR2 Subunit in AMPA Receptor Function and Synaptic Plasticity. Neuron. 2007; 54:859–871. [PubMed: 17582328]

Isoo N, Ohno T, Isowaki M, Fukuda S, Murabe N, Mizukami H, Ozawa K, Mishina M, Sakurai M. The decline in synaptic GluN2B and rise in inhibitory neurotransmission determine the end of a critical period. Sci Rep. 2016; 6:34196. [PubMed: 27677249]

Jacono FJ, Mayer CA, Hsieh Y-H, Wilson CG, Dick TE. Lung and brainstem cytokine levels are associated with breathing pattern changes in a rodent model of acute lung injury. Respir Physiol Neurobiol. 2011; 178:429–438. [PubMed: 21569869]

Jacono FJ, Peng Y-J, Nethery D, Faress JA, Lee Z, Kern JA, Prabhakar NR. Acute lung injury augments hypoxic ventilatory response in the absence of systemic hypoxemia. J Appl Physiol. 2006; 101:1795–1802. [PubMed: 16888052]

Jarman E, Jarai G, Egger C, Cannet C, Ge C, Suply T, Micard A, Dunbar A, Tigani B, Beckmann N. Administration of Bleomycin via the Oropharyngeal Aspiration Route Leads to Sustained Lung Fibrosis in Mice and Rats as Quantified by UTE-MRI and Histology. 2013:8.

Jin Y, Bailey TW, Andresen MC. GABA Release onto Second-Order Neurons via Distinctly Segregated Metabotropic Glutamate Receptors. 2004; 24:9332–9340.

Johnson SM, Randhawa KS, Epstein JJ, Gustafson E, Hocker AD, Huxtable AG, Baker TL, Watters JJ. Gestational intermittent hypoxia increases susceptibility to neuroinflammation and alters respiratory motor control in neonatal rats. Respir Physiol Neurobiol. 2017

Kamendi HW, Cheng Q, Dergacheva O, Gorini C, Jameson HS, Wang X, McIntosh JM, Mendelowitz D. Abolishment of Serotonergic Neurotransmission to Cardiac Vagal Neurons During and After Hypoxia and Hypercapnia With Prenatal Nicotine Exposure. J Neurophysiol. 2009; 101:1141–1150. [PubMed: 19091927]

Kaminski N, Allard JD, Pittet JF, Zuo F, Griffiths MJD, Morris D, Huang X, Sheppard D, Heller RA. Global analysis of gene expression in pulmonary fibrosis reveals distinct programs regulating lung inflammation and fibrosis. Proc Natl Acad Sci. 2000; 97:1778–1783. [PubMed: 10677534]

Karperien A, Ahammer H, Jelinek HF. Quantitating the subtleties of microglial morphology with fractal analysis. Front Cell Neurosci. 2013; 7:3. [PubMed: 23386810]

Kerchner GA, Nicoll RA. Silent synapses and the emergence of a postsynaptic mechanism for LTP. Nat Rev Neurosci. 2008; 9:813–825. [PubMed: 18854855]

Kessler J, Baude A. Distribution of AMPA Receptor Subunits GluR1-4 in the Dorsal Vagal Complex of the Rat: A Light and Electron Microscope Immunocytochemical Study. Synapse. 1999; 34:55–67. [PubMed: 10459172]

Khlaifia A, Farah H, Gackiere F, Tell F. Anandamide, cannabinoid type 1 receptor, and NMDA receptor activation mediate non-Hebbian presynaptically expressed long-term depression at the first central synapse for visceral afferent fibers. J Neurosci. 2013; 33:12627–12637. [PubMed: 23904599]

Kiernan EA, Smith SMC, Mitchell GS, Watters JJ. Mechanisms of microglial activation in models of inflammation and hypoxia: Implications for chronic intermittent hypoxia. J Physiol. 2016; 594:1563–1577. [PubMed: 26890698]

King TL, Heesch CM, Clark CG, Kline DD, Hasser EM. Hypoxia activates nucleus tractus solitarii neurons projecting to the paraventricular nucleus of the hypothalamus. Am J Physiol Regul Integr Comp Physiol. 2012; 302:R1219–32. [PubMed: 22403798]

Kline DD. Plasticity in glutamatergic NTS neurotransmission. Respir Physiol Neurobiol. 2008; 164:105–111. [PubMed: 18524694]

Kline DD. Plasticity in Glutamatergic NTS Neurotransmission. 2009; 164:105–111.

Kline DD, Ramirez-Navarro A, Kunze DL. Adaptive depression in synaptic transmission in the nucleus of the solitary tract after in vivo chronic intermittent hypoxia: evidence for homeostatic plasticity. J Neurosci. 2007; 27:4663–4673. [PubMed: 17460079]

Kronschlager MT, Drdla-Schutting R, Gassner M, Honsek SD, Teuchmann HL, Sandkuhler J. Gliogenic LTP spreads widely in nociceptive pathways. Science (80−). 2016; 354:1144–1148.

Kubin L. Central pathways of pulmonary and lower airway vagal afferents. J Appl Physiol. 2006; 101:618–627. [PubMed: 16645192]

Kumar SS, Bacci A, Kharazia V, Huguenard JR. A developmental switch of AMPA receptor subunits in neocortical pyramidal neurons. J Neurosci. 2002; 22:3005–3015. [PubMed: 11943803]

Lachamp P, Balland B, Tell F, Crest M, Kessler JP. Synaptic localization of the glutamate receptor subunit GluR2 in the rat nucleus tractus solitarii. Eur J Neurosci. 2003; 17:892–896. [PubMed: 12603280]

Lalanne T, Oyrer J, Mancino A, Gregor E, Chung A, Huynh L, Burwell S, Maheux J, Farrant M, Sjöström PJ. Synapse-specific expression of calcium-permeable AMPA receptors in neocortical layer 5. J Physiol. 2016; 594:837–861. [PubMed: 26537662]

Lanuza MA, Garcia N, Santafé M, González CM, Alonso I, Nelson PG, Tomàs J. Pre- and postsynaptic maturation of the neuromuscular junction during neonatal synapse elimination depends on protein kinase C. J Neurosci Res. 2002; 67:607–617. [PubMed: 11891773]

Lenth RV. Some practical guidelines for effective sample size determination. Am Stat. 2001; 55:187–193.

Levelt CN, Hubener M. Critical-Period Plasticity in the Visual Cortex. Annu Rev Neurosci. 2012:309–330. [PubMed: 22462544]

Lewitus GM, Konefal SC, Greenhalgh AD, Pribiag H, Augereau K, Stellwagen D. Microglial TNF-alpha Suppresses Cocaine-Induced Plasticity and Behavioral Sensitization. Neuron. 2016; 90:483–491. [PubMed: 27112496]

Li J, Zhang M-M, Tu K, Wang J, Feng B, Zhang Z-N, Lei J, Li Y-Q, Du J-Q, Chen T. The excitatory synaptic transmission of the nucleus of solitary tract was potentiated by chronic myocardial infarction in rats. PLoS One. 2015; 10:e0118827. [PubMed: 25756354]

Li P, Janczewski WA, Yackle K, Kam K, Pagliardini S, Krasnow MA, Feldman JL. The peptidergic control circuit for sighing. Nature. 2016; 530:293–297. [PubMed: 26855425]

Lin HC, Wan FJ, Kang BH, Wu CC, Tseng CJ. Systemic administration of lipopolysaccharide induces release of nitric oxide and glutamate and c-fos expression in the nucleus tractus solitarii of rats. Hypertension. 1999; 33:1218–1224. [PubMed: 10334815]

Litvin D, Dick T, Jacono F. The FASEB Journal. San Diego, CA: 2016. Apr 2-6. Acute Lung Injury Alters Receptor Subunit Density in the Dorsal Vagal Complex. pp Abstract number 988.10

Liu Q, Fehring C, Lowry TF, Wong-Riley MT. Postnatal development of metabolic rate during normoxia and acute hypoxia in rats: implication for a sensitive period. J Appl Physiol. 2009; 106:1212–1222. [PubMed: 19118157]

Liu Q, Wong-Riley MTT. Postnatal developmental expressions of neurotransmitters and receptors in various brain stem nuclei of rats. J Appl Physiol. 2005; 98:1442–1457. [PubMed: 15618314]

Liu Q, Wong-Riley MTT. Postnatal development of N-methyl-d-aspartate receptor subunits 2A, 2B, 2C, 2D, and 3B immunoreactivity in brain stem respiratory nuclei of the rat. Neuroscience. 2010a; 171:637–654. [PubMed: 20887777]

Liu Q, Wong-Riley MTT. Postnatal changes in the expressions of serotonin 1A, 1B, and 2A receptors in ten brain stem nuclei of the rat: implication for a sensitive period. Neuroscience. 2010b; 165:61–78. [PubMed: 19800944]

Liu Q, Wong-Riley MTT. Postnatal development of Na+-K+-2Cl− co-transporter 1 and K+-Cl− co-transporter 2 immunoreactivity in multiple brain stem respiratory nuclei of the rat. Neuroscience. 2012; 210:1–20. [PubMed: 22441038]

Liu Q, Wong-Riley MTT. Postnatal development of glycine receptor subunits α1, α2, α3, and β immunoreactivity in multiple brain stem respiratory-related nuclear groups of the rat. Brain Res. 2013; 1538:1–16. [PubMed: 24080401]

Liu SJ, Cull-Candy SG. Activity-dependent change in AMPA receptor properties in cerebellar stellate cells. J Neurosci. 2002; 22:3881–3889. [PubMed: 12019307]

Liu SQ, Cull-Candy SG. Synaptic activity at calcium-permeable AMPA receptors induces a switch in receptor subtype. Nature. 2000; 405:454–458. [PubMed: 10839540]

Liu Y, Formisano L, Savtchouk I, Takayasu Y, Szabó G, Zukin RS, Liu SJ. A single fear-inducing stimulus induces a transcription-dependent switch in synaptic AMPAR phenotype. Nat Neurosci. 2010; 13:223–231. [PubMed: 20037575]

Lu F-M, Hawkins RD. Presynaptic and postsynaptic Ca(2+) and CamKII contribute to long-term potentiation at synapses between individual CA3 neurons. Proc Natl Acad Sci U S A. 2006; 103:4264–4269. [PubMed: 16537519]

Lüscher C, Malenka RC. NMDA receptor-dependent long-term potentiation and long-term depression (LTP/LTD). Cold Spring Harb Perspect Biol. 2012; 4:1–15.

Malinow R, Tsien RW. Presynaptic enhancement shown by whole-cell recordings of long-term potentiation in hippocampal slices. Nature. 1990; 346:177–180. [PubMed: 2164158]

Mameli M, Balland B, Lujan R, Luscher C. Rapid Synthesis and Synaptic Insertion of GluR2 for mGluR-LTD in the Ventral Tegmental Area. Science (80−). 2007; 317:530–533.

Martin RJ, Miller MJ, Carlo WA. Pathogenesis of apnea in preterm infants. J Pediatr. 1986; 109:733–741. [PubMed: 3095518]

Marty V, El Hachmane M, Amédée T. Dual modulation of synaptic transmission in the nucleus tractus solitarius by prostaglandin E2 synthesized downstream of IL-1beta. Eur J Neurosci. 2008; 27:3132–3150. [PubMed: 18598258]

Matute-Bello G, Frevert CW, Martin TR. Animal models of acute lung injury. Am J Physiol. 2008:379–399.

McDougall SJ, Guo H, Andresen MC. Dedicated C-fibre viscerosensory pathways to central nucleus of the amygdala. J Physiol. 2017; 595:901–917. [PubMed: 27616729]

McDougall SJ, Peters JH, Andresen MC. Convergence of cranial visceral afferents within the solitary tract nucleus. J Neurosci. 2009; 29:12886–12895. [PubMed: 19828803]

Mifflin SW, Felder RB. An intracellular study of time-dependent cardiovascular afferent interactions in nucleus tractus solitarius. J Neurophysiol. 1988; 59:1798–1813. [PubMed: 3404205]

Miyamoto A, Wake H, Ishikawa AW, Eto K, Shibata K, Murakoshi H, Koizumi S, Moorhouse AJ, Yoshimura Y, Nabekura J. Microglia contact induces synapse formation in developing somatosensory cortex. Nat Commun. 2016; 7:12540. [PubMed: 27558646]

Morrison HW, Filosa JA. A quantitative spatiotemporal analysis of microglia morphology during ischemic stroke and reperfusion. J Neuroinflammation. 2013; 10:782.

Naka A, Gruber-Schoffnegger D, Sandk??hler J. Non-Hebbian plasticity at C-fiber synapses in rat spinal cord lamina i neurons. Pain. 2013; 154:1333–1342. [PubMed: 23707311]

Newbern JM, Li X, Shoemaker SE, Zhou J, Zhong J, Wu Y, Bonder D, Hollenback S, Coppola G, Geschwind DH, Landreth GE, Snider WD. Specific Functions for ERK/MAPK Signaling during PNS Development. Neuron. 2011; 69:91–105. [PubMed: 21220101]

Nikodemova M, Duncan ID, Watters JJ. Minocycline exerts inhibitory effects on multiple mitogen-activated protein kinases and IκBα degradation in a stimulus-specific manner in microglia. J Neurochem. 2006; 96:314–323. [PubMed: 16336636]

Nikodemova M, Watters JJ, Jackson SJ, Yang SK, Duncan ID. Minocycline down-regulates MHC II expression in microglia and macrophages through inhibition of IRF-1 and protein kinase C (PKC) α/βII. J Biol Chem. 2007; 282:15208–15216. [PubMed: 17395590]

Ninan I, Arancio O. Presynaptic CaMKII Is Necessary for Synaptic Plasticity in Cultured Hippocampal Neurons. 2004; 42:129–141.

Nosyreva ED, Huber KM. Developmental switch in synaptic mechanisms of hippocampal metabotropic glutamate receptor-dependent long-term depression. J Neurosci. 2005; 25:2992–3001. [PubMed: 15772359]

Park J-S, Voitenko N, Petralia RS, Guan X, Xu J-T, Steinberg JP, Takamiya K, Sotnik A, Kopach O, Huganir RL, Tao Y-X. Persistent inflammation induces GluR2 internalization via NMDA receptor-triggered PKC activation in dorsal horn neurons. J Neurosci. 2009; 29:3206–3219. [PubMed: 19279258]

Physiol JA, August F, Jacono FJ, Peng Y, Nethery D, Faress JA, Lee Z, Kern JA, Prabhakar NR. Acute lung injury augments hypoxic ventilatory response in the absence of systemic hypoxemia Acute lung injury augments hypoxic ventilatory response in the absence of systemic hypoxemia. 2013; 44106:1795–1802.

Poon C, Zhou Z, Champagnat J. NMDA Receptor Activity In Utero Averts Respiratory Depression and Anomalous Long-Term Depression in Newborn Mice. 2000; 20:1–6.

Pozo K, Goda Y. Unraveling mechanisms of homeostatic synaptic plasticity. Neuron. 2010; 66:337–351. [PubMed: 20471348]

Pribilla I, Takagi T, Langosch D, Bormann J, Betz H. The atypical M2 segment of the beta subunit confers picrotoxinin resistance to inhibitory glycine receptor channels. EMBO J. 1992; 11:4305–4311. [PubMed: 1385113]

Ragaller M, Richter T. Acute lung injury and acute respiratory distress syndrome. J Emerg Trauma Shock. 2010; 3:43. [PubMed: 20165721]

Ramirez JM, Garcia AJ, Anderson TM, Koschnitzky JE, Peng YJ, Kumar GK, Prabhakar NR. Central and peripheral factors contributing to obstructive sleep apneas. Respir Physiol Neurobiol. 2013; 189:344–353. [PubMed: 23770311]

Razavi-Azarkhiavi K, Ali-Omrani M, Solgi R, Bagheri P, Haji-Noormohammadi M, Amani N, Sepand M. Silymarin alleviates bleomycin-induced pulmonary toxicity and lipid peroxidation in mice. Pharm Biol. 2014; 52:1267–1271. [PubMed: 25026360]

Ren K, Dubner R. Interactions between the immune and nervous systems in pain. Nat Med. 2010; 16:1267–1276. [PubMed: 20948535]

Reuter S. Respiratory distress in the newborn patient. Paediatr Rev. 2014; 35:59–64. Sanford S of M.

Riazi K, Galic MA, Kentner AC, Reid AY, Sharkey KA, Pittman QJ. Microglia-Dependent Alteration of Glutamatergic Synaptic Transmission and Plasticity in the Hippocampus during Peripheral Inflammation. J Neurosci. 2015; 35:4942–4952. [PubMed: 25810524]

Riazi K, Galic MA, Kuzmiski JB, Ho W, Sharkey KA, Pittman QJ. Microglial activation and TNFalpha production mediate altered CNS excitability following peripheral inflammation. Proc Natl Acad Sci U S A. 2008; 105:17151–17156. [PubMed: 18955701]

Riquier AJ, Sollars SI. Microglia density decreases in the rat rostral nucleus of the solitary tract across development and increases in an age-dependent manner following denervation. Neuroscience. 2017; 355:36–48. [PubMed: 28478126]

Roberts AC, Díez-García J, Rodriguiz RM, López IP, Luján R, Martínez-Turrillas R, Picó E, Henson MA, Bernardo DR, Jarrett TM, Clendeninn DJ, López-Mascaraque L, Feng G, Lo DC, Wesseling JF, Wetsel WC, Philpot BD, Pérez-Otaño I. Downregulation of NR3A-Containing NMDARs Is Required for Synapse Maturation and Memory Consolidation. Neuron. 2009; 63:342–356. [PubMed: 19679074]

Rogers RC, Hermann GE. Tumor Necrosis Factor Activation of Vagal Afferent Terminal Calcium Is Blocked by Cannabinoids. J Neurosci. 2012; 32:5237–5241. [PubMed: 22496569]

Roumier A, Pascual O, Bechade C, Wakselman S, Poncer JC, Real E, Triller A, Bessis A. Prenatal activation of microglia induces delayed impairment of glutamatergic synaptic function. PLoS One. 2008; 3

Sandkuhler J. Models and Mechanisms of Hyperalgesia and Allodynia. Physiol Rev. 2009; 89:707–758. [PubMed: 19342617]

Sara Y, Bal M, Adachi M, Monteggia LM, Kavalali ET. Use-Dependent AMPA Receptor Block Reveals Segregation of Spontaneous and Evoked Glutamatergic Neurotransmission. J Neurosci. 2011; 31:5378–5382. [PubMed: 21471372]

Savani RC, et al. Respiratory distress after intratracheal bleomycin: selective deficiency of surfactant proteins B and C. 2001:4399.

Schafer DP, Lehrman EK, Kautzman AG, Koyama R, Mardinly AR, Yamasaki R, Ransohoff RM, Greenberg ME, Barres BA, Stevens B. Microglia Sculpt Postnatal Neural Circuits in an Activity and Complement-Dependent Manner. Neuron. 2012; 74:691–705. [PubMed: 22632727]

Schindelin J, Arganda-Carreras I, Frise E, Kaynig V, Longair M, Pietzsch T, Preibisch S, Rueden C, Saalfeld S, Schmid B, Tinevez J-Y, White DJ, Hartenstein V, Eliceiri K, Tomancak P, Cardona A. Fiji: an open-source platform for biological-image analysis. Nat Methods. 2012; 9:676–682. [PubMed: 22743772]

Schwartz DR, Homanics GE, Hoyt DG, Klein E, Abernethy J, Lazo JS. The neutral cysteine protease bleomycin hydrolase is essential for epidermal integrity and bleomycin resistance. Proc Natl Acad Sci. 1999; 96:4680–4685. [PubMed: 10200322]

Sekizawa SI, Chen CY, Bechtold AG, Tabor JM, Bric JM, Pinkerton KE, Joad JP, Bonham AC. Extended secondhand tobacco smoke exposure induces plasticity in nucleus tractus solitarius second-order lung afferent neurons in young guinea pigs. Eur J Neurosci. 2008a; 28:771–781. [PubMed: 18657181]

Sekizawa SI, Chen CY, Bechtold AG, Tabor JM, Bric JM, Pinkerton KE, Joad JP, Bonham AC. Extended secondhand tobacco smoke exposure induces plasticity in nucleus tractus solitarius second-order lung afferent neurons in young guinea pigs. Eur J Neurosci. 2008b; 28:771–781. [PubMed: 18657181]

Sen A, Hongpaisan J, Wang D, Nelson TJ, Alkon DL. Protein Kinase Cε (PKCε) promotes synaptogenesis through membrane accumulation of the postsynaptic density protein PSD-95. J Biol Chem. 2016; 291:16462–16476. [PubMed: 27330081]

Sipe GO, Lowery RL, Tremblay M-È, Kelly EA, Lamantia CE, Majewska AK. Microglial P2Y12 is necessary for synaptic plasticity in mouse visual cortex. Nat Commun. 2016; 7:10905. [PubMed: 26948129]

Skurikhin EG, Pershina OV, Reztsova AM, Ermakova NN, Khmelevskaya ES, Krupin VA, Stepanova IE, Artamonov AV, Bekarev AA, Madonov PG, Dygai AM. Modulation of bleomycin-induced lung fibrosis by pegylated Hyaluronidase and dopamine receptor antagonist in mice. PLoS One. 2015; 10:1–24.

Smith S, Doig A, Dudley W. Impaired parasympathetic response to feeding in ventilated preterm babies. Arch Dis Child Fetal Neonatal Ed. 2005; 90:F505–F508. [PubMed: 15941824]

Smith DV, Uteshev VV. Heterogeneity of nicotinic acetylcholine receptor expression in the caudal nucleus of the solitary tract. Neuropharmacology. 2008; 54:445–453. [PubMed: 18078963]

Sollars SI. Chorda tympani nerve transection at different developmental ages produces differential effects on taste bud volume and papillae morphology in the rat. J Neurobiol. 2005; 64:310–320. [PubMed: 15898061]

Soto D, Coombs ID, Kelly L, Farrant M, Cull-Candy SG. Stargazin attenuates intracellular polyamine block of calcium-permeable AMPA receptors. Nat Neurosci. 2007; 10:1260–1267. [PubMed: 17873873]

Soto D, Coombs ID, Renzi M, Zonouzi M, Farrant M, Cull-Candy SG. Selective regulation of long-form calcium-permeable AMPA receptors by an atypical TARP, γ-5. Nat Neurosci. 2009; 12:277–285. [PubMed: 19234459]

Stokes JA, Arbogast TE, Moya EA, Fu Z, Powell FL. Minocycline blocks glial cell activation and ventilatory acclimatization to hypoxia. J Neurophysiol:jn. 2017; 2016:00525.

Streit WJ, Walter SA, Pennell NA. Reactive microgliosis. Prog Neurobiol. 1999; 57:563–581. [PubMed: 10221782]

Stumm S. Respiratory Distress Syndrome Degrades the Fine Structure of the Non-Nutritive Suck In Preterm Infants Susan. J Neonatal Nurs Neonatal Nurs. 2008; 14:9–16. University of K.

Sugawara T, Hisatsune C, Miyamoto H, Ogawa N, Mikoshiba K. Regulation of spinogenesis in mature Purkinje cells via mGluR/PKC-mediated phosphorylation of CaMKIIβ. Proc Natl Acad Sci. 2017 201617270.

Sullivan SJ, Farrant M, Cull-Candy SG. TARP y-2 Is Required for Inflammation-Associated AMPA Receptor Plasticity within Lamina II of the Spinal Cord Dorsal Horn. J Neurosci. 2017; 37:6007–6020. [PubMed: 28559374]

Szalay G, Martinecz B, Lénárt N, Környei Z, Orsolits B, Judák L, Császár E, Fekete R, West BL, Katona G, Rózsa B, Dénes Á. Microglia protect against brain injury and their selective elimination dysregulates neuronal network activity after stroke. Nat Commun. 2016; 7

Teran FA, Massey CA, Richerson GB. Serotonin neurons and central respiratory chemoreception: Where are we now? Prog Brain Res. 2014; 209:207–233. [PubMed: 24746050]

Thibault K, Lin WK, Rancillac A, Fan M, Snollaerts T, Sordoillet V, Hamon M, Smith GM, Lenkei Z, Pezet S. BDNF-Dependent Plasticity Induced by Peripheral Inflammation in the Primary Sensory and the Cingulate Cortex Triggers Cold Allodynia and Reveals a Major Role for Endogenous BDNF As a Tuner of the Affective Aspect of Pain. J Neurosci. 2014; 34:14739–14751. [PubMed: 25355226]

Tsukamoto K, Sved AF. Enhanced gamma-Aminobutyric Acid-Mediated Responses in Nucleus Tractus Solitarius of Hypertensive Rats. Hypertension. 1993; 22:819–825. [PubMed: 7902334]

Turner SMF, Johnson SM. Abrupt changes in pentobarbital sensitivity in preBötzinger complex region, hypoglossal motor nucleus, nucleus tractus solitarius, and cortex during rat transitional period (P10-P15). Respir Physiol Neurobiol. 2015; 207:61–71. [PubMed: 25550216]

Tyzio R, Holmes GL, Ben-Ari Y, Khazipov R. Timing of the developmental switch in GABAA mediated signaling from excitation to inhibition in CA3 rat hippocampus using gramicidin perforated patch and extracellular recordings. Epilepsia. 2007:96–105.

Vadász I, Sznajder JI. Gas exchange disturbances regulate alveolar fluid clearance during acute lung injury. Front Immunol. 2017; 8

Vitkovic L, Konsman JP, Bockaert J, Dantzer R, Homburger V, Jacque C. Cytokine signals propagate through the brain. Mol Psychiatry. 2000; 5:604–615. [PubMed: 11126391]

Wang P, Slaughter MM. Effects of GABA receptor antagonists on retinal glycine receptors and on homomeric glycine receptor alpha subunits. J Neurophysiol. 2005; 93:3120–3126. [PubMed: 15728760]

Warren JB, et al. Newborn respiratory disorders. Pediatr Rev. 2010; 31:487–95. quiz 496. [PubMed: 21123510]

Wong-Riley MTT, Liu Q. Neurochemical and physiological correlates of a critical period of respiratory development in the rat. Respir Physiol Neurobiol. 2008; 164:28–37. [PubMed: 18524695]

Xu J, Mora AL, LaVoy J, Brigham KL, Rojas M. Increased bleomycin-induced lung injury in mice deficient in the transcription factor T-bet. Am J Physiol Lung Cell Mol Physiol. 2006; 291:L658–67. [PubMed: 16648243]

Yashiro K, Philpot BD. Regulation of NMDA receptor subunit expression and its implications for LTD, LTP, and metaplasticity. Neuropharmacology. 2008; 55:1081–1094. [PubMed: 18755202]

Yrjänheikki J, Tikka T, Keinänen R, Goldsteins G, Chan PH, Koistinaho J. A tetracycline derivative, minocycline, reduces inflammation and protects against focal cerebral ischemia with a wide therapeutic window. Proc Natl Acad Sci. 1999; 96:13496–13500. [PubMed: 10557349]

Zhang J, Malik A, Choi HB, Ko RWY, Dissing-Olesen L, MacVicar BA. Microglial CR3 activation triggers long-term synaptic depression in the hippocampus via NADPH oxidase. Neuron. 2014; 82:195–207. [PubMed: 24631344]

Zhang W, Carren FR, Cunningham JT, Mifflin SW. Chronic sustained hypoxia enhances both evoked EPSCs and norepinephrine inhibition of glutamatergic afferent inputs in the nucleus of the solitary tract. J Neurosci. 2009a; 29:3093–3102. [PubMed: 19279246]

Zhang W, Carreño FR, Cunningham JT, Mifflin SW. Chronic sustained and intermittent hypoxia reduce function of ATP-sensitive potassium channels in nucleus of the solitary tract. Am J Physiol Regul Integr Comp Physiol. 2008; 295:R1555–R1562. [PubMed: 18784334]

Zhang W, Carreño FR, Cunningham JT, Mifflin SW. Chronic sustained hypoxia enhances both evoked EPSCs and norepinephrine inhibition of glutamatergic afferent inputs in the nucleus of the solitary tract. J Neurosci. 2009b; 29:3093–3102. [PubMed: 19279246]

Zhao H, Peters JH, Zhu M, Page SJ, Ritter RC, Appleyard SM. Frequency-dependent facilitation of synaptic throughput via postsynaptic NMDA receptors in the nucleus of the solitary tract. J Physiol. 2015; 593:111–125. [PubMed: 25281729]

Zhou Z, Champagnat J, Poon CS. Phasic and long-term depression in brainstem nucleus tractus solitarius neurons: differing roles of AMPA receptor desensitization. J Neurosci. 1997; 17:5349–5356. [PubMed: 9204919]

Highlights

- Lung injury (LI) decreases synaptic efficacy and evokes inflammation in the nTS.
- Mechanisms decreasing glutamatergic synaptic efficacy depend on maturation.
- In P9–11 rats, LI causes microglia to *hyper*-ramify and *post*-synaptic depression.
- Minocycline treatment prevents *hyper*-ramification and synaptic depression.
- In P17–19 rats, LI evokes microglia to *hypo*-ramify and *pre*-synaptic depression.

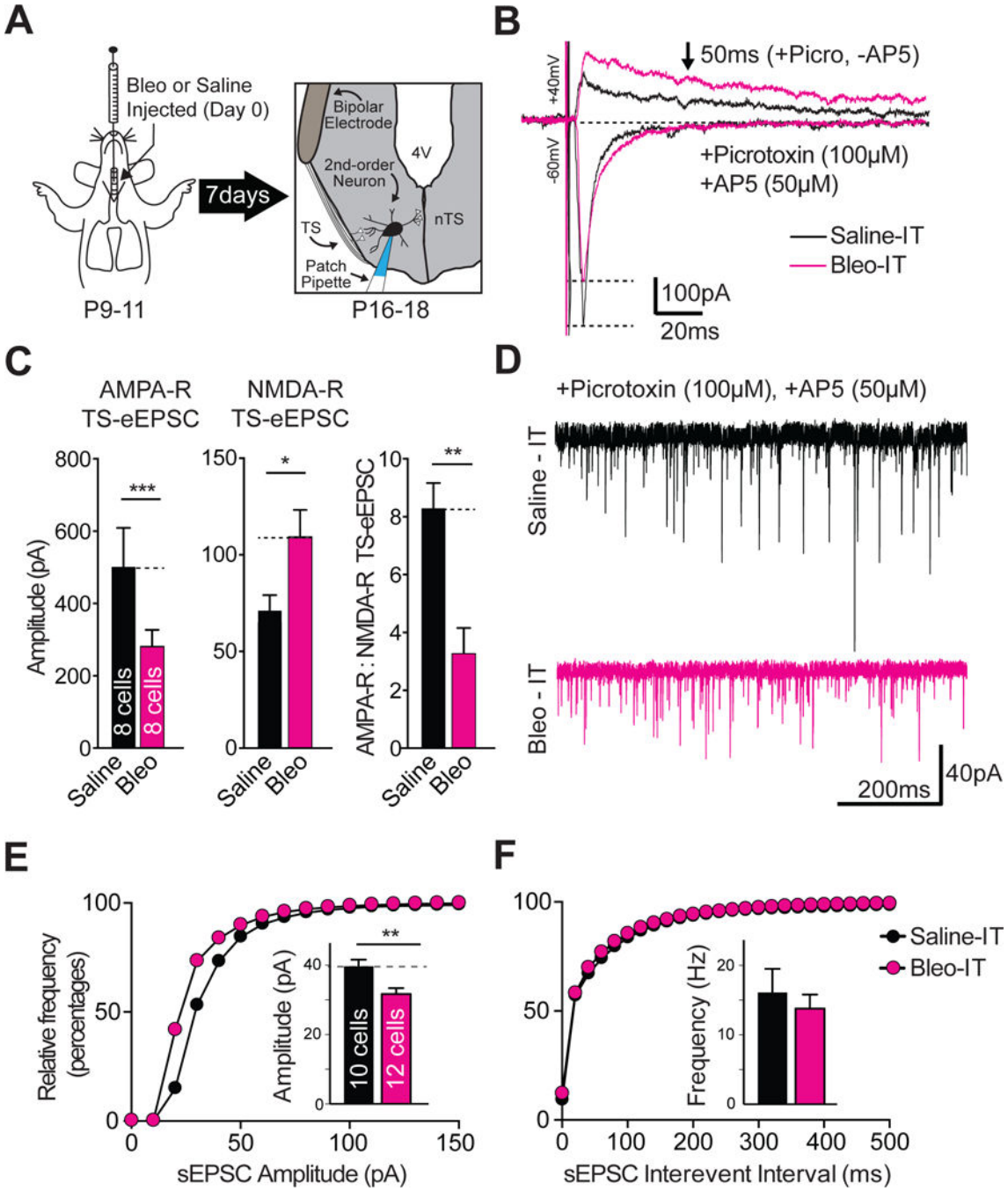

Figure 1.

Lung injury in pre-transition period rats-pups depresses the amplitude of spontaneous and evoked excitatory postsynaptic currents (sEPSCs and eEPSCs), but not the frequency of sEPSCs recorded from neurons located in the nucleus Tractus Solitarii (nTS) that receive monosynaptic input from the Tractus Solitarii (TS➔nTS synapses).

A Protocol. Neonatal rats (P9–11) received Bleomycin (Bleo) or saline intratracheally, recovered and were euthanized 7-days later for electrophysiological recordings from nTS

neurons in a horizontal brainstem slice that retained TS-fibers; which were stimulated using a bipolar electrode.

B Representative raw recordings showing TS-evoked (TS-e) AMPAR and NMDAR components of TS-eEPSCs from a Bleo-treated (magenta) and saline-treated rat (black). The NMDAR component of TS-eEPSCs was recorded at +40 mV in the presence of Picrotoxin (100 μM), and was considered NMDAR-dependent at 50 ms from the stimulus artifact. The AMPAR component of TS-evoked currents was recorded at −60 mV in the presence of Picrotoxin and AP5 (50 μM). All TS-evoked currents were recorded with a cesium based intrapipette solution containing spermine (0.1 μM) and QX-314 (5 μM).

C The mean amplitude of TS-eEPSCs recorded at −60 mV (AMPAR-dependent) was significantly reduced in the Bleo-treated group (n = 8 cells/slices/rats) compared to the saline-treated group (n = 8 cells/slices/rats, $*P = 0.03$). The amplitude of TS-eEPSCs recorded at +40 mV (NMDAR-dependent) was significantly increased in Bleo-treated rats compared to saline-treated rats ($*P = 0.018$). The AMPAR/NMDAR ratio in Bleo-treated rats was significantly reduced ($**P = 0.002$, Two-tail t-Test.). Graphs presented as mean ± SEM.

D Representative raw sEPSC traces recorded 7-days following intratracheal Bleo (magenta) or saline (black) instillation made from nTS neurons receiving monosynaptic TS-input.

E Cumulative probability graph for amplitudes of sEPSC recorded from Bleo-treated (magenta, n = 12 cells, 11 slices, 11 rats) and saline-treated (black, 10 cells/slices/rats) rats. The Bleo-treated group was shifted to the left from the saline treated group. Inset: The mean of means for the sEPSC amplitude was reduced in Bleo compared to saline treated rats ($**P = 0.006$, Two-tail t-Test).

F The cumulative probability graph of interevent-intervals overlapped and (inset) the mean of means for the frequency of sEPSCs was not significantly different for Bleo-treated and saline-treated (black) treated rats ($P = 0.56$, Two-tail t-Test).

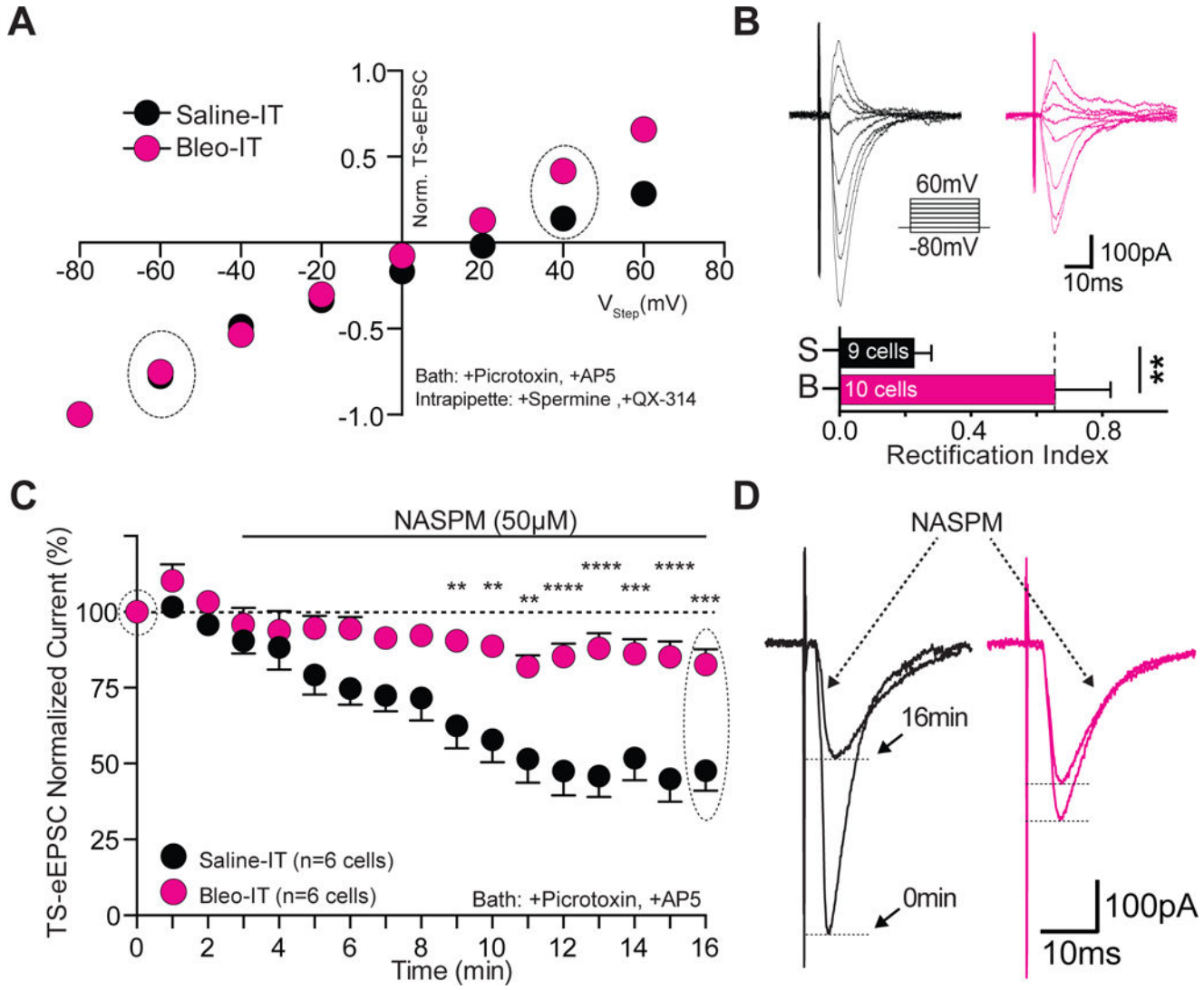

Figure 2.

Lung injury in pre-transition period rats-pups increases the contribution of Ca^{2+}-impermeable AMPA Receptors at TS➔nTS synapses.

A Current-voltage plots for TS-eEPSCs recorded from Bleo-treated (magenta, n = 10 cells/slices/rats) and saline-treated (black, n = 9 cells/slices/rats) rats. Rectification was assessed in the presence of bath applied Picrotoxin (100 μM) and *DL*-AP5 (50 μM), and with a cesium based intrapipette solution containing spermine (0.1 μM) and QX-314 (5 μM). TS-eEPSCs were normalized to responses at −80 mV. The rectifying current was less in the Bleo-treated compared to saline-treated rats.

B top: raw representative traces of TS-eEPSCs recorded from Bleo-treated and saline-treated rats at holding potentials ranging from −80 to +60 mV. bottom: The rectification index; defined as the ratio of TS-eEPSC at +40 to that at −60 mV, was greater in Bleo-treated than saline-treated rats (** $P = 0.008$, unpaired two-tail t-test).

C Average normalized amplitude of TS-eEPSCs from Bleo-treated (n = 6 cells/slices/rats) and saline-treated (n = 6 cells/slices/rats) rats at baseline (0-3 min) and for 13 min after bath

application of NASPM (at 3 min), an antagonist of Ca^{2+}-permeable AMPARs. NASPM-dependent depression was evident in the TS-eEPSCs from saline-treated rats and was significantly reduced in Bleo-treated rats ($P < 0.0001$, Two-way ANOVA with Bonferroni correction).

D Representative raw recordings of TS-eEPSCs from saline-treated and Bleo-treated rats at 0 min and 16 min (13 min after NASPM application).

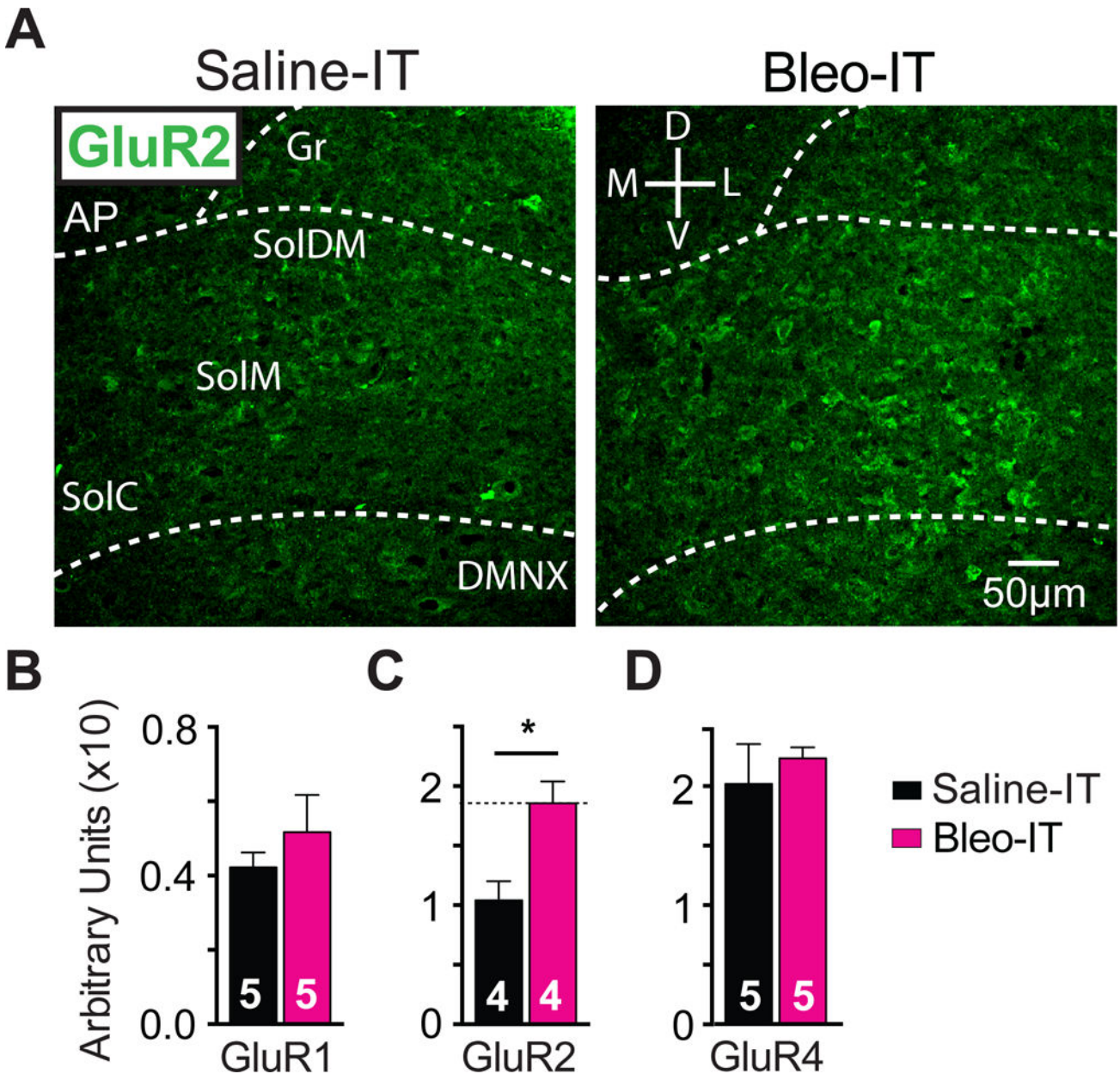

Figure 3.

Lung injury in pre-transition period rats-pups augments $GluR_2$-containing AMPA receptor (GluA2) expression in the nTS

A Representative images of coronal brainstem sections from saline-treated (black) and Bleo-treated (magenta) groups showing immunohistochemical staining that is GluA2+ in commissural (SolC), medial (SolM) and dorsomedial (SolDM) subnuclei of the nTS.

B GluA1+ staining in the nTS was not significantly different in Bleo-treated (n = 5) and saline-treated (n = 5) rats ($P = 0.40$, Two-tail t-Test).

C GluA2+ staining in the nTS was significantly greater in Bleo-treated (n=4), than of saline-treated rats (n=4, $*P = 0.016$, Two-tail t-Test).

D GluA4+ staining in the nTS was not significantly different in Bleo-treated (n=5) and saline-treated (n = 5) rats ($P = 0.55$, Two-tail t-Test)

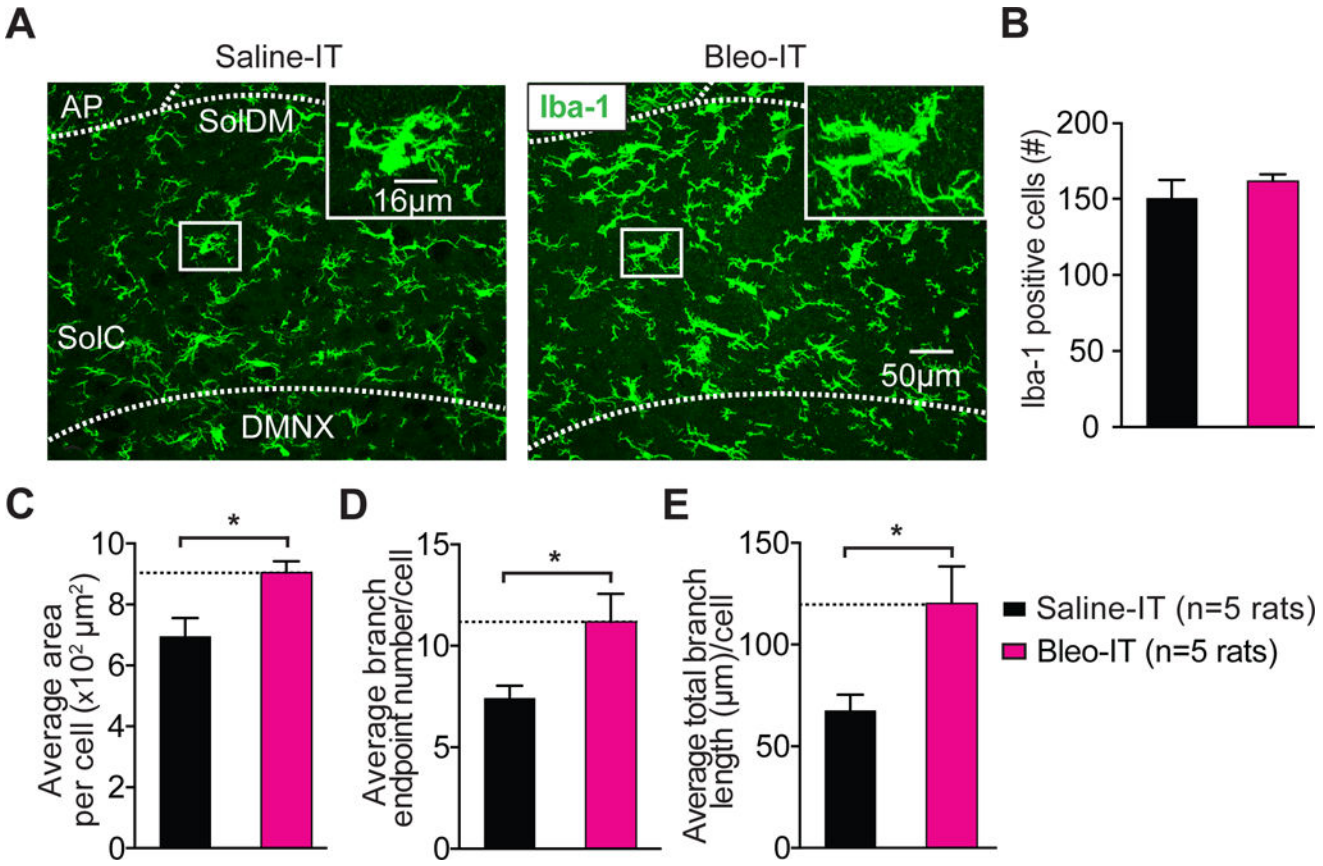

Figure 4.

Lung injury in pre-transition period rats-pups promotes *hyper*-ramification of Iba-1+ microglia in the nTS and IL-1β/pro-IL-1β production throughout the dorsomedial brainstem.

A Representative images of coronal brainstem sections from saline-treated (black) and Bleo-treated (magenta) groups (7-days after injury) showing immunohistochemical staining for Iba-1+ cells (microglia) in the commissural (SolC), and dorsomedial (SolDM) subnuclei of the nTS. Inset: magnified images showing microglia localized to a medial region of the nTS.

B The number of microglia in the nTS was not significantly different in Bleo-treated (n = 5) or saline-treated (n = 5) rats ($P = 0.411$, Mean ± SEM, Two-tail t-Test).

C The area of individual microglia from Bleo-treated rats was greater than that of saline-treated rats (*$P = 0.018$, Two-tail t-Test).

D The number of branch endpoints per microglia increased in Bleo-treated compared to saline-treated rats (*$P = 0.038$, Two-tail t-Test).

E The total branch length per microglia increased in Bleo-treated compared to saline-treated rats (*$P = 0.03$, Two-tail t-Test).

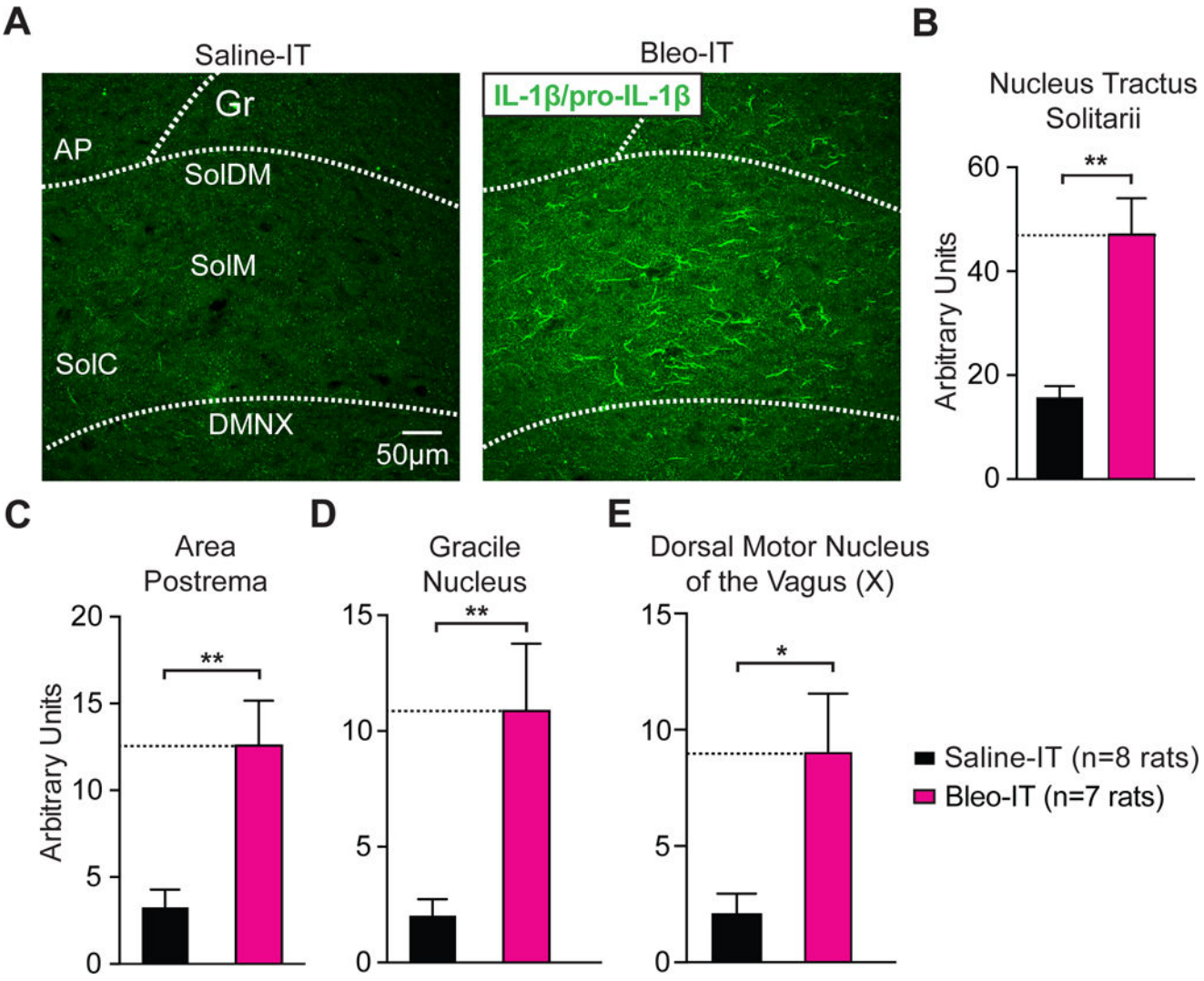

Figure 5.

Lung injury in pre-transition period rats-pups promotes IL-1β/pro-IL-1β production throughout the dorsomedial brainstem.

A Representative images of coronal brainstem sections from saline and Bleo-treated groups that show immunohistochemical staining with an antibody that shows specificity for interleukin 1 beta and its pro-peptide (IL-1β/pro-IL-1β) throughout the nTS.

B Bleo-treated rats (n = 7) exhibited a significant increase in IL-1β/pro-IL-1β immunoreactivity throughout the nTS when compared to saline-treated rats (n = 8, $^{**}P = 0.0022$, Two-tail T-test).

C Bleo-treated rats exhibited a significant increase in IL-1β/pro-IL-1β immunoreactivity in the area postrema (AP) compared to saline-treated rats ($^{**}P = 0.0032$).

D Bleo-treated rats exhibited a significant increase in IL-1β/pro-IL-1β immunoreactivity in the gracile nucleus (Gr) compared to saline-treated rats ($^{**}P = 0.0071$).

E Bleo-treated rats exhibited a significant increase in IL-1β/pro-IL-1β immunoreactivity in the dorsal motor nucleus of the vagus (DMNX) compared to saline-treated rats ($^{*}P = 0.0145$).

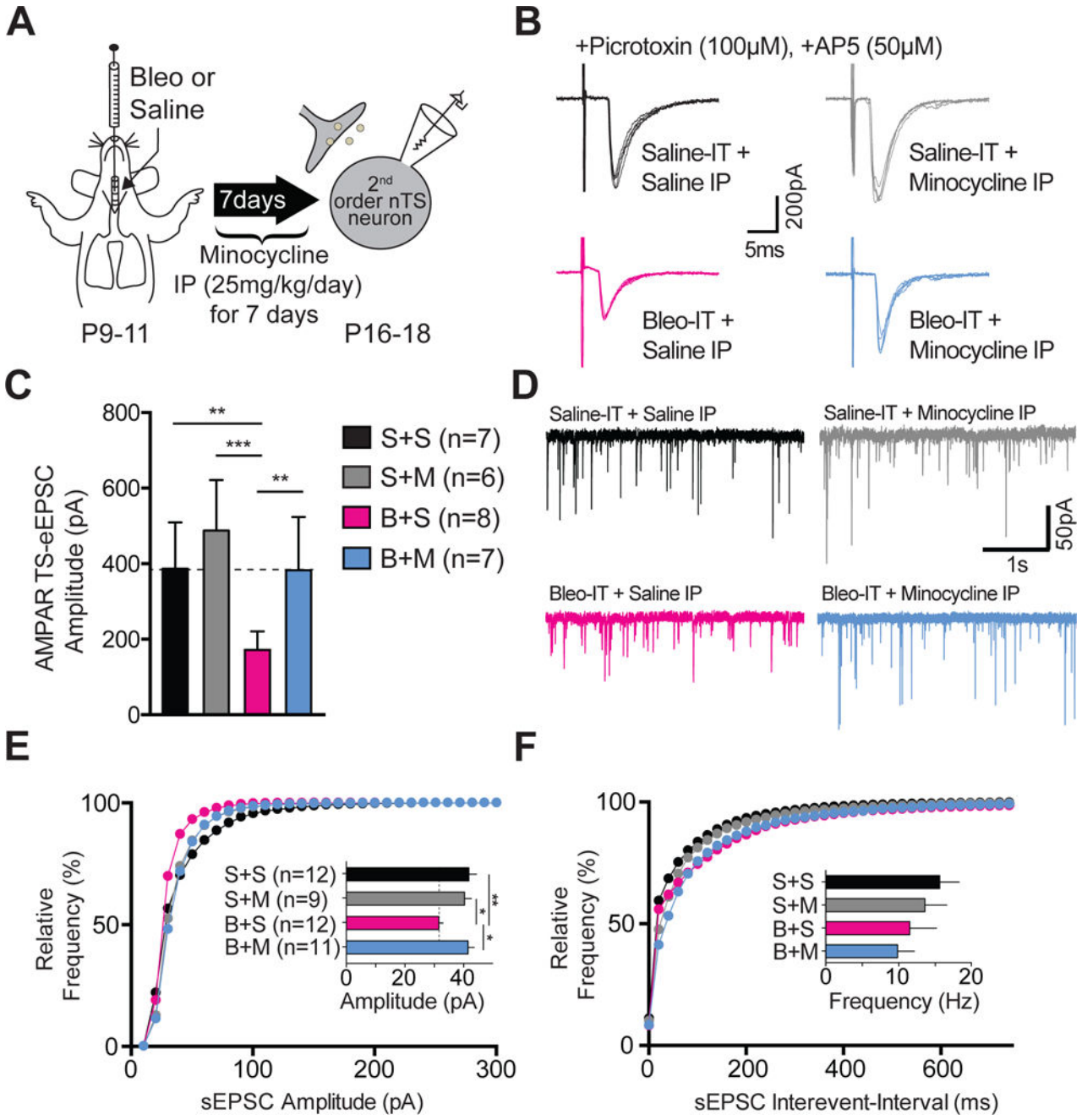

Figure 6.

Minocycline treatment in pre-transition period lung-injured rat-pups prevents synaptic depression.

A Protocol. Neonatal rats (P9–11) were intratracheally (IT) instilled with Bleomycin (Bleo) or saline and then intraperitoneally (IP) injected once daily with minocycline or saline for 7-days, and euthanized for electrophysiological experiments on day 7.

B Representative raw traces showing AMPAR mediated TS-eEPSCs (at −60 mV) from saline-IT + saline-IP (S+S, black, n=7 cells/slices/rats), saline-IT + minocycline-IP (S+M,

grey, n = 6 cells/slices/rats), Bleo-IT + saline-IP (B+S, magenta, n = 8 cells/slices/rats), Bleo-IT + minocycline-IP (B+M, blue, n = 7 cells/slices/rats) treated groups.

C Minocycline treatment prevented the lung-injury dependent reduction in TS-eEPSC amplitude. B+M treated rats exhibited significantly greater TS-eEPSC amplitudes compared to B+S treated rats (** $P = 0.0082$), which was not significantly different from S+S− ($P = 0.999$) or S+M− treated rats ($P = 0.373$, Mean ± SEM, One-way ANOVA with Tukey test).

D Representative raw traces showing spontaneous (s) EPSCs recorded from S+S−, (n = 12 cells, 9 slices, 9 rats), S+M− (n = 9 cells, 7 slices, 7 rats), B+S− (n = 12 cells, 7 slices, 7 rats), and B+M− treated rats (n = 11 cells, 7 slices, 7 rats).

E Cumulative probability graph for the amplitude of sEPSCs shows that the leftward shift in distribution exhibited by B+S-treated rats was absent in B+M-treated rats. The mean sEPSC amplitude was significantly reduced in B+S treated rats, compared to B+M− (* $P = 0.01$), S +S− (** $P = 0.006$), and S+M-treated rats (* $P = 0.041$, One-way ANOVA with Tukey test).

F Cumulative probability graph for the interevent interval of sEPSCs. Inset bar graph shows B+S treatment did not promote significant changes in mean frequency of sEPSCs when compared to B+M− ($P = 0.999$), S+S− ($P = 0.47$) and S+M− treated rats ($P > 0.999$, Kruskal-Wallis with Dunn's test).

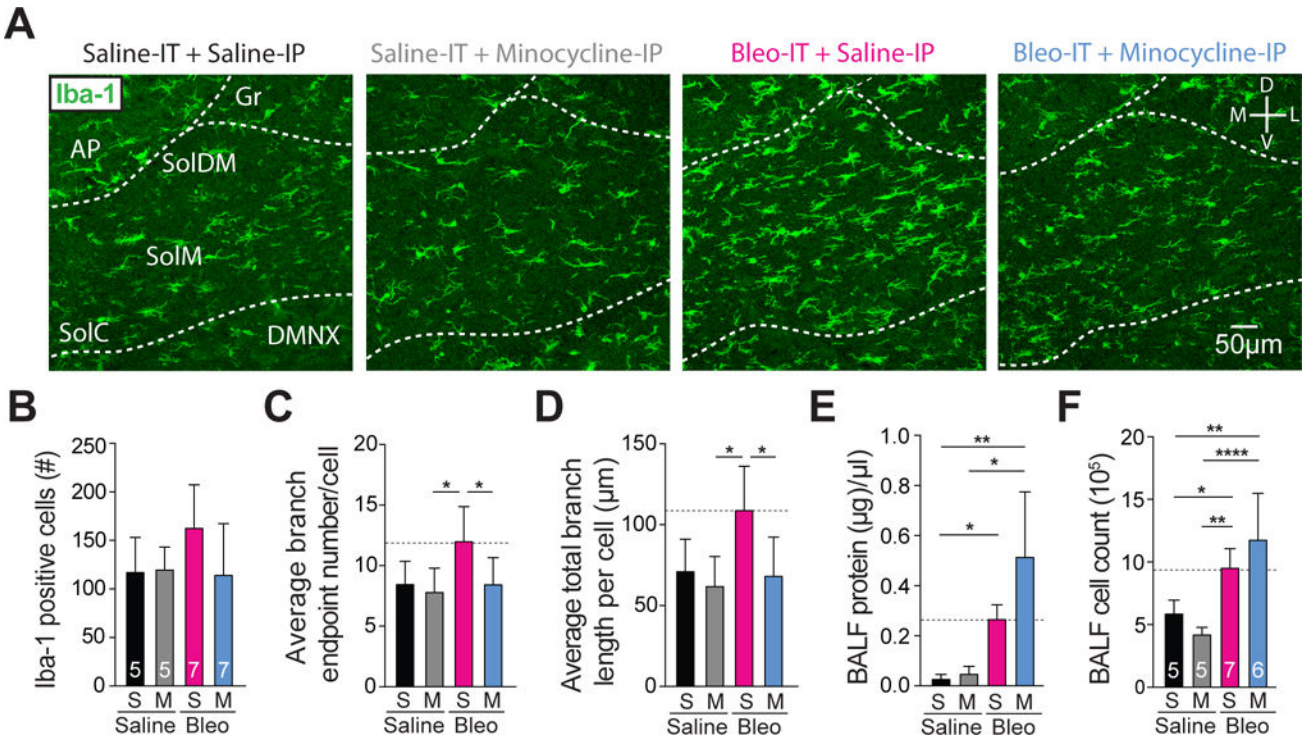

Figure 7.

Minocycline treatment in pre-transition period lung-injured rat-pups prevents *hyper*-ramification of Iba-1+ microglia, but does not significantly alter protein levels or the number of nucleated cells measured in BAL fluid.

A Representative images of coronal brainstem sections from saline-IT + saline-IP (S+S, black, n = 5), saline-IT + minocycline-IP (S+M grey, n = 5) Bleo-IT + saline-IP (B+S, magenta, n = 7) Bleo-IT + minocycline-IP (B+M, blue, n = 7) treated groups showing immunohistochemical staining in the commissural (SolC), medial (SolM), and dorsomedial (SolDM) subnuclei of the nTS.

B The number of microglia localized to the nTS was not significantly different in B+S− compared to B+M− ($P = 0.353$), S+S− ($P = 0.499$), or S+M-treated rats ($P = 0.499$, Kruskal-Wallis with Dunn's test).

C The number of branch endpoints per microglia in B+M-treated rats was significantly reduced compared to B+S treated rats (*$P = 0.048$), but not significantly different compared to S+S− ($P > 0.999$) or S+M− treated rats ($P = 0.967$, One-way ANOVA and Tukey multiple comparison's correction).

D The total branch length per microglia in B+M treated rats was significantly reduced compared to B+S treated rats (*$P = 0.0198$), but was not significantly different compared to S+S− ($P = 0.996$) and S+M− treated rats ($P = 0.967$, One-way ANOVA and Tukey test).

E The protein concentration present in bronchial alveolar lavage fluid (BALF) was augmented by lung injury, but not affected by minocycline treatment. The B+M− and B+S− treated rats exhibited significantly higher protein concentrations compared to their corresponding saline controls (B+M: n = 6 vs. S+M: n = 5, **$P = 0.0016$; B+S: n = 7 vs. S+S: n = 5, *$P = 0.035$), but were not significantly different from eachother (B+M vs. B+S: $P > 0.999$, Kruskal-Wallis with Dunn's test).

F The number of nucleated cells in BALF was augmented by lung injury, but was not affected by minocycline treatment. B+M and B+S treated rats exhibited significantly greater cell counts compared to their respective controls (B+M vs. S+M, ****P < 0.0001; B+S vs. S +S, *$P = 0.0479$), however the number of nucleated cells in B+M− and B+S− treated rats was not significantly different ($P = 0.287$, One-way ANOVA with Tukey test).

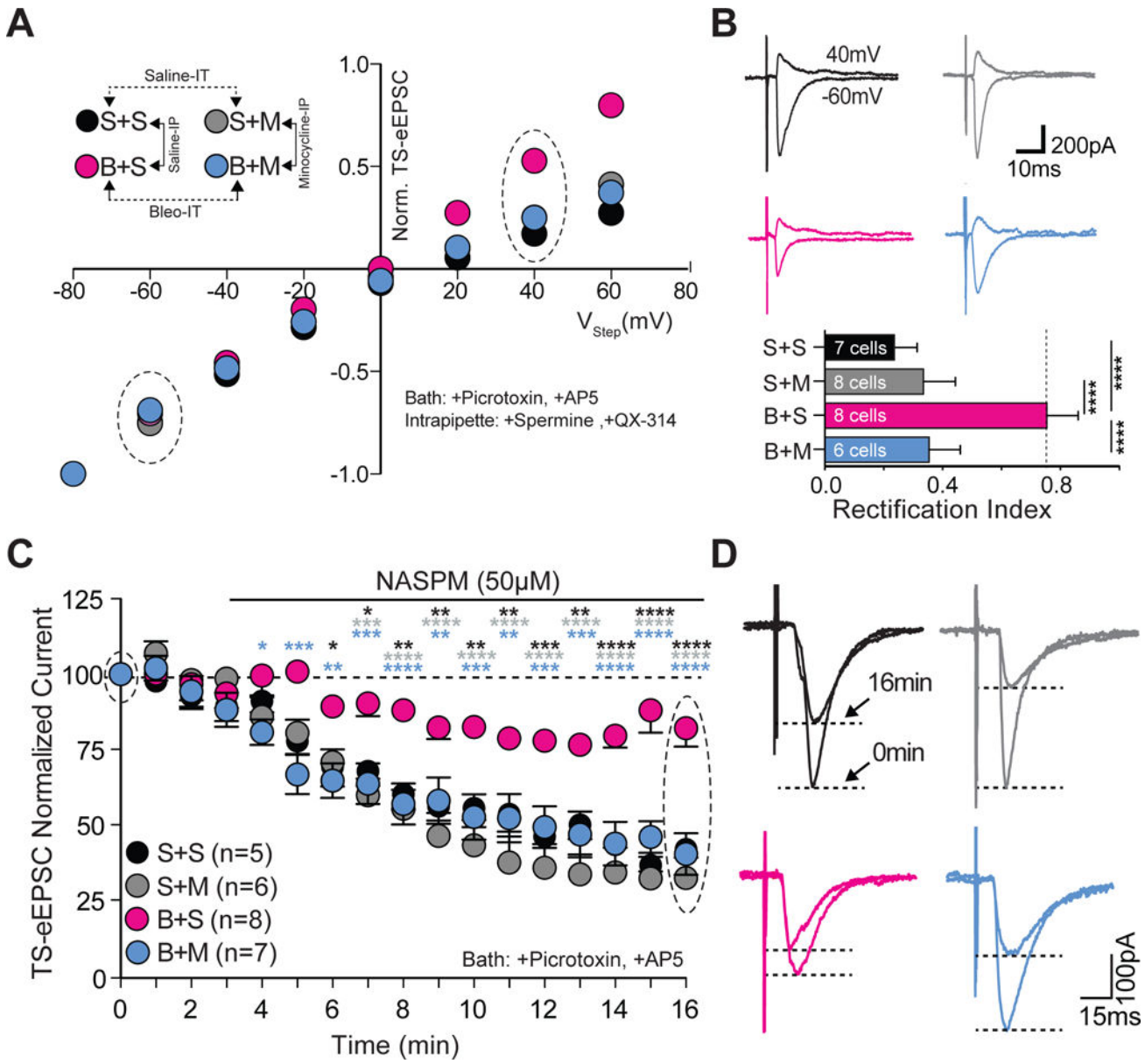

Figure 8.

Minocycline treatment in pre-transition period lung-injured rat-pups prevents loss of current-rectification and diminished polyamine sensitivity at TS➔nTS synapses.

A Current-voltage plots for TS-eEPSCs recorded from saline-IT + saline-IP (S+S, black; n = 7 cells, 5 slices, 5 rats), saline-IT + minocycline-IP (S+M, grey; n = 8 cells/slices/rats), Bleo-IT + saline-IP (B+S, magenta; n = 8 cells/slices/rats), and Bleo-IT + minocycline-IP (B +M, blue; n = 6 cells, 5 slices, 5 rats) treated rats.

B top: Raw representative traces of TS-eEPSCs recorded at −60mV and +40 mV (circled in the I–V plot) bottom: B+M treated rats exhibited a significant reduction in the rectification index compared to B+S treated rats (****P < 0.0001), which was not significantly different from S+S ($P = 0.187$) or S+M treated groups ($P = 0.985$, One-way ANOVA and Tukey test).

C Average normalized amplitudes of TS-eEPSCs from S+S− (n = 5 cells/slices/rats), S+M− (n = 6 cells/slices/rats), B+S (n = 8 cells/slices/rats), and B+M-treated (n = 7 cells/slices/rats) rats at base line and for 13 min after bath application of NASPM (after the 3rd min). B+M treated rats exhibited significantly greater NASPM dependent depression compared to B+S treated groups at 16 min (****P < 0.0001, Two-way ANOVA and Tukey test).
D Representative raw recordings showing TS-eEPSCs at baseline (0 min) and 13 min after bath application of NASPM.

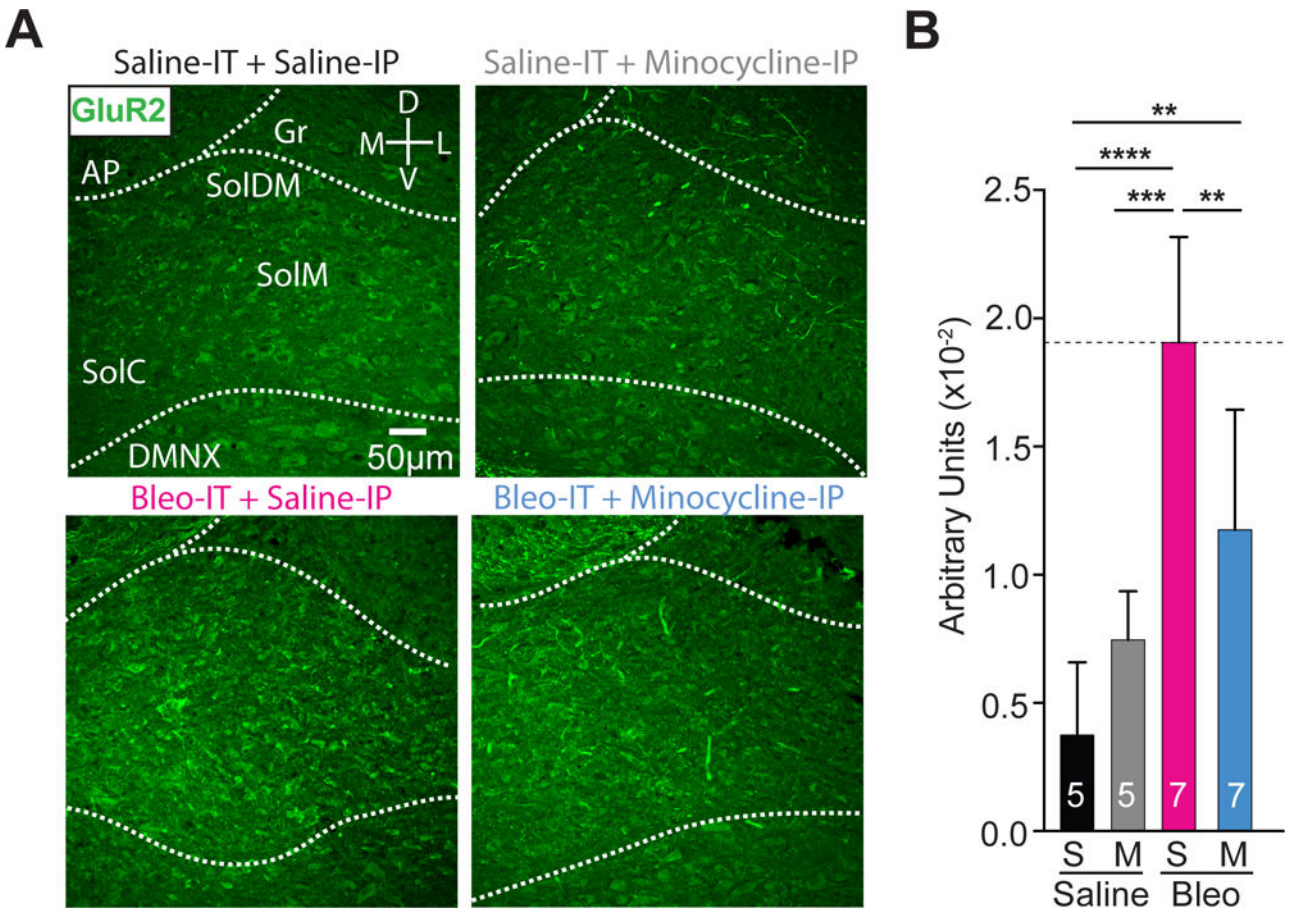

Figure 9.

Minocycline treatment in pre-transition period lung-injured rat-pups reduces GluA2+ immunostaining in the nTS

A Representative images showing coronal brainstem sections from saline-IT + saline-IP (S+S, n = 5) saline-IT + minocycline-IP (S+M, n = 5), Bleo-IT + saline-IP (B+S, n=7) and Bleo-IT + minocycline-IP (B+M, n = 7) treated groups immunostained for GluA2 in commissural (SolC), medial (SolM) and dorsomedial (SolDM) subnuclei of the nTS.

B GluA2+ staining in the nTS was significantly reduced in B+M (blue) treated rats compared to B+S (magenta) treated rats (**P = 0.008), but significantly greater than S+S (black) treated rats (**P = 0.0079), and was not significantly different from S+M (grey) treated rats (P = 0.234, One-way ANOVA with Tukey multiple comparisons test). There were no significant differences between S+S and S+M treated groups (P = 0.419).

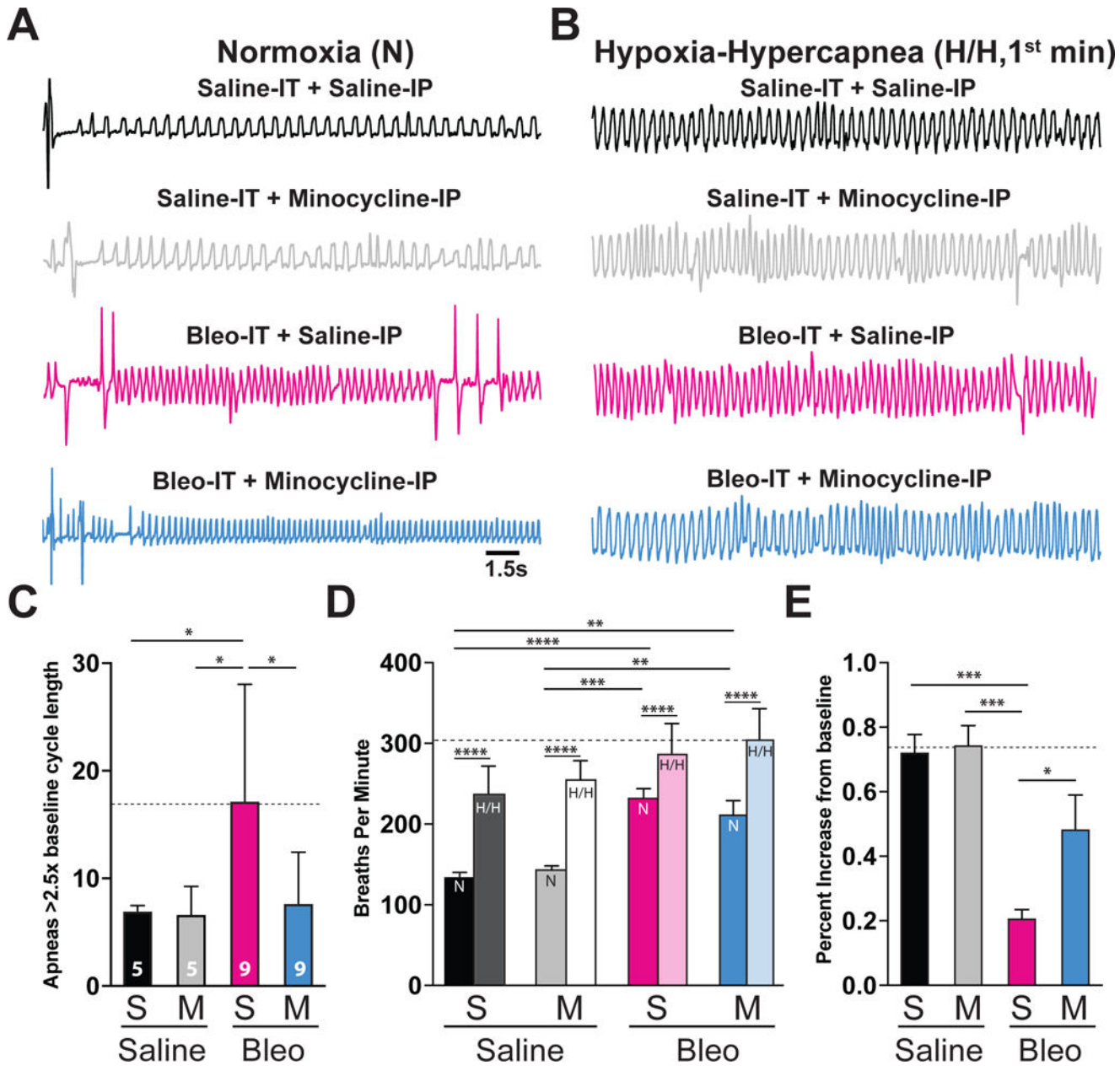

Figure 10.

Pre-transition period lung-injury promotes apnea and blunts the ventilatory response to acute hypoxic-hypercapnea (H/H) exposure.

A Representative baseline plethysmographic traces recorded in normoxia from saline-IT + saline-IP (black, S+S, n = 5) saline-IT + minocycline-IP (grey, S+M, n = 5), Bleo-IT + saline-IP (magenta, B+S, n=9) and Bleo-IT + minocycline-IP (blue, B+M, n = 9) treated rat-pups.

B Representative plethysmographic traces for S+S−, S+M−, B+S−, B+M− treated rats that were recorded during the 1st min of an acute (5 min) H/H exposure (5% CO_2, 10% CO_2).

C. B+S treated rats exhibited a significantly higher number of apneas (>2.5× baseline respiratory cycle length) compared to S+S or S+M treated rats, which was significantly

lower in B+M treated rats (B+S: vs. S+S: $P = 0.041$; B+S vs. S+M: $P = 0.041$; B+S vs. B +M: $P = 0.027$, One way ANOVA with Tukey test). There were no significant differences in the number of apneas measured in the B+M treated group and saline-treated controls (B+M vs. S+S: $P = 0.998$; B+M vs. S+M: $P = 0.998$).

D. LI promoted significant increases to the respiratory frequency (breaths per minute) in both Bleo-treated groups (B+S vs. S+S: $P < 0.0001$; B+S vs. S+M: $P = 0.0002$; B+M vs. S +S: $P = 0.002$; B+M vs. S+M: $P = 0.0078$, Two-way ANOVA with Sidak's test). In all treatment groups, the 1st min of acute H/H exposure promoted significant respiratory rate increases from baseline (baseline vs. 1st min H/H: S+S: $P < 0.0001$; S+M: $P < 0.0001$; B+S: $P < 0.0001$; B+M: $P < 0.0001$, Two-way ANOVA with Sidak's test).

E. B+S treated rat-pups exhibited a significantly smaller respiratory rate increase during the 1st min of H/H compared to S+S or S+M treated rats, which was significantly increased in B +M treated rats (B+S: vs. S+S: $P = 0.0008$; B+S vs. S+M: $P = 0.0005$; B+S vs. B+M: $P = 0.04$; One way ANOVA with Tukey test). There was no significant difference in the ventilatory response to H/H in B+M-treated rats compared to rats from saline-treated control groups (B+M vs. S+S: $P = 0.187$; B+M vs. S+M: $P = 0.131$).

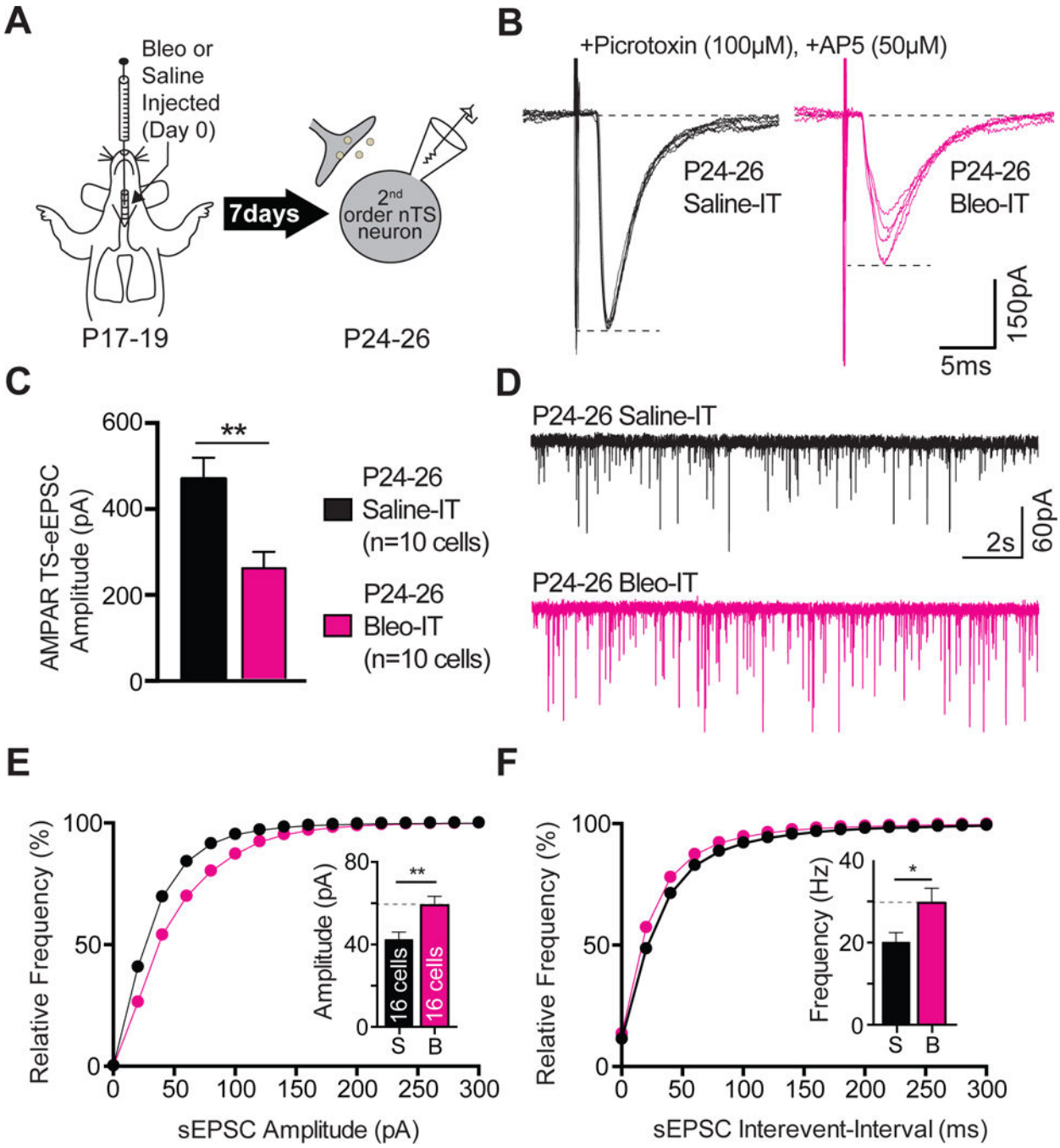

Figure 11.

Lung injury in post-transition period rat-pups alters TS➔nTS synaptic efficacy by attenuating the amplitude TS-eEPSCs and potentiating the amplitude and frequency of sEPSCs.

A Protocol. More mature rats pups (P17–19) received Bleo or saline intratracheally, recovered and where euthanized 7-days later (P24–26) for electrophysiological recordings.

B Representative raw recordings showing TS-eEPSCs (at −60 mV) from Bleo-treated (magenta) and saline-treated rats (black).

C The mean amplitude of TS-eEPSCs recorded at −60 mV was significantly smaller in Bleo-treated rats than in saline-treated rats (Bleo: n = 10 cells, 8 slices, 8 rats vs. saline: n = 10 cells, 8 slices, 8 rats, $P = 0.007$, Two-Tail T-test)

D Representative raw traces showing sEPSCs from Bleo-treated (magenta, n = 16 cells, 13 slices, 13 rats) and saline-treated rats (black, n = 16 cells, 13 slices, 13 rats).

E The cumulative probability graph for the amplitude of sEPSCs was rightward shifted in Bleo treated rats. Inset: The mean amplitude of sEPSCs was significantly increased in Bleo-treated rats compared to saline-treated rats (** $P = 0.0061$, Two-Tail T-test).

F The cumulative probability graph for the sEPSC interevent-interval was leftward shifted in Bleo-treated rats. Inset: The mean sEPSC frequency was significantly increased in Bleo-treated rats compared to saline-treated rats (* $P = 0.0322$, Two-Tail T-test).

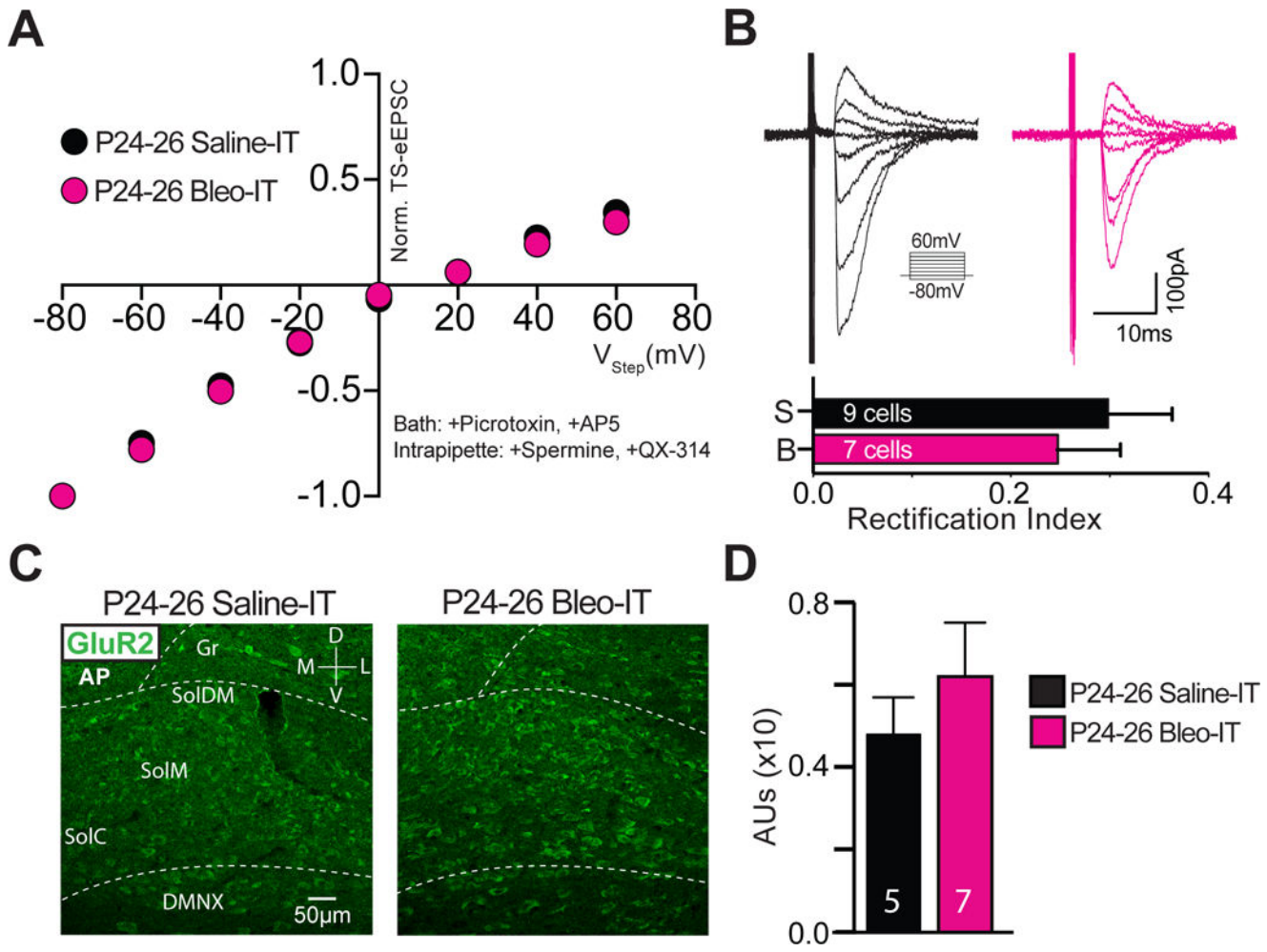

Figure 12.

Lung injury in post-transition period rat-pups alters TS➔nTS synaptic transmission through a GluA2-independent mechanism.

A Current-voltage plots for TS-eEPSCs recorded from Bleo-treated (magenta, n = 7 cells, 6 slices, 6 rats) and saline-treated rats (black, n = 9 cells, 6 slices, 6 rats).

B top: raw representative traces of TS-eEPSCs recorded at holding potentials ranging from −80 to +60 mV. bottom: The rectification index was not significantly different between Bleo- and saline- treated groups ($P = 0.1259$, Two-tail t-Test).

C Representative images showing coronal brainstem sections from Bleo-treated and saline-treated rats with GluA2+ immunostaining in commissural (SolC), medial (SolM) and dorsomedial (SolDM) subnuclei of the nTS.

D GluA2+ staining in the nTS was not significantly different between Bleo-treated (n = 5) and saline-treated (n = 7) rats ($P = 0.4405$, Two-tail t-Test).

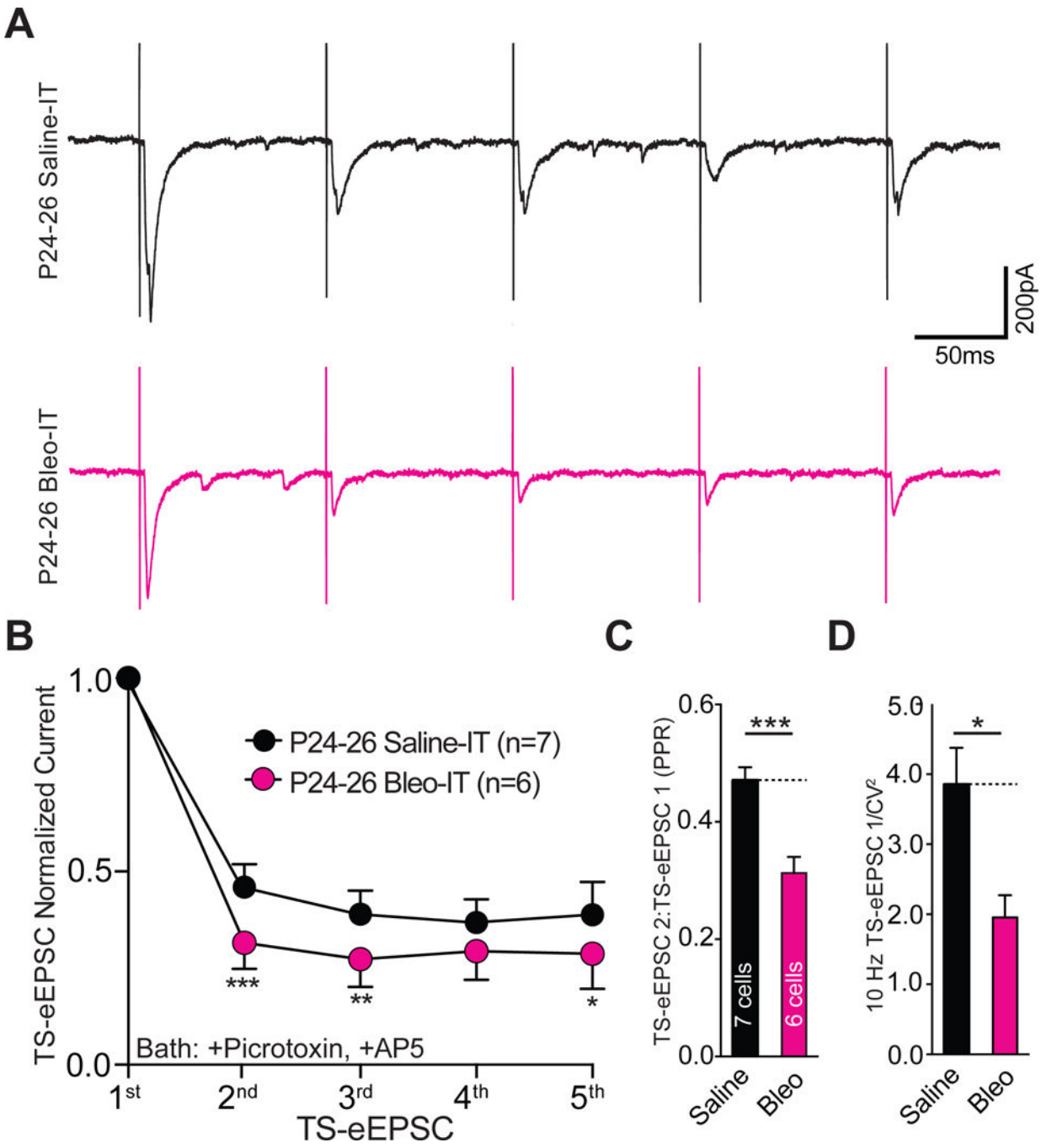

Figure 13.

Lung injury in post-transition period rat-pups augments short-term use-dependent depression and reduces the paired pulse ratio and $1/CV^2$.

A Representative raw TS-eEPSCs (events) from a 10 Hz stimulus train applied to Bleo-treated (n = 6 cells, 5 slices, 5 rats) and saline-treated rats (n = 7 cells, 6 slices, 6 rats).

B Bleo treatment promoted significant depression in normalized TS-eEPSC amplitudes within bleo-treated (stimulus 1 vs. 2, 3, 4 & 5, $P < 0.0001$) and saline-treated (stimulus 1 vs. 2, 3, 4 & 5, $P < 0.0001$, Two-way ANOVA with Tukey test), which was significantly greater

in Bleo-treated than saline-treated rats between stimulus 2 (***P = 0.0008), stimulus 3 (**P = 0.0091), and stimulus 5 (*P = 0.0318, Two-way ANOVA with Tukey test.
C The paired pulse ratio (PPR; TS-eEPSC 2/TS-eEPSC 1) for Bleo-treated rats was significantly reduced compared to saline-treated rats (***P = 0.0009, Two-Tail T-test).
D The $1/CV^2$ (measured at 10 Hz) was significantly reduced for Bleo-treated rats compared to saline-treated rats (*P = 0.0128, Two-Tail T-test).

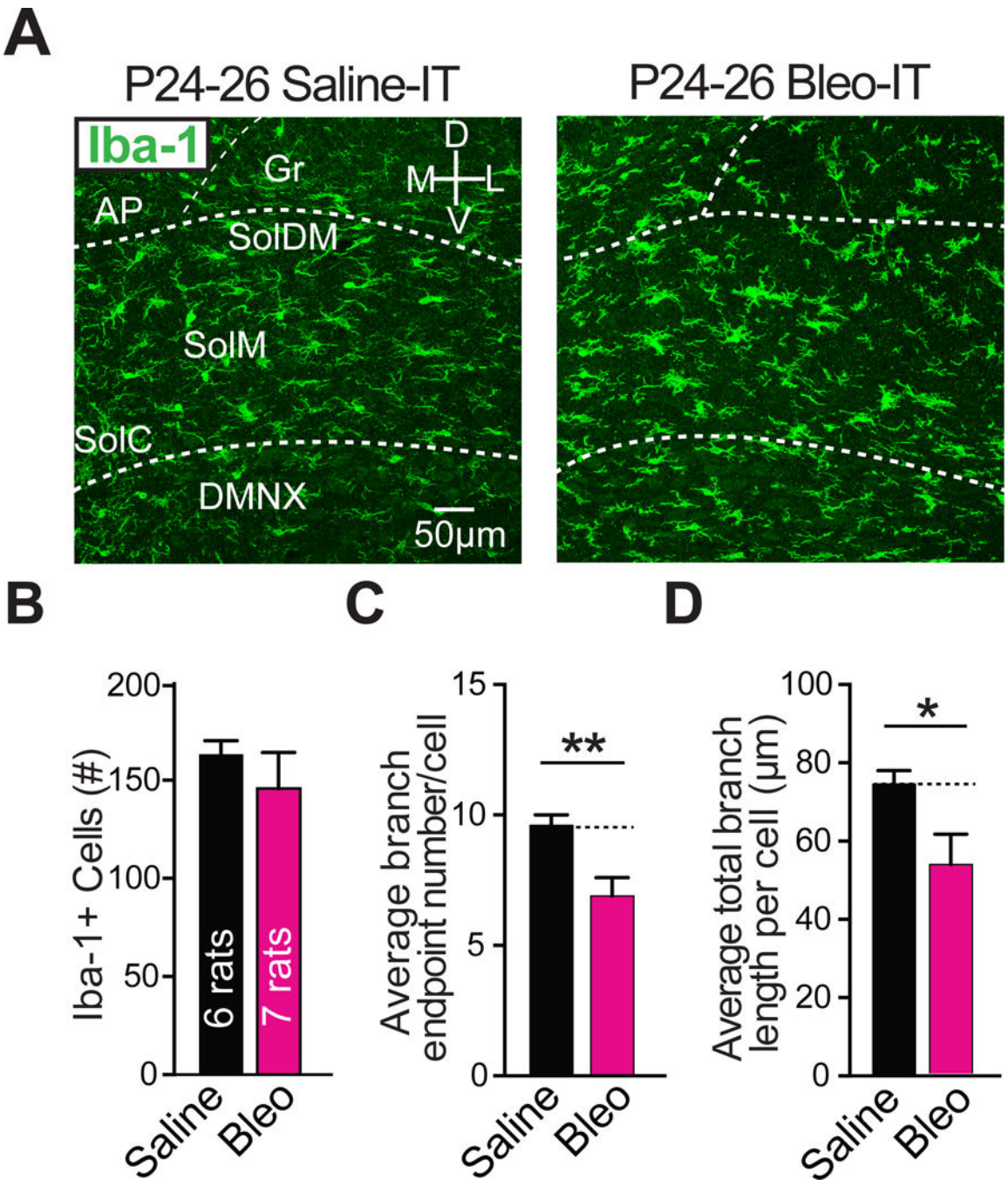

Figure 14.

Lung injury in post-transition period rat-pups promotes microglia *hypo*-ramification in the nTS.

A Representative images of coronal brainstem sections from Bleo-treated (n = 7) and saline-treated (n = 6) rats stained for the microglia marker Iba-1.

B The number of microglia in the nTS was not significantly different in Bleo-treated and saline-treated rats ($P = 0.431$, Two-Tail T-test).

C The number of branch endpoints per microglia decreased in Bleo-treated versus saline-treated rats (** $P = 0.0080$, Two-Tail T-test).
D The total branch length per microglia decreased in Bleo-treated compared to saline-treated rats (* $P = 0.0345$).